Technische Universität München

Fakultät für Medizin
Institut für Diabetes und Adipositas

Leptin sensitizer celastrol, glial calcineurin and hypothalamic glutathione peroxidase 7 – novel entities in weight control and glucose homeostasis

Katrin Hannelore Pfuhlmann

Vollständiger Abdruck der von der Fakultät für Medizin der Technischen Universität München zur Erlangung des akademischen Grades eines

Doktors der Naturwissenschaften

genehmigten Dissertation.

Vorsitzender: Prof. Dr. Carsten Schmidt-Weber
Prüfer der Dissertation: 1. Prof. Dr. Matthias Tschöp
2. Prof. Dr. Martin Hrabě de Angelis

Die Dissertation wurde am 26.01.2018 bei der Technischen Universität München eingereicht und durch die Fakultät für Medizin am 10.10.2018 angenommen.

Summary

Obesity and comorbid sequelae such as diabetes type 2 are global health burdens of the first order. Our current lack of efficacious therapeutic weight loss strategies, and a still incomplete understanding of the underlying mechanisms of pathogenesis of obesity and type 2 diabetes are thus scientists' challenges of the highest priority. This thesis aims to address this unmet scientific need by exploring three partially independent topics that focus on central vs. peripheral mechanisms of weight and glucose control.

The first aim of the thesis was to assess, whether celastrol, a plant-derived constituent of traditional Chinese medicine, is of use as putative weight loss drug based on its central action as sensitizer for hypothalamic leptin action, or via browning of white adipose tissue and/or brown adipose tissue thermogenesis. Results of this thesis largely corroborate celastrol as potent anti-obesity drug. The thesis demonstrates considerable anorectic and weight-lowering effects of celastrol that are independent from inguinal white adipose tissue browning, brown adipose tissue activation and uncoupling protein 1 (UCP1)-mediated thermogenesis. Rather, weight loss is strictly leptin dependent - shown by the lack of effect of celastrol administration in Lep^{ob} or Lep^{db} mice - and a result of hypophagia induced by inhibition of protein tyrosine phosphatases (PTP)1B and T-cell (TC)PTP.

The second aim of the thesis was to explore, whether the phosphatase calcineurin, a regulator of skeletal muscle metabolism and systemic energy and glucose homeostasis, affects the activation of hypothalamic astrocytes and microglia. The activation of both non-neuronal hypothalamic cell populations, termed astrocytosis and microgliosis, is observed in response to high fat diet (HFD) feeding and associated with the etiology of hypothalamic inflammation and metabolic dysfunction. Astrocytosis was previously shown to induce changes in calcium (Ca^{2+}) homeostasis, and was linked with activation of calcium-sensitive serine-threonine phosphatase calcineurin. However, the role of calcineurin in hypothalamic astrocytosis as a response to chronic HFD exposure had not been studied. The results of the thesis show that deficiency for the catalytic calcineurin subunit Ppp3cb results in a decrease in astrocytosis marker Glial fibrilary acidic protein (GFAP) in the dorsomedial hypothalamus (DMH), ventromedial hypothalamus (VMH) and arcuate nucleus (ARC) of mice chronically exposed to HFD. A reduction of ionized calcium binding adaptor molecule 1 (IBA1) positive microglia, a marker for microgliosis, is detected in the VMH of HFD-fed Ppp3cb deficient mice.

Third, the thesis aims to delineate whether glutathione peroxidase 7 (GPx7), a putative oxygen sensor involved in endoplasmic reticulum (ER)-stress, exerts its weight lowering actions via peripheral or central mechanisms. GPx7 was previously shown to regulate

adipocyte differentiation, and GPx7 deficiency was linked with systemic oxidative stress and pathophysiologies ranging from carcinogenesis to obesity. The results of this thesis extend those earlier reports and show increased body weight in globally deficient male GPx7 knockout (KO) mice on chow and high fat diet, and impaired glucose tolerance in globally deficient male GPx7 knockout mice after 8 weeks of HFD feeding. Higher body weight is linked *in vivo* with a decrease in energy expenditure in GPx7 knockout mice, and *in vitro* with a cell-autonomous increase of adipogenesis of white but not brown adipocytes. Hypothalamus-specific conditional ablation of GPx7 (driven by NK2 Homeobox 1 (Nkx2.1)-Cre) has no impact on body weights compared to Nkx2.1-Cre positive wildtype (WT) mice, but impairs glucose tolerance after 8 weeks of HFD feeding.

In summary, results of this thesis reflect the plurality of central and peripheral pathways and mechanisms responsible for the regulation of energy and glucose homeostasis. The three projects further highlight that targeting of central circuitry by pharmacological agents (celastrol) or genetic manipulation (GPx7, calcineurin) may be key in developing successful treatment strategies against metabolic diseases.

Zusammenfassung

Adipositas und Folgeerkrankungen wie Typ 2 Diabetes zählen zu den weltweit schwerwiegendsten Gesundheitsproblemen. Das derzeit noch unvollständige Verständnis der Mechanismen, die diesen Krankheiten zugrunde liegen, sowie der Mangel an therapeutischen Strategien zur effizienten Gewichtsreduzierung machen die wissenschaftliche Untersuchung dieser Themen zu einer wichtigen Aufgabe. Die vorliegende Arbeit zielt darauf ab, einen Beitrag zu diesen Forschungsgebieten zu leisten, indem in drei – teilweise unabhängigen – Projekten periphere und zentrale Mechanismen der Gewichtsreduzierung und der Glukosekontrolle untersucht werden.

Der erste Teil der Arbeit befasst sich mit Celastrol, einem pflanzlichen Bestandteil der traditionellen chinesischen Medizin, dem eine gewichtsreduzierende Wirkung zugeschrieben wird. Der gewichtsreduzierende Effekt von Celastrol wird entweder zentral durch hypothalamische Sensibilisierung des Fettgewebshormons Leptin oder durch Thermogenese des weißen bzw. braunen Fettgewebes vermittelt. Die im Rahmen der Arbeit erzielten Ergebnisse bestätigen weitestgehend die Wirkung von Celastrol als potentes Medikament gegen Adipositas. Zudem wird eine deutliche anorektische und gewichtsreduzierende Wirkung von Celastrol gezeigt, die unabhängig von der Bräunung des inguinalen weißen Fettgewebes, sowie von Uncoupling Protein 1 (UCP1)-mediierter Thermogenese und Aktivierung von braunem Fettgewebe ist. Der Gewichtsverlust scheint vielmehr stark von Leptin abhängig - was durch die Unwirksamkeit von Celastrol in Lep^{ob} und Lep^{db} Mäusen gezeigt werden konnte - und ein Ergebnis der Hypohagie zu sein, welche durch eine Inhibierung der Protein-Tyrosin-Phosphatase (PTP)1B und T-Zell (TC)PTP ausgelöst wird.

Zweiter Gegenstand dieser Arbeit ist die Untersuchung der Phosphatase Calcineurin, einem Regulator des Skelettmuskel-Metabolismus und der systemischen Energie- und Glukosehomöostase. Ziel ist es, herauszufinden, ob Calcineurin für die Aktivierung hypothalamischer Astrozyten und Microglia von Bedeutung ist. Es wurde festgestellt, dass die Aktivierung dieser beiden nicht-neuronalen Zellpopulationen – Astrozytose oder Mikrogliose genannt – unter anderem als Folge der Verabreichung einer fettreichen Diät auftritt und mit hypothalamischer Inflammation und metabolischer Dysfunktion einhergeht. In vorhergehenden Forschungsarbeiten wurde gezeigt, dass Astrozytose Veränderungen in der Calcium Homeostase hervorruft und mit der Aktivierung der Calcium-sensitiven Serine-Threonin-Phosphatase Calcineurin einhergehen kann. Bis heute wurde jedoch nicht untersucht, ob Calcineurin eine Wirkung auf die durch fettreiche Diät induzierte hypothalamische Astrozytose besitzt. Die Ergebnisse dieser Forschungsarbeit deuten darauf hin, dass das Fehlen der katalytischen Calcineurin Untereinheit Ppp3cb bei Mäusen, die chronisch mit fettreichem Futter gefüttert werden, zu einer reduzierten Astrozytose im

dorsomedialen und ventromedialen Hypothalamus sowie im Arcuate Nucleus des Hypothalamus führt. Als Marker kommt dabei Glia-fibrilläres Protein (GFAP) zum Einsatz. Als Marker für Mikrogliose wird das ionisierte Calcium bindende Adaptormolekül 1 (IBA1) verwendet, wobei hier eine Reduktion von IBA1-positiven Mikroglia nur im VMH festgestellt wird.

Ziel des dritten Projektes ist es, zu erforschen, ob das Enzym Glutathion Peroxidase 7 (GPx7), welchem eine Rolle als Sauerstoffsensor bei Endoplasmatischem Retikulum (ER)-Stress zugeschrieben wird, eine Rolle in der Regulation von Körpergewicht und Glukosehomöostase spielt. In vorherigen Studien wurde gezeigt, dass GPx7 die Adipozyten-Differenzierung reguliert und dass die Abwesenheit von GPx7 zu systemischem oxidativem Stress sowie der Ausbildung von Krankheiten wie Karzinogenese und Adipositas führt. Die Ergebnisse dieser Arbeit erweitern diese vorausgehenden Veröffentlichungen und zeigen ein erhöhtes Körpergewicht in männlichen Mäusen mit globaler GPx7-Defizienz. Dieser Befund ist unabhängig davon, ob Wildtyp-Kontrollmäuse bzw. GPx7 Knockout-Mäuse mit normaler oder mit fettreicher Nahrung gefüttert werden. Glukoseintoleranz wird lediglich bei mit fettreicher Nahrung gefütterten GPx7 Knockout-Mäusen nach 8-wöchiger Fütterung beobachtet. Das erhöhte Körpergewicht der GPx7-defizienten Mäuse wird *in vivo* mit einer Abnahme des Energieverbrauchs und *in vitro* mit einer zell-autonomen Zunahme der Adipogenese von weißen, aber nicht von braunen Adipozyten verknüpft. Eine Hypothalamus-spezifische Ausschaltung von GPx7 (verursacht durch NK2 Homeobox 1 (Nkx2.1)-Cre) hat keinen Einfluss auf das Körpergewicht im Vergleich zu Nkx2.1-Cre-positiven Wildtyp-Kontrollmäusen, verschlechtert jedoch die Glukosetoleranz nach 8-wöchiger Fütterung mit fettreicher Diät.

Zusammenfassend werden im Rahmen dieser Arbeit verschiedene zentrale und periphere Signalwege und Mechanismen aufgezeigt, die für die Regulierung der Energie- und Glukosehomöostase verantwortlich sind. Die drei Projekte zeigen, dass die Einflussnahme auf zentrale Netzwerke durch pharmakologische Wirkstoffe (Celastrol) oder durch genetische Manipulation (GPx7, Calcineurin) für die Entwicklung erfolgreicher Behandlungsstrategien gegen Stoffwechselerkrankungen entscheidend sein kann.

Table of contents

I Introduction

1 Hypothalamic regulation of glucose and energy homeostasis and novel drugs against the global obesity threat

Diabetes and obesity are world wide occurring diseases with epidemic character [2-4]. In 2016, 39% men and 40% of women of the world population were classified as overweight and 11% of men and 15% of women are diagnosed as obese [3]. Moreover, in 2014, 8.5% of the adult world population were diagnosed with diabetes [4]. Reasons for the development of obesity are genetics on the one hand and environmental factors on the other. Although multiple genes are known to be involved in the development of diabetes and obesity, numerous genes still await discovery. More importantly, the interplay between genetic factors, especially in relation to environmental cues is far from being understood. An unhealthy lifestyle including insufficient movement and consumption of noxious food containing high amounts of sugar and fat are environmental influences that are accountable for the development of obesity and diabetes.

In our body many different organs and cell types contribute to the regulation of energy and glucose balance. The hypothalamus, as a center for glucose and energy homeostasis containing many different neuronal cell types and a large variety of glia cells, is one of them. Neuronal cells within the arcuate nucleus of the hypothalamus receive nutritional and hormonal signals from the periphery and orchestrate adaptive physiological responses including calorie intake, glucose metabolism and energy expenditure. Important hormones acting on the hypothalamus in terms of energy and glucose metabolism include insulin, leptin [5] and the gastrointestinal hormones ghrelin [6], glucagon-like peptide 1 (GLP-1), peptide YY (PYY)3-36 and cholecystokinin (CCK). Insulin acts mainly via the insulin receptor substrate (IRS)2 – phosphatidylinositol 3-kinase (PI3K) pathway. Further, insulin action on the brain

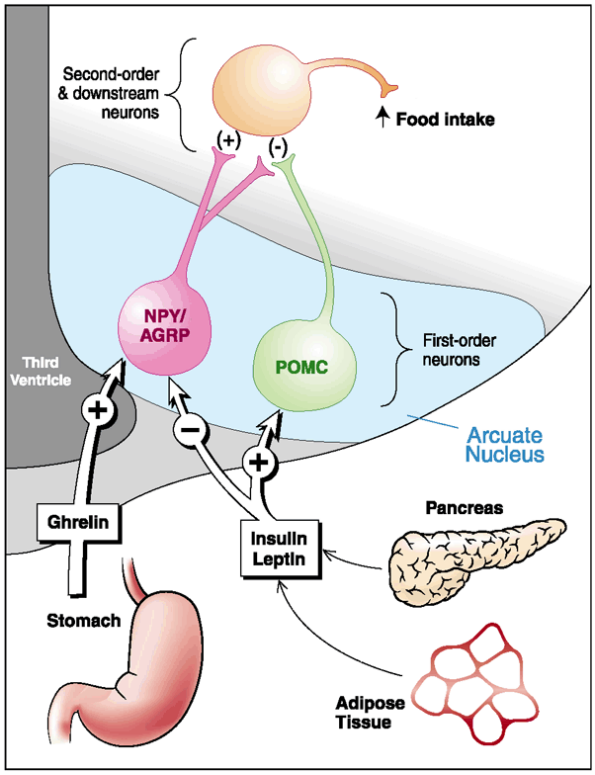

Figure 1. Hypothalamic regulation of food intake by peripheral hormones
Insulin is secreted by the pancreas and leptin is released from adipose tissue, in proportion to the amount of adipose tissue. Both hormones stimulate POMC neurons and inhibit NPY/AgRP neurons. Ghrelin is released from the stomach and activates NPY/AgRP neurons. In case of activation of the orexigenic NPY/AgRP neurons, food intake is increased, while activation of POMC neurons leads to a decrease in food intake. Figure adapted from [1].

regulates hepatic glucose metabolism and the hypothalamus regulates pancreatic insulin and glucagon secretion via the parasympathetic and sympathetic efferent nerves. Leptin in the hypothalamus acts via janus kinase (JAK)–signal transducers and activators of transcription (STAT) pathway, IRS–PI3K, AMP-activated protein kinase (AMPK), extracellular signal-regulated kinase (ERK), and the mammalian target of rapamycin-S6 kinase signaling [5].
In the ARC, two distinct neuronal cell populations with contrary functions are present that are important for the regulation of glucose and energy balance: the anorexigenic pro-opiomelanocortin (POMC) expressing neurons and the orexigenic agouti-related protein (AgRP) and neuropeptide Y (NPY) expressing neurons. POMC is further cleaved to neuropeptides including α-melanocyte-stimulating hormone (α-MSH), which activates melanocortin receptor 3/4 (MC3/4R) on second order neurons to decrease food intake (FI) and increase energy expenditure. Second order neurons reside in hypothalamic nuclei such as the VMH, DMH, paraventricular hypothalamic nucleus (PVN) and lateral hypothalamus (LH). After processing of the information, these second order neurons project to neurons outside the hypothalamus, leading to a response in energy intake and expenditure. AgRP/NPY neurons are activated by fasting and project to the PVN and the LH. They release the neuropeptides AgRP and NPY. AgRP is an inverse agonist of MC3/4R and therefore increases food intake (simplified overview: figure 1). NPY activates NPY Y1 and Y5 receptors to stimulate food intake and Y1 receptors to further reduce energy expenditure. Moreover, AgRP/NPY neurons directly inhibit POMC neurons via inhibitory γ-aminobutyric acid (GABA) action [7]. Overall, the hypothalamus is considered as key brain region for the control of glucose and energy homeostasis.

At current, novel anti-obesity drug candidates often phenocopy the central action of peptide hormones from the gastrointestinal tract or adipose tissue [8] on homeostatic and hedonic neuronal circuitry in the hypothalamus or related brain areas. Direct action against these complex gut-brain and fat-brain axes alters the release of anorexic/orexigenic signals and neurotransmitters, ultimately curbing appetite and food intake [9, 10]. Current efforts are further focusing on brown adipose tissue (BAT) as target for anti-obesity medicines [11]. BAT is present in infants and adult humans and is characterized by a high number of large mitochondria that contain UCP1. UCP1 is paramount for BAT thermogenesis by dissipating the inner membrane proton motive force, thereby converting nutrient energy into heat instead of adenosine triphosphate (ATP) [11]. Early, anti-obesity therapies often targeted the central nervous system (CNS) control of metabolism. However, few CNS-based drugs succeeded in decreasing appetite and body weight (BW), and those are associated with severe side effects that prohibit chronic usage. Rimonabant, a selective cannabinoid receptor type 1 (CB1) blocker, is one example for a drug targeting the CNS that was on the market for a couple of years and was withdrawn in 2009 due to serious psychiatric side effects [12].

Another example is the potent anti-obesity drug fenfluramine/phentermine (Fen-Phen), which consists of the amphetamine analog phentermine and serotonin uptake inhibitor and stimulant fenfluramine. The drug combination was withdrawn from the marked due to severe side effects like pulmonary hypertension and valvular heart disease [13, 14]. Central acting anti-obesity molecules that were recently approved by the Food and Drug Administration (FDA) of the United States of America (US) are lorcaserin and the combinatorial drug phentermine-topiramate (Phen-Top). Lorcaserin is a molecular agent with high affinity to 5-HT2c receptor, which is present in hypothalamic POMC neurons. Phentermine increases norepinephrine release and therefore decreases food intake. Topiramate is believed to increase energy expenditure, decrease energetic efficiency and decrease caloric intake. Minor secondary effects such as headache or constipation were reported for lorcaserin, Phen-Top might cause psychiatric disturbances and teratogenicity. Approved doses of lorcaserin cause a modest weight loss of approximately 5.8% in one year and approved doses of Phen-Top reduce body weight up to 10.9% within one year [12]. Increasing attention is nowadays also given towards developing weight lowering drugs that act on peripheral thermogenesis, mostly activated via UCP1-mediated uncoupling in inguinal white adipose tissue (iWAT) or BAT. Mitochondrial uncouplers such as 2,4-dinitrophenol are effective as anti-obesity drugs, but their use is highly dangerous due to severe side effects [15]. Accordingly, novel strategies to induce UCP1-mediated uncoupling are warranted, which requires a better understanding of the exact mechanisms. Moreover, the development of novel CNS-acting anti-obesity drugs demands a full understanding of the molecular circuitry governing energy and glucose homeostasis.

2 Medical use of triterpenoid compound celastrol as anti-obesity drug

Parts of this project have been published in: Pfuhlmann K. *et al.* (2018), ”Celastrol-Induced Weight Loss Is Driven by Hypophagia and Independent From UCP1.” Diabetes 67(11): 2456-2465.

Celastrol, a pentacyclic triterpenoid naturally occurring in the chinese thunder of god vine *Tripterygium wilflordii*, has been proposed as anti-obesity agent [16-18]. Celastrol-containing plant extracts find use as traditional chinese medicine to treat fever, chills, joint pain and edema [19]. Medicinal celastrol has been described as nuclear factor kappa B (NF-κB) inhibitor [20-24] with anti-inflammatory [24, 25] and anti-carcinogenic potential [26-28]. The interaction of celastrol with heat-shock protein 90 and co-chaperones such as cell division cycle 37 (Cdc37) or prostaglandin E synthase 3 (p23) has been shown to impair complex stability and downstream kinase activation [29]. The potential use of celastrol as novel anti-obesity drug was first described in 2013 by Jung Kim and colleagues and corroborated by

Weisberg and co-workers. 1 or 3 mg/kg celastrol were shown to lower body weight and blood glucose levels and to increased insulin sensitivity in leptin receptor deficient (Lep^{db}) mice, respectively [18, 30]. Recently, celastrol was described as a potent leptin sensitizer at 10- to 30-fold lower doses by Liu and colleagues [16]. Celastrol was shown to lower body weight and hypothalamic as well as hepatic ER-stress, inhibit food intake and improve glucose tolerance in diet-induced obese mice. None of these improvements could be detected in lean or leptin (receptor) deficient Lep^{ob} or Lep^{db} mice [16]. *In vitro*, celastrol was shown to increase lipolysis and to inhibit adipocyte differentiation of 3T3 cells [31]. Others found a decreased in hepatic steatosis in mice after celastrol administration (dose: 200 µg/kg, injection every two days) due to increased sirtuin 1 (*Sirt1*) expression [32]. Further, activation of a heat shock transcription factor 1 (HSF1) – Peroxisome proliferator-activated receptor gamma coactivator 1α (PGC-1α) axis and mitochondrial gene programs that lead to increased muscle and BAT thermogenesis and iWAT browning were suggested to be responsible for the weight lowering effects of celastrol (figure 2) [17].

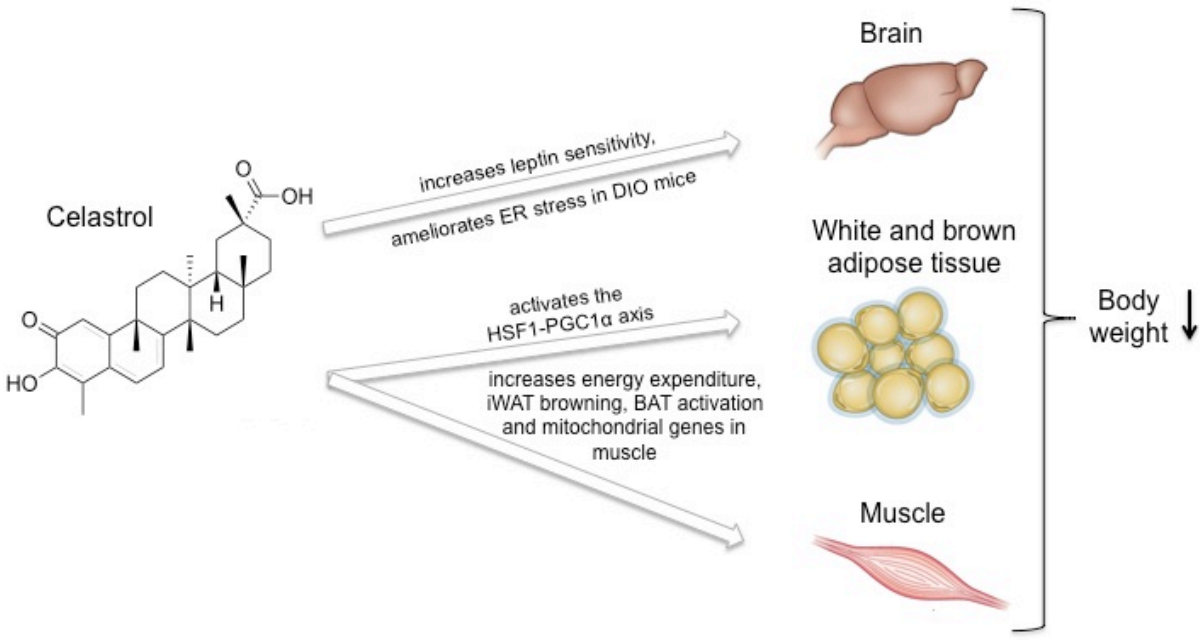

Figure 2. Celastrol decreases body weight via leptin sensitization and/or activation of the HSF1/PGC-1α axis
Celastrol decreases body weight via leptin sensitization and amelioration of ER-stress in diet induced obese (DIO) mice [16]. Moreover, celastrol activates the HSF1-PGC1α axis, leading to an increase in energy expenditure, inguinal white adipose tissue browning, brown adipose tissue activation and mitochondrial genes in muscle [17]. Activation of both mechanisms lead to a reduction in body weight.

3 Calcineurin Aβ and its function in HFD-induced hypothalamic astrocytosis

Parts of this project have been published in: Pfuhlmann K. *et al.* (2018), “Calcineurin A beta deficiency ameliorates HFD-induced hypothalamic astrocytosis in mice.“ Journal of Neuroinflammation 15(1): 35.

3.1 Discovery of glia cells

In 1856, Rudolf Virchow documented glia cells for the first time and assigned the name “glia” for glue to these cells. In 1906, Santiago Ramón y Cajal and Camillo Golgi won the Nobel Prize for their work on the structure of the nervous system. Describing the “Neuron Doctrine”, they highlight the presence and interconnectivity of individual cells but also the presence of non-connected cells, which were shown to exist in high numbers. Until 20 years ago, glia cells were not studied in detail and were considered as structural elements of the brain. Today, many different glia cell types in the CNS are known with a multitude of functions, including astrocytes, microglia, tanycytes, polydendrocytes, and oligodendrocytes [33, 34].

3.2 Astrocytes and their function within the CNS

More than 90% of all cells in the human brain are estimated to be glia cells. Astrocytes account for more than 50% of all brain cells, and represent the most frequent glial cell type in the brain [35]. Astrocytes are located at the interface between neurons and blood vessels, and together with pericytes and endothelial cells from microvessels, they form the neurovascular system [36], which is important for the blood brain barrier function and glucose entry into the brain [37]. Glucose is taken up by astrocytes via glucose transporter (GLUT) 1 and can be stored as glycogen. Glycogen can later be used in energy deficient states, or directly be converted to lactate and used by neurons in the oxidative metabolism as alternative source of energy [38-41]. Astrocytes contain receptors for neurotransmitters as well as for metabolically relevant hormones such as leptin, insulin, ghrelin or glucocorticoids and are further able to send molecules and ions back and forth between neurons and blood vessels. Therefore, astrocytes are important regulators for the type and quantity of nutrients reaching their neighboring neurons [38, 42]. Astrocytes and neurons can directly interact via small finger-like processes to influence synaptic transmission and plasticity. Another important function of astrocytes is the ability to take up the primary neurotransmitter glutamate from the synaptic cleft, which protects neurons from highly toxic glutamate receptor overstimulation. Glutamate in the astrocytes can be converted to glutamine and transported back to neurons, were glutamine can be reconverted to glutamate. Further, astrocytes are the only natural cells in the brain that express pyruvate carboxylase and can therefore effectively replenish glutamate from glucose [41]. Furthermore, astrocytes produce

reactive oxygen species (ROS)-detoxifying enzymes and are important for the defense against oxidative stress [41]. Each astrocyte occupies a specific territory, referred to as the astrocytic domain [43-46]. These domains are dynamic and can change depending on the surrounding microenvironment due to neuronal activity or the physiological status [47].

3.3 Activation of astrocytes

Astrocytes are dynamic cells that transform into an activated state in response to brain injury, pathophysiological conditions, or HFD feeding [48, 49]. The activation of astrocytes is known as astrocytosis, reactive gliosis or astrogliosis, and is often found in conjunction with the activation of microglia and an increased expression of cytokines [50, 51]. Morphologically, astrocytosis is characterized by hypertrophy of the soma and cellular processes (figure 3). Mechanistically, astrocytosis involves the up-regulation of intermediate filaments such as GFAP and vimentin as well as extracellular matrix molecules, growth factors, inflammatory cytokines and oxidative stress markers [52]. Depending on the cellular and environmental context, the induction of astrocytosis is governed by various cellular signaling pathways and linked with a number of downstream processes ranging from gene expression changes to progressive cellular hypertrophy or proliferation and scar formation [49]. In consequence, astrocytosis can be linked with both a gain or loss of astrocytic function that, dependent on the cellular or physiological context, may exert beneficial or detrimental effects on surrounding neurons or cells.

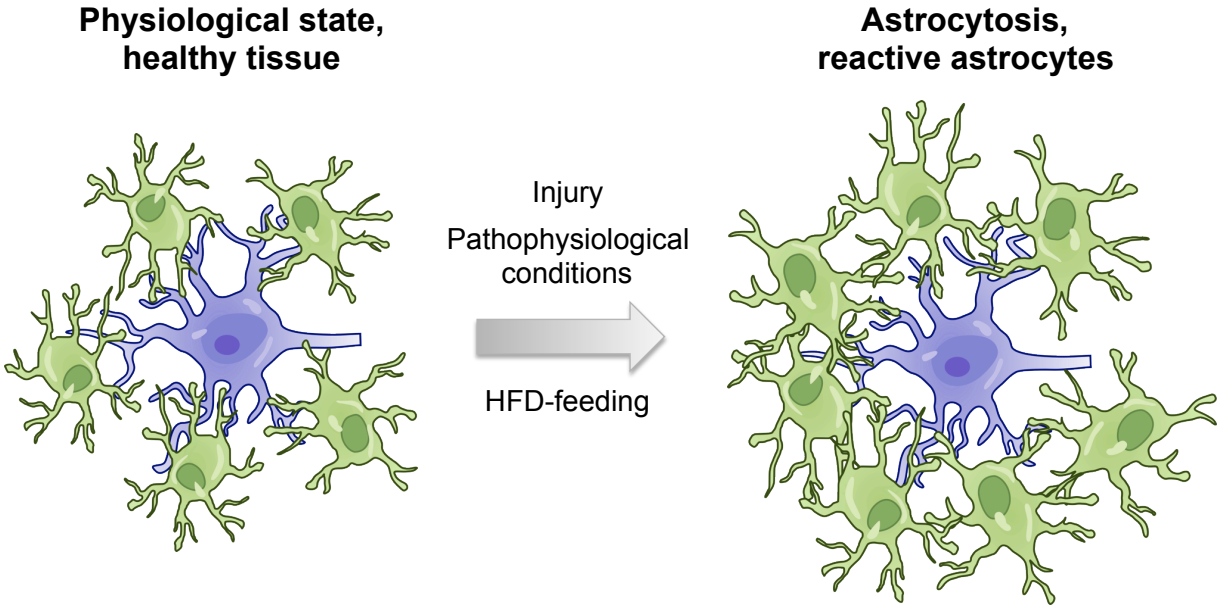

Figure 3. Activation of astrocytes induces changes in morphology and number
Astrocytosis is induced by injury, pathophysiological conditions or high fat diet (HFD)-feeding and is morphologically characterized by thickening of the soma and cellular processes. Astrocytes are shown in green, neurons in blue. Figure adapted from [38].

3.4 Calcineurin as modulator of astrocytosis

Besides morphological, molecular and functional changes in astrocytes, astrocytosis also induces alterations in Ca^{2+} homeostasis. Calcineurin is a calcium-sensitive serine-threonine phosphatase (gene name: protein phosphatase 3, Ppp3), that consists of 2 subunits, a 61 kD calmodulin-binding catalytic subunit A (Ppp3c) and a 19 kD Ca^{2+}-binding regulatory subunit B (Ppp3r) [53]. The catalytic subunit can be encoded by three genes: Protein phosphatase 3 catalytic subunit alpha (Ppp3ca), protein phosphatase 3 catalytic subunit beta (Ppp3cb) or protein phosphatase 3 catalytic subunit gamma (Ppp3cc). The regulatory subunit B is encoded by the genes protein phosphatase 3 regulatory subunit B, alpha (Ppp3r1) and protein phosphatase 3 regulatory subunit B, beta (Ppp3r2).

Several reports link alterations of calcineurin with astrocytosis development. Indeed, calcineurin overexpression was sufficient to trigger pro-inflammatory astrocytosis in rat hippocampal cultured astrocytes and intense calcineurin staining was observed in activated hippocampal astrocytes in murine models of aging and Alzheimers disease [54]. Another study pointed out that calcineurin is a crucial part of an intracellular machinery that determines the activation of pro-inflammatory versus anti-Inflammatory signals in activated astrocytes [55]. Recently, we showed that mice with a global knockout of Ppp3cb were protected from diet-induced obesity [56]. However, the role of calcineurin in the CNS or specifically in astrocytes in the context of an obesogenic environment with chronic HFD exposure remains unclear.

4 Glutathione peroxidase 7 as novel regulator of metabolic homeostasis

4.1 Glutathione peroxidases

Mammalian glutathione peroxidase (GPx) family members GPx1, GPx2, GPx3, GPx4, GPx5, GPx6, GPx7 and GPx8 vary in their enzymatic function, their tissue expression patterns and their localization within the cell. Their enzymatic function is largely determined by either a selenocystein in their catalytic center, which classifies mammalian GPx1 to 4 and human GPx6 as selenoproteins (SecGPx), or by a cysteine (Cys) residue in GPx5 and mouse/rat GPx6 to 8 (CysGPx) [57].

4.1.1 Mechanism and localization

The first identified glutathione peroxidases were the selenocysteine (Sec) containing glutathione peroxidases 1 to 4. They catalyze the “classical” glutathione peroxidase reduction of hydrogen peroxide (H_2O_2) or organic hyroperoxides to water or the corresponding alcohols. Two molecules of glutathione (GSH) are used as substrate and are typically

converted to glutathione disulfide (GSSG) [57-60]. Notably, GSH is not used as a reductant by all GPx and is not strictly conserved in SecGPx [57]. Glutathione peroxidases containing cysteine as catalytic center (CysGPx) typically use thioredoxin as a substrate and are referred to as thioredoxin peroxidases [61]. In CysGPx the thiol moiety (-SH) of the cysteine residues is oxidized. As a consequence either reversible disulfide bonds, including intramolecular disulfide bonds (R-S-S-R) and sulphenyl moiety (R-SOH) or irreversible sulphinic ($R\text{-}SO_2H$) and sulphonic ($R\text{-}SO_3H$) acids are formed [61-65]. The N-terminal active cysteine oxidized by the peroxide is called peroxidatic Cys (C_P). Within the cysteine block, another cysteine termed resolving cysteine (C_R) forms an intramolecular disulfide bond with C_P, thereby enhancing its catalytic activity [61, 66, 67]. Mainly thioredoxin reduces the C_P-C_R disulfide bond and is therefore transformed in the oxidized form [57, 61].

Glutathione peroxidases are localized in various tissues. GPx1 is ubiquitously expressed, GPx2 can mostly be found in the gastrointestinal system including the epithelium of the esophagus and in humans high GPx2 expression is detected in the liver, whereas GPx3 is present in the plasma [57]. GPx4 is ubiquitously expressed, but highest expression levels can be found in male germ cells [57, 68]. GPx5 is present in the caput and cauda epididymides lumen [69] and GPx6 shows its highest expression in embryos and in the olfactory epithelium [70]. GPx7 and GPx8 are widely expressed at low transcriptional levels [71]. Glutathione peroxidases are also detected in various cellular compartments. GPx1 is located ubiquitously in the cytosol and mitochondria [57], GPx2 is found in the cytosol [72, 73], GPx4 is, dependent on the isoform, either expressed in the cytosol, mitochondria or in the nucleus of sperm [57], GPx5 is secreted as well as membrane associated [69]. The isoenzymes of GPx6 vary in their cellular localization [74]. GPx7 is located in the lumen of the ER and GPx8 sits in the membrane of the ER [57, 71]. GPx1, GPx2, GPx3, GPx5 and GPx6 form homotetramers while GPx4, GPx7 and GPx8 are monomers [57, 59].

4.1.2 Glutathione peroxidase 7

4.1.2.1 Function and target proteins

Mammalian GPx7, also known as non-selenocysteine containing phospholipid hydroperoxide glutathione peroxidase (NPGPx) [61, 75], has a size of 21 kilo Dalton (kDa) [61] and is 191 amino acids in length [71]. GPx7 was identified as an ER-residing protein [71] with an ER-signaling peptide at the N-terminus and an atypical KDEL motif (amino acid sequence: Lysine, aspartic acid, glutamic acid, leucine) at the C-terminus, which functions as an ER-retrieval signal [61, 76]. In rare cases, cleavage of the N-terminus signal allows the translocation of GPx7 from the ER to the Golgi along the secretory pathway [61, 77]. GPx7 is wildly expressed but at low transcriptional levels [71]. In 2004, Utomo and colleagues

assessed GPx7 messenger ribonucleic acid (mRNA) and protein levels and showed GPx7 expression in testis, lung, kidney, adipose tissue, and mammary gland. GPx7 mRNA and protein levels were not detected in the liver [75]. Further, highest GPx7 expression was found in gonadal fat and inguinal fat, followed by BAT, lung, heart, muscle, brain, kidney, liver spleen and small intestine [78].

The C_P in GPx7 is Cys57 and is located in the NVASxC(U)G reactive (seleno) cysteine-containing motive. However, the classical C_R is typically localized within the cysteine block and does not exist in GPx7. Another cysteine residue of importance is Cys86, which is localized in the highly conserved FPCNQF motif, where it forms an intramolecular disulfide bridge with Cys57. Notably, thioredoxin peroxidase activity is not involved in disulfide bond formation in GPx7, and GPx7 is not considered a classical CysGPx [61, 77]. Rather, through interaction and the oxidization of various substrates GPx7 was shown to detoxify reactive oxygen species and to simultaneously support protein re-folding.

GPx7 displayed interaction with endoplasmic reticulum oxidoreductase 1 alpha (ERO1α), protein disulfide isomerase (PDI), glucose-regulated protein, 78 kDa (GRP78), cytoplasmic polyadenylation element binding protein 2 (CPEB2) and 5'-3' exoribonuclease 2 (XRN2) via disulfide bonding. In 2011, Nguyen and colleagues identified GPx7 as a protein disulfide isomerase [71]. Furthermore, in 2013 Bosello-Travain and co-workers described PDI and GSH as alternative substrates for GPx7 [77]. *In vitro* GPx7 enables the efficient oxidative refolding of a reduced denatured protein when in addition to GPx7 PDI and peroxide were added to a folding protein. GPx7 was shown to interact with ERO1α and to increase oxygen consumption by ERO1α [71]. The complete mechanism of the ERO1α/PDI/GPx7 triad was described by Wang and co-workers in 2014. H_2O_2 produced by ERO1α oxidizes Cys57 of GPx7 to sulfenic acid. Oxidized Cys57 forms an intra-molecular disulfide bond with Cys86 of GPx7. PDI is oxidized by the sulfenic acid form and by the disulfide form of GPx7. The oxidized PDI transfers disulfides into substrates for oxidative folding. The harmful H_2O_2 is converted into water (H_2O) and oxygen (O_2) within this reaction [62]. Recombinant GPx7 oxidizes PDI at a much faster rate than GSH and competition between GSH and PDI takes place at physiological conditions [62, 79]. The rate of oxidized PDI seems to be limited by GSH. In contrast to the above listed publications, Maiorino and colleagues postulate that the Cys57 of GPx7 is the only cysteine of the glutathione peroxidase being involved in the reduction of H_2O_2 and oxidization of PDI. Cys86 rather is catalytically inactive and functions as a stabilizer of the oxidized GPx7 in the absence of the substrate [79].

GPx7 is also able to bind to GRP78, also known as BIP. Due to the binding, protein refolding is facilitated. The intra-molecular disulfide bond that is initially formed between Cys57 and Cys86 in GPx7 is transferred, connecting Cys86 of GPx7 with Cys41/Cys420 of GRP78.

Binding of GPx7 to GRP78 in stressed cells was shown to increase GRP78 chaperone activity and to attenuate stress-induced protein misfolding (figure 4) [80].

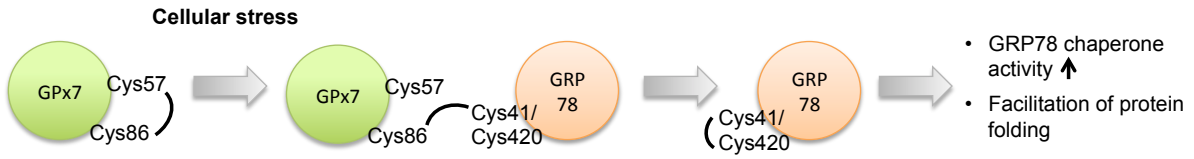

Figure 4. Binding of GPx7 to GRP78 in stressed cells
Cellular stress induces binding of GPx7 to GRP78, followed by an increase of GRP78 chaperone activity and a facilitation of protein folding. Figure adapted from [80].

GPx7 can furthermore bind to CPEB2 via the formation of a covalent bond between Cys57 of GPx7 and Cys157 of CPEB2. This binding leads to an enhancement in the binding activity of CPEB2 to the hypoxia inducible factor 1 alpha subunit (HIF1α) RNA and decreases HIF1α translation [81]. HIF1α activates the transcription of genes important for angiogenesis, metabolism and cell survival, as a response to hypoxia or various oxidative stressors [81]. Exposure to excessive non-target siRNA (NT-siRNA) leads to the increase in GPx7 expression and depletion of GPx7 leads to accumulation of NT-siRNA and apoptosis. During NT-siRNA stress, binding of GPx7 to the exoribonuclease XRN2 was displayed and shown to facilitate NT-siRNA removal [82].

4.1.2.2 Importance of GPx7 in adipose tissue, pancreatic islets and the brain

In adipose tissue single nucleotide polymorphisms (SNPs) in methylation quantitative trait loci (mQTLs) were associated with the expression of GPx7 [83]. In a genome wide mQTL analysis in human pancreatic islets, GPx7 was identified, amongst other genes, as a genetic locus that interacts with the epigenome. Further it was shown in a functional analysis, that GPx7 directly affects key biological processes such as proliferation and apoptosis in pancreatic β-cells [84].

The regulation of GPx7 expression in the brain is to date published in three articles. Overexpression of GPx7 was shown in the CA1 hippocampal area after injury [85]. Down-regulation of GPx7 was detected in the ventral tegmental area as well as in the nucleus accumbens after chronic treatment of human immunodeficiency virus (HIV)-1 transgenic mice with nicotine [86]. In mice undergoing binge-drinking-like alcohol exposure, GPx7 expression was decreased in the frontal cortex, hippocampus, striatum and cerebellum [87]. Potential functions of GPx7 in the hypothalamus as center for glucose and energy homeostasis have not been studied to date.

4.1.2.3 Impact of GPx7 on cancer, metabolic and systemic diseases

A differential regulation of GPx7 was reported for various types of cancer, and GPx7 was postulated as potential tumor suppressor gene [88]. Accumulation of misfolded proteins due to GPx7 removal was shown to lead to systemic oxidative stress, a shortened live span and increased carcinogenesis [80]. During Barret's carcinogenesis GPx7 mRNA levels were shown to be down-regulated, CpG islands were detected around transcription start sites [89] and location-specific promoter desoxyribonucleic acid (DNA) methylation was inversely correlated with mRNA levels of GPx7 [88, 89]. Up-regulated inflammatory markers were shown to be down-regulated after reconstitution of GPx7 in esophageal cells and the promotion of tumor necrosis factor (TNF)-α induced NF-κB activation was shown to be induced by GPx7 silencing [88] during Barrett's carcinogenesis. Furthermore, reconstitution of GPx7 in esophageal cells led to resistance to H_2O_2 induced oxidative stress and to lower levels of ROS signaling, indicated by reduced phospho-c-jun N-terminal kinase (JNK) and phospho-p38 level and lower levels of apoptosis upon bile acid treatment and normalized phosphorylation of NF-kB. GPx7 reconstitution may thus exert a potential anti-inflammatory and oxidative stress protective function in cancer cells [88]. In hepatocellular carcinoma GPx7 was up-regulated [90, 91] and GPx7 expression increased with cancer progression [91]. GPx7 was furthermore up-regulated in hepatitis C virus related cirrhosis [91]. In lung cancer, GPx7 variations were associated with hazardous effects on overall survival [92] and SNPs in the GPx7 gene were correlated with chemotherapy-induced peripheral neuropathy in diabetes patients suffering from lung cancer [93]. GPx7 presence was very low to none in breast cancer cell lines and in fibroblasts of Brca1-null mice. Nevertheless, overexpression of GPx7 alleviated oxidative stress generated from polyunsaturated fatty acid metabolism [75]. Furthermore, GPx7 was shown to be up-regulated in intestinal ischemia [94, 95].

The involvement of GPx7 in metabolic and systemic diseases was published by Wei and colleagues and Chang and co-workers [78, 80]. Deficiency of GPx7 was shown to lead to obesity in mice and human via the accumulation of ROS. GPx7-deficient mice exhibit a marked increase in fat mass and adipocyte hypertrophy when fed with high fat diet compared to chow-fed mice. GPx7 KO mice further displayed normal fasting blood glucose and food intake levels, but higher fasting insulin blood levels, pointing towards a critical role in glucose homeostasis. SNPs in the GPx7 gene in humans were correlated with a decrease in GPx7 expression in adipose tissue and were related with an increased body mass index (BMI) [78]. Chang and colleagues suggested that GPx7 deficiency promotes pre-adipocytes to differentiate to adipocytes via ROS-dependent dimerization of protein kinase A regulatory subunits and activation of CCAAT/enhancer–binding protein beta (C/EBPβ). In humans, SNPs near the GPx7 gene were associated with adiposity. Specifically, a significant association of the genetic variant rs835337 with BMI was shown in 3 independent cohorts.

People carrying the above mentioned risk allele furthermore exhibited lower GPx7 gene expression in abdominal fat depots and higher plasma levels of the oxidative stress marker malondialdehyde. Two other genetic variants, rs7529595 and rs6588432 were also associated with BMI. In conclusion, GPx7 risk allele carriers might have a higher BMI due to reduced GPx7 expression in adipose tissue [78].

5 Scope of this thesis

This PhD thesis aims to identify novel pathways in the control of glucose and energy homeostasis both in the CNS and in peripheral tissues. Moreover, the thesis aims to assess novel avenues of treatment against obesity and diabetes type 2. Specifically, the first project aims to assess the impact of the natural compound celastrol on body weight in mice, and possible molecular mechanisms involved were investigated. The second project of this thesis aims to explore the impact of calcineurin, a calcium sensitive phosphatase, for the development of high-fat diet-induced hypothalamic astrocytosis and microgliosis. The third project focuses on glutathione peroxidase 7, a putative oxygen-stress sensor and ER-stress modulator, and its influence on glucose- and energy metabolism.

In detail, the current PhD thesis is based on the following three partly independent projects, which are currently in preparation or revision for publication in peer-reviewed journals:

Celastrol-induced weight loss depends on leptin signaling and is independent from UCP1-mediated thermogenesis

A drug that efficiently reduces body weight is in great need. Celastrol was proposed to be a potent and promising weight loss drug candidate for humans. However, to date its exact mechanism of action remains unknown. Identifying celastrol target proteins would be an important step for the further development of celastrol as safe and efficacious drug in humans. The overall objective of this study was to identify celastrol targets and its mechanism of action. The focus of the study was directed towards central action on leptin signaling and downstream anorexigenic pathways. Moreover, the study aimed to delineate effects of celastrol treatment on peripheral organs such as skeletal muscle or adipose tissue.

Calcineurin Aβ deficiency ameliorates HFD-induced hypothalamic astrocytosis in mice

It was investigated whether calcineurin plays an important role in the induction of hypothalamic astrocytosis induced by chronic HFD feeding. Specifically, it was aimed to delineate whether calcineurin ablation can protect from HFD-induced astrocytosis in the arcuate-, ventromedial- and dorsomedial nucleus of the hypothalamus in mice. To elucidate mechanistical underpinnings, it was planed to assess whether results observed *in vivo* can be reproduced *in vitro* by applying calcineurin inhibitor Fk506 to primary cultured astrocytes.

Global and hypothalamic deletion of GPx7 impair glucose and energy homeostasis

The aim of this study was to clarify the potential function of GPx7 in diabetes and obesity. Primarily, the role of GPx7 in the hypothalamus as the center of glucose and energy homeostasis should be evaluated. The hypothesis that GPx7 serves as primary sensor for oxidative stress in hypothalamic neurons, and that the lack of GPx7 in these neuronal populations will lead to systemic changes in glucose and energy homeostasis was tested. Moreover, the aim was to discern effects of hypothalamic GPx7 from effects of GPx7 in the peripheral tissues, namely white and brown fat, liver and muscle. The effect of GPx7 knockout on metabolic parameters like food intake, energy expenditure and locomotor activity was further evaluated (figure 5).

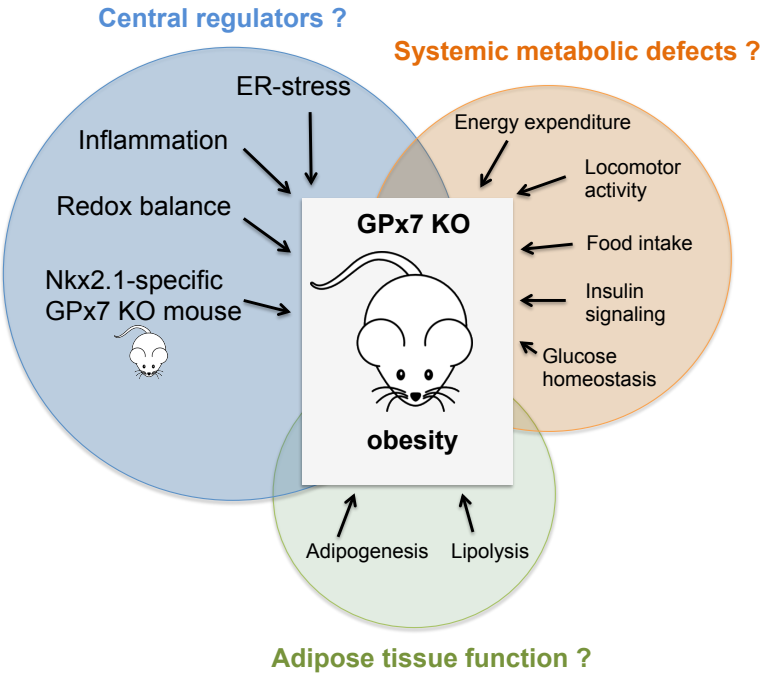

Figure 5. Overview on obesity and diabetes influencing parameters, investigated in global GPx7 KO mice
In a first step it was studied whether the KO of GPx7 leads to an obesogenic and/or diabetic phenotype in mice, by assessing body weight as well as glucose and insulin tolerance on chow and high fat diet in mice. Secondly central and peripheral regulators as well as metabolic parameters influencing this phenotype were observed in detail.

II Material and methods

1 Material

1.1 Mouse strains and diets

Table 1. Mouse strains

Mouse strain	Strain name	Supplier
C57BL/6J	C57BL/6J	Janvier Lab, Saint-Berthevin Cedex, France
UCP1 KO	B6.129-Ucp1tm1Kz/J	Jackson Laboratory, Bar Harbor, ME, USA
Lep^{ob}	B6.Cg-Lepob/J/+	Jackson Laboratory, Bar Harbor, ME, USA
Lep^{db}	BKS.Cg-Dock7m +/+ Leprdb/J	Jackson Laboratory, Bar Harbor, ME, USA
Ppp3cb KO	B6;129S6-Ppp3cbtm1Jmk/J	Jackson Laboratory, Bar Harbor, ME, USA
Global GPx7 KO	GPx7tm1a(EUCOMM) Hmgu	Dr. Marcus Conrad, HMGU, Munich
Conditional GPx7 KO	GPx7tm1c(EUCOMM) Hmgu	Dr. Marcus Conrad, HMGU, Munich
Nkx2.1-Cre	C57BL/6J-Tg(Nkx2-1-cre) 2Sand/J	Jackson Laboratory, Bar Harbor, ME, USA

Table 2. Mouse diets

Diet	Reference	Supplier
Regular rodent chow diet	1314	Altromin Spezialfutter GmbH & Co. KG, Lage, Germany
High-fat diet, 45% kilocalories (kcal) from fat	D12451	Research diets Inc., New Brunswick, NJ, USA
High-fat diet, 58% kcal from fat	D12331	Research diets Inc., New Brunswick, NJ, USA
High-fat diet, 40% kcal from butter fat	D03082706	Research diets Inc., New Brunswick, NJ, USA

UCP1 knockout mice were kindly provided by Dr. Müller and Dr. Clemmensen, Molecular Pharmacology Group, Institute for Diabetes and Obesity (IDO), Helmholtz-Zentrum München. Heterozygous Lep^{ob} mice purchased from Jackson were bred in our own mouse facility to generate homozygous Lep^{ob} mice. All studies performed for the celastrol part of the thesis were conducted in male mice. HFD, that was fed to mice within the celastrol project contained 58% calories from fat (table 2). Ppp3cb wildtype and knockout [96, 97] mice were generated as described previously [56]. Sudies in Ppp3cb knockout and corresponding wildtype animals were performed in male mice. Ppp3cb mice were exposed to high fat diet containing 40% of calories from butter fat (table 2) for 16 weeks. GPx7 global knockout first and wildtype control mice on a C57BL/6J genetic background (strain name: table 1) were a gift from Marcus Conrad's lab, Institute for Developmental Genetics, Helmholtz-Zentrum München. Colonies were expanded in our own mouse facilities, to obtain enough wildtype

and knockout mice to perform the studies. For the creation of the knockout of GPx7 in Nkx2.1 expressing cells, the Cre-lox system was used. The conditional GPx7 knockout mouse (strain name: table 1), in which the GPx7 gene is flanked from two locus of X-over P1 (loxP) sides, was also kindly provided by Marcus Conrad's lab, Institute for Developmental Genetics, Helmoltz-Zentrum München. Conditional GPx7 knockout mouse colonies were expanded in our own mouse facilities and bred with Nkx2.1-Cre (strain name: table 1) mice. The Nkx2.1-Cre mouse expresses the Cre-recombinase under the control of the Nkx2.1 promoter/enhancer. Stock colonies are maintained at the IDO. Studies in global and Nkx2.1-Cre specific GPx7 KO mice were performed in male and female mice. HFD that was fed to mice within the GPx7 project contained 45% calories from fat (table 2).

1.2 Genotyping

Primers for genotyping were purchased from Sigma-Aldrich Co. LLC., St. Louis, MO, USA and had the following sequences and resulted in the following product sizes:

Table 3. Genotyping primers and product sizes, WT polymerase chain reaction (PCR) for the global GPx7 KO mouse

Primer	Primer Sequence	Product Size
Primer 1	ACTTTCTCACCCTAGCACTTTCCCGA	163 base pairs (bp)
Primer 2	CTTGATCAGCCTTCTCCAGGTGTGT	

Table 4. Genotyping primers and product sizes, KO PCR for the global GPx7 KO mouse

Primer	Primer Sequence	Product Size
Primer 1	ACTTTCTCACCCTAGCACTTTCCCGA	184 bp
Primer 3	AAGAGACTCCCAGTCGCCCATAACTT	

Table 5. Genotyping primers and product sizes for the tissue specific GPx7 KO mouse

Primer	Primer Sequence	WT Product Size	KO Product Size
Primer 1	TGCCTCTCTGTGAATGTGCTATGT	248 bp	350 bp
Primer 2	ACTCCTTCACACAGGCAAGAATACCAT		

Table 6. Genotyping primers and product sizes for the Cre PCR

Primer	Primer Sequence	Product Size
Primer 1 (transgene forward (fwd))	GCGGTCTGGCAGTAAAAACTATC	100 bp
Primer 2 (transgene reverse (rev))	GTGAAACAGCATTGCTGTCACTT	
Primer 3 (positive control fwd)	CTAGGCCACAGAATTGAAAGATCT	324 bp
Primer 4 (positive control rev)	GTAGGTGGAAATTCTAGCATCATCC	

Table 7. Reagents for genotyping

Reagent	Supplier
5x Green buffer (GoTaq® flexi)	Promega Corporation, Madison, WI, USA
Betaine	Sigma-Aldrich Co. LLC., St. Louis, MO, USA
Deoxynucleotides (dNTPs)	Life technologies/Thermo Fisher Scientific Inc., Waltham, MA, USA
Magnesium chloride ($MgCl_2$;25 mM)	Promega Corporation, Madison, WI, USA
Polymerase (GoTaq® flexi; 5 U/µl)	Promega Corporation, Madison, WI, USA

1.3 Primary cultures

1.3.1 Primary glia cells

Primary hypothalamic astrocytes were isolated from C57BL/6J mice that were originally obtained from Janvier Lab, Saint-Berthevin Cedex, France, and were bred in our own facilities.

Table 8. Cell culture products primary glia cells

Product	Supplier
Fetal bovine serum (FBS)	GibcoTM/Life technologies/Thermo Fisher Scientific Inc., Waltham, MA, USA
Fk506 (Tacrolimus), #SEL-S5003	Selleck Chemicals Co. Ltd., Houston, TX, USA
Minimum essential medium (MEM), #11095080	GibcoTM/Life technologies/Thermo Fisher Scientific Inc., Waltham, MA, USA
Phosphate buffered saline (PBS)	GibcoTM/Life technologies/Thermo Fisher Scientific Inc., Waltham, MA, USA
Poly-L-lysine hydrobromide	Sigma-Aldrich Co. LLC., St. Louis, MO, USA
Trypsin-Ethylenediaminetetraacetic acid (EDTA) (0.05%), phenol red	GibcoTM/Life technologies/Thermo Fisher Scientific Inc., Waltham, MA, USA

Obese serum was obtained form blood of obese mice with a body weight higher than 45 g by centrifugation of blood at 2500 x g for 15 min at 4°C.

1.3.2 Primary adipocytes

Primary white and brown adipocytes were gained out of GPx7 global KO and C57BL/6J control mice from the GPx7 global KO breeding (strain name: table 1).

Table 9. Cell culture products primary adipocytes

Product	Supplier
Dulbecco's modified eagle medium (DMEM)/F12 + glutaMAX™	GibcoTM/Life technologies/Thermo Fisher Scientific Inc., Waltham, MA, USA
FBS	GibcoTM/Life technologies/Thermo Fisher Scientific Inc., Waltham, MA, USA
PBS	GibcoTM/Life technologies/Thermo Fisher Scientific Inc., Waltham, MA, USA

Penicillin-Streptomycin (10,000 U/ml)	GibcoTM/Life technologies/Thermo Fisher Scientific Inc., Waltham, MA, USA
Trypsin-EDTA (0.05%), phenol red	GibcoTM/Life technologies/Thermo Fisher Scientific Inc., Waltham, MA, USA

1.4 Cell survival assays

Table 10. Cell survival assays

Product	Supplier
Alamar Assay	Life technologies/Thermo Fisher Scientific Inc., Waltham, MA, USA
Isopropanol	Carl Roth GmbH + Co. KG, Karlsruhe, Germany
MTT (3-(4,5-Dimethylthiazol-2-yl)-2,5-diphenyltetrazolium bromide)	Sigma-Aldrich Co. LLC., St. Louis, MO, USA
Triton X 100	Sigma-Aldrich Co. LLC., St. Louis, MO, USA

1.5 Chemicals

Table 11. Chemicals

Chemical	Supplier
2-Deoxy-glucose	Sigma-Aldrich Co. LLC., St. Louis, MO, USA
2,4-Dinitrophenol	Sigma-Aldrich Co. LLC., St. Louis, MO, USA
3-Isobutyl-1-methylxanthine (IBMX)	Biomol GmbH, Hamburg, Germany
Albumin bovine serum, protease free	VWR International LLC., Randor, PA, USA
Antimycin A	Sigma-Aldrich Co. LLC., St. Louis, MO, USA
BSA lyophilized powder, essentially fatty acid free	Sigma-Aldrich Co. LLC., St. Louis, MO, USA
Calcium chloride ($CaCl_2$)	Sigma-Aldrich Co. LLC., St. Louis, MO, USA
Celastrol (#34157-83-0)	BOC Science, Shirlex, NY, USA
Chlorophorm	VWR International LLC., Randor, PA, USA
Collagenase type II and IV	Life technologies/Thermo Fisher Scientific Inc., Waltham, MA, USA
Dexamethasone	Sigma-Aldrich Co. LLC., St. Louis, MO, USA
Disodium hydrogen phosphate (Na_2HPO_4)	Sigma-Aldrich Co. LLC., St. Louis, MO, USA
Dispase II	Sigma-Aldrich Co. LLC., St. Louis, MO, USA
Dithiothreitol (DTT)	Sigma-Aldrich Co. LLC., St. Louis, MO, USA
ECL substrate	Bio-Rad Laboratories Inc., Hercules, CA, USA
Ethanol, absolute	VWR International LLC., Randor, PA, USA
Free glycerol reagent	Sigma-Aldrich Co. LLC., St. Louis, MO, USA
Gelatine	Sigma-Aldrich Co. LLC., St. Louis, MO, USA

Glucose	Carl Roth GmbH + Co. KG, Karlsruhe, Germany
Glycerol standard solution	Sigma-Aldrich Co. LLC., St. Louis, MO, USA
Hydrogen chloride (HCl)	Carl Roth GmbH + Co. KG, Karlsruhe, Germany
Indomethacine	Santa Cruz Biotechnology Inc., Dallas, TX, USA
Insulin (Actrapid)	Novo Nordisk A/S, Bagsvaerd, Denmark
Insulin solution, human	Sigma-Aldrich Co. LLC., St. Louis, MO, USA
Isopropanol	Carl Roth GmbH + Co. KG, Karlsruhe, Germany
Isoproterenol	Sigma-Aldrich Co. LLC., St. Louis, MO, USA
Non-esterified free fatty acids (NEFA) standard	Wako Chemicals GmbH, Neuss, Deutschland
Norepinephrine	Sigma-Aldrich Co. LLC., St. Louis, MO, USA
NuPAGE, LDS sample buffer (4x)	Noves/Life techonologies/Thermo Fisher Scientific Inc., Waltham, MA, USA
Oil Red O	Sigma-Aldrich Co. LLC., St. Louis, MO, USA
Oligomycine	Sigma-Aldrich Co. LLC., St. Louis, MO, USA
Paraformaldehyde (PFA)	Sigma-Aldrich Co. LLC., St. Louis, MO, USA
Phenyl-methane-sulfonyl fluorid (PMSF)	Carl Roth GmbH + Co. KG, Karlsruhe, Germany
Phosphatase inhibitor cocktail	Thermo Fisher Scientific Inc., Waltham, MA, USA
Ponceau S solution	Sigma-Aldrich Co. LLC., St. Louis, MO, USA
Pyruvate	Sigma-Aldrich Co. LLC., St. Louis, MO, USA
Qiazol	Qiagen N.V., Hilden, Germany
Radioimmunoprecipitation assay buffer (Ripa) buffer	Sigma-Aldrich Co. LLC., St. Louis, MO, USA
Rosiglitazone	Santa Cruz Biotechnology Inc., Dallas, TX, USA
Rotenone	Sigma-Aldrich Co. LLC., St. Louis, MO, USA
Sodium chloride (NaCl, 0.9%)	SteriPharm Pharmazeutische Produkte GmbH & Co. KG, Berlin, Germany
Sodium chloride (NaCl; powder)	Carl Roth GmbH + Co. KG, Karlsruhe, Germany
Sodium phosphate monobasic (NaH2PO4)	Sigma-Aldrich Co. LLC., St. Louis, MO, USA
Sucrose	Carl Roth GmbH + Co. KG, Karlsruhe, Germany
Triiodthyronin (T3)	Sigma-Aldrich Co. LLC., St. Louis, MO, USA
Tris(hydroxymethyl)aminomethane (Tris)	Carl Roth GmbH + Co. KG, Karlsruhe, Germany
Tween® 20	Sigma-Aldrich Co. LLC., St. Louis, MO, USA

1.6 Commercially available kits

Table 12. Kits

Kits	Supplier
Genomic DNA extraction kit, FavorPrep	Favorgene Corp., Ping-Tung, Taiwan
Mouse ultra sensitive insulin enzyme-linked immunosorbent assay (ELISA) kit	Alpco Diagnostics, Salem, NH, USA
NucleoSpin® RNA extraction kit	Macherey-Nagel GmbH + Co. KG, Düren, Germany
QuantiTect reverse transcription kit	Qiagen N.V., Hilden, Germany

1.7 Antibodies for western blotting

Chemicals used for protein extraction and western blotting are listed within section 1.5 Chemicals. Gels and nitrocellulose membranes were purchased from Biorad, Hercules, CA, USA. All Blue prestained protein standard was purchased from Bio-Rad Laboratories Inc., Hercules, CA, USA.

Table 13. Primary antibodies for western blot

Antibody	Reference	Supplier
Anti-GAPDH	#sc-166545	Santa Cruz Biotechnology, Inc., Dallas, TX, USA
Anti-GFAP	#3893	Sigma-Aldrich Co. LLC., St. Louis, MO, USA
Anti-GPX7	#GTX108578-100	GeneTex, Inc., Irvine, CA, USA
Anti-HSL	#4107	Cell Signaling Technology, Inc., Danver, MA, USA
Anti-NFATc4	#sc-13036	Santa Cruz Biotechnology, Inc., Dallas, TX, USA
Anti-pathScan multiplex western cocktail	#5301	Cell Signaling Technology, Inc., Danver, MA, USA
Anti-phospho-HSL (Ser660)	#4126	Cell Signaling Technology, Inc., Danver, MA, USA
Anti-PPARγ	#2435	Cell Signaling Technology, Inc., Danver, MA, USA
Anti-pSTAT3^{T705}	#9145	Cell Signaling Technology, Inc., Danver, MA, USA
Anti-STAT3	#9139	Cell Signaling Technology, Inc., Danver, MA, USA
Anti-STAT5	#9363	Cell Signaling Technology, Inc., Danver, MA, USA
Anti-UCP1	#14670	Cell Signaling Technology, Inc., Danver, MA, USA
Anti-Vimentin	#V5255	Sigma-Aldrich Co. LLC., St. Louis, MO, USA
Anti-β-Actin	#4970	Cell Signaling Technology, Inc., Danver, MA, USA

Table 14. Secondary antibodies for western blot

Antibody	Reference	Supplier
Anti-mouse immunoglobulin G-horseradish peroxidase (IgG-HRP; donkey)	#sc-2318	Santa Cruz Biotechnology, Inc., Dallas, TX, USA
Anti-rabbit IgG-HRP (goat)	#sc-2004	Santa Cruz Biotechnology, Inc., Dallas, TX, USA

1.8 Antibodies and reagents for immunohistochemical stainings

Table 15. Primary antibodies for immunohistochemical stainings

Antibody	Reference	Supplier
Anti-GFAP	#Z0334	Dako/Agilent Technologies Inc., Santa Clara, CA, USA
Anti-IBA1	#234 003	Synaptic Systems GmbH, Göttingen, Germany
Anti-POMC	#H-029-30	Phoenix Pharmaceuticals Inc., Burlingame, CA, USA
Anti-pSTAT3	#sc-7993	Santa Cruz Biotechnology, Inc., Dallas, TX, USA

Table 16. Secondary antibodies for immunohistochemical stainings

Antibody	Reference	Supplier
Alexa fluor 488 goat anti-rabbit IgG (H+L)	#A11008	Life technologies/Thermo Fisher Scientific Inc., Waltham, MA, USA
Alexa fluor 555 conjugate, Streptavidin	#S32355	Life technologies/Thermo Fisher Scientific Inc., Waltham, MA, USA
Anti-rabbit biotinylated, IgG (H+L)	#BA-1000	Vector Laboratories Inc., Peterborough, UK
Biotin-SP-conjugated affiniPure fab fragment goat anti mouse IgG (H+L)	#115-067-033	Jackson Immunoresearch Inc, West Grove, PA, USA

Table 17. Material for 3,3'-Diaminobenzidine (DAB) stainings

Product	Supplier
ABC HRP Kit	Vector Laboratories Inc., Burlingame, CA, USA
DAB substrate	Sigma-Aldrich Co. LLC., St. Louis, MO, USA
H_2O_2	Carl Roth GmbH + Co. KG, Karlsruhe, Germany
Xylene	Sigma-Aldrich Co. LLC., St. Louis, MO, USA

For immunohistochemical stainings mounting media containing DAPI (Vector Laboratories Inc., Burlingame, CA, USA) or no DAPI (Permount, Fisher Scientific/Thermo Fisher Scientific Inc., Waltham, MA, USA) were used.

1.9 Primers, TaqMan assays and reagents for qPCR

For quantitative analysis of mRNA levels, RNA was transcribed to complementary DNA (cDNA) and quantitative polymerase chain reactions (qPCRs) using primers (Sigma-Aldrich, Co. LLC., St. Louis, MO, USA; table 18) or TaqMan probs (Applied Biosystems/Thermo Fisher Scientific, Inc., Waltham, MA, USA; table 19, table 20) were performed. Power

SybrGreen master mix or TaqMan universal master mix II no UNG (both: Applied biosystems/Thermo Fisher Scientific, Inc., Waltham, MA, USA) were used respectively.

Table 18. Primers for SybrGreen qPCR

Gene	Forward primer	Reverse primer
Mouse A2	ATGGGGCCACACGGGAACGA	GTGACGTGGTCTGGCGC
Mouse A3	AAGCCCTCAGCATCCCAAGCTA	CCTGGCAGAACCTGAGGCAACC
Mouse Agrp	GGCCTCAAGAAGACAACTGC	GCAAAAGGCATTGAAGAAGC
Mouse Atf4	GGGTTCTGTCTTCCACTCCA	AAGCAGCAGAGTCAGGCTTTC
Mouse Atgl	CACAGCGCTGGTCACTGGGG	CCGGGCCTCCTTGGACACCT
Mouse Bip	TTCAGCCAATTATCAGCAAACTCT	TTTTCTGATGTATCCTCTTCACCAGT
Mouse Cart	CGAGAAGAAGTACGGCCAAG	GGAATATGGGAACCGAAGGT
Mouse Cebpa	CAAGAACAGCAACGAGTACCG	GTCACTGGTCAACTCCAGCAC
Mouse Cebpb	GACACGGGACTACGCAACAC	AACCCCGCAGGAACATCTTTA
Mouse Chop	CCACCACACCTGAAAGCAGAA	AGGTGAAAGGCAGGGACTCA
Mouse Cidea	TGACATTCATGGGATTGCAGAC	CGAGCTGGATGTATGAGGGG
Mouse Cox4β	CTGCCCGGAGTCTGGTAATG	CAGTCAACGTAGGGGGTCATC
Mouse Cpeb2	ACACTCTTACCCTTACAGGATCG	ACCTCGTCTTCGCCCATAAC
Mouse Cyt c	AAATCTCCACGGTCTGTTCGG	GGGTATCCTCTCCCCAGGTG
Mouse Erdj4	CTTAGGTGTGCCAAAGTCTGC	GGCATCCGAGAGTGTTTCATA
Mouse Fgf21	GCTGCTGGAGGACGGTTACA	CACAGGTCCCCAGGATGTTG
Mouse Foxo1	CGCCTCCTACTACTCTGAGC	TGTCTGTACTTAGGCGCACA
Mouse Grp78	ATTGGAGGTGGGCAAACCAA	TCGCTGCGCATCATTGAAGT
Mouse Hprt	AAGCTTGCTGGTGAAAAGGA	TTGCGCTCATCTTAGGCTTT
Mouse Hsf1	GCTCTGGACCCATAATCTC	CTCTTGCTTGACACGGAC
Mouse Hsl	CCGTTCCTGCAGACTCTCTC	CCACGCAACTCTGGGTCTAT
Mouse Il-1ß	TACAAGGAGAACCAAGCAACGAC	GATCCACACTCTCCAGCTGCA
Mouse Il-6	GTGGCTAAGGACCAAGACCA	GGTTTGCCGAGTAGACCTCA
Mouse LepR	CGTGGTGAAGCATCGTACTG	GGGCCATGAGAAGGTAAGGT
Mouse Mc3r	TCAAACGCGAAGAAAGTGCA	AGACAACGCACTTACCAGGA
Mouse Mc4r	GGACTCTGAAAAGACCCCGA	TGCCTGTAGAAGTTGGGAGG
Mouse Mcad	ATGACGGAGCAGCCAATGAT	TCGTCACCCTTCTTCTCTGCTT
Mouse Nf-κb	TGCCTGGCCAGTGTAGCAGTCTT	CAAAGTCACCAAGTGCTCCACGAT
Mouse Npy	TCGCTCTATCTCTGCTCGTG	AATCAGTGTCTCAGGGCTGG
Mouse Pgc-1α	AGCCGTGACCACTGACAACGAG	GCTGCATGGTTCTGAGTGCTAAG
Mouse Plin	GTCTGCTGCACGTGGAGAGTAAGGA	ACCACAGGCAGCTGCAGAACTC
Mouse Pomc	CATTAGGCTTGGAGCAGGTC	TCTTGATGATGGCGTTCTTG
Mouse Pppary	CCAGAGCATGGTGCCTTCGCT	CAGCAACCATTGGGTCAG
Mouse Prdm16	CCACCAGCGAGGACTTCAC	GGAGGACTCTCGTAGCTCGAA
Mouse Pref	CAGTACGAATGCTCCTGCAC	AGGGAGAACCATTGATCACG
Mouse Ptp1b	CCGAGATGTCAGCCCTTTTG	CCACACCATCTCCCAGAAGT
Mouse Shp2	GAAACGGTCATTCAGCCACT	GCAGCCAAGGAGTCATCTTC
Mouse Stat3	AATGGAAATTGCCCGGATCG	TCCTGAAGATGCTGCTCCAA

Mouse sXbp1	GGTCTGCTGAGTCCGCAGCAGG	AGGCTTGGTGTATACATGG
Mouse Tcptp	AGAGTGGCCAAGTTTCCAGA	CACACCATGAGCCAGAAATG
Mouse Ucp1	GGCCTCTACGACTCAGTCCA	TAAGCCGGCTGAGATCTTGT
Mouse Xbp1	GAACCAGGAGTTAAGAACACG	AGGCAACAGTGTCAGAGTCC

Table 19. TaqMan assays

Gene abbreviation	Assay ID
Hprt	Mm01545399_m1
Mfn1	Mm00612599_m1
Mfn2	Mm00500120_m1
Socs3	Mm00545913_s1
Ucp1	Mm01244861_m1
Atp2a1	Mm01275320_m1
Atp2a2	Mm01201431_m1
Atp2a3	Mm00443898_m1

Gene abbreviation	Assay ID
Itpr1	Mm01306070_m1
Sln	Mm00481536_m1
Slc8b1	Mm00519262_m1
Plb	Mm00452263_m1
Itpr3	Mm00439907_m1
Il-1ß	Mm00434228_m1
Il-6	Mm00446190_m1
Tnf	Mm00443258_m1

Table 20. TaqMan assays LDA card

Gene abbreviation	Assay ID
Arg1	Mm00475988_m1
Atf3	Mm00476032_m1
Bip	Mm00517691_m1
Calr	Mm00482936_m1
Cat	Mm00437992_m1
Ccl2	Mm99999056_m1
Ccl3	Mm00441259_g1
Ccl5	Mm01302427_m1
Cd68	Mm03047340_m1
Cd8b	Mm00438116_m1
Cebpd	Mm00786711_s1
Chop	Mm00492097_m1
Chuk (IKKα)	Mm00432529_m1
Emr1	Mm00802529_m1
Erdj4	Mm01622956_s1
Fap	Mm00484254_m1
Foxp3	Mm00475162_m1
Gadd45a	Mm00432802_m1

Gene abbreviation	Assay ID
Gpx1	Mm00656767_g1
Gpx4	Mm00515041_m1
Grp94 (Hsp90b1)	Mm00441926_m1
Hif1α	Mm00468869_m1
Hprt	Mm01545399_m1
Il-1β	Mm00434228_m1
Il-6	Mm00446190_m1
IRE1α	Mm00470233_m1
Itgax	Mm00498698_m1
Nf-κb1	Mm00476361_m1
Nfe2l2	Mm00477784_m1
Perk	Mm00438708_m1
Pgc-1α	Mm01208835_m1
Slc25a4	Mm01207393_m1
Sod1	Mm01344233_g1
Sod2	Mm01313000_m1
Tnf	Mm99999068_m1
Xbp1	Mm00457359_m1

2 Methods

2.1 Animal experiments

2.1.1 Animals

Studies in lean and obese C57BL/6J, UCP1 WT and KO, Lep^{ob} WT and KO, Lep^{db} WT and KO mice were performed in male mice. Studies in obese Ppp3cb (calcineurin A beta) WT and KO mice were performed in male mice. Studies in global GPx7 knockout and GPx7;Nkx2.1-Cre mice were performed in male and female mice. Mice were maintained on a 12-h dark-light cycle and had free access to diet and water. Tissues were collected for Immunohistochemical stainings, RNA and protein extraction. All studies were based on power analyses to assure adequate sample sizes, and approved by the State of Bavaria, Germany.

2.1.2 Genotyping

To determine the genotype of mice, ear punches were taken from mice and DNA was extracted with a genomic DNA extraction kit.

Genotyping protocol global GPx7 KO mouse

Three different primers (section II, 1.2 Genotyping, table 3 and 4) were used and KO and WT PCRs were performed separately by combining primer 1 with primer 2 for the WT PCR and primer 1 with primer 3 for the KO PCR. 2 µl genomic DNA was used and mixed with 8.7 µl water, 3.3 µl 5x promega rxn buffer, 1 µl $MgCl_2$, 0.3 µl dNTPs, 0.9 µl of each primer and 0.2 µl polymerase. In a PCR cycler, the samples were run under the following temperature profile: 95°C for 5 min, the following 3 temperature steps were repeated 35 times: 95°C for 30 sec, 63°C for 30 sec, 72°C for 30 sec, followed by a 72°C step for 5 min. Afterwards samples were cooled down to 4°C.

Genotyping Protocol GPx7;Nkx2.1-Cre mouse

For genotyping of the GPx7;Nkx2.1-Cre mouse, two different PCRs were performed: The GPx7 flox PCR, to determine if the GPx7 gene is enclosed by loxP sides and can potentially be cut out, and the Cre PCR to determine expression of the Cre-recombinase. Therefore GPx7;Nkx2.1-Cre KO mice had a KO and no WT product in the GPx7 flox PCR and a Cre transgene product in the Cre PCR. WT control animals had a WT and no KO product in the GPx7 flox PCR and a Cre transgene product in the Cre PCR.

GPx7 flox PCR

For the GPx7 flox PCR, two primers (section II, 1.2 Genotyping, table 5) were used, resulting in different product sizes for the WT and KO product. The PCR product for the KO is larger

compared to the WT product due to inserted loxP sequences (section II, 1.2 Genotyping, table 5). 2 µl of genomic DNA was mixed with 13.9 µl water, 5 µl 5x promega rxn buffer, 0.75 µl $MgCl_2$, 0.5 µl dNTPs, 1.3 µl of each primer and 0.3 µl polymerase. Samples were placed in a PCR Cycler and underwent the following temperature cycles: 95°C for 5 min, the following 3 temperature steps were repeated 35 times: 95°C for 30 sec, 61°C for 30 sec, 72°C for 30 sec, followed by 72°C for 5 min. Samples were cooled down to 4°C afterwards.

Cre PCR

For the detection of Cre-recombinase, four primers (section II, 1.2 Genotyping, table 6) were used. Primer 1 (transgene fwd) and Primer 2 (transgene rev) detected the presence of the Cre-recombinase. Primer 3 (positive control fwd) and primer 4 (positive control rev) served as an internal positive control, showing the presence of DNA. 2 µl of genomic DNA was mixed with 4 µl water, 3 µl 5x promega rxn buffer, 1.3 µl $MgCl_2$, 0.32 µl dNTPs, 0.3 µl of each primer, 3 µl betaine, 0.13 µl polymerase. The following program was run on a PCR cycler: 3 min at 94°C, the following cycles were repeated 36 times: 94°C for 45 sec, 60°C for 45 sec, 72°C for 1 min, followed by 72°C for 2 min. Samples were cooled down to 4°C afterwards.

PCR products of all genotypings were analyzed with a Qiaxel Analysis system (Qiagen N.V., Hilden, Germany).

2.1.3 Body composition and indirect calorimetry

Celastrol project

Fat and lean mass were measured via nuclear magnetic resonance (NMR) technology (EchoMRI, Houston, TX, USA). Energy expenditure, locomotor activity and food intake were analyzed by a combined indirect calorimetry system (TSE System, Bad Homburg, Germany), as described [56]. Mice were acclimatized to the calorimetry system for at least 24 h before data collection for 3 days (d) and 21 h at 23°C. For the assessment of the impact of celastrol on basal metabolic rates and maximum respiration, housing temperatures were changed to 30°C for 17 h. 2.5 h after light onset mice were injected with 0.5 µg/g BW norepinephrine in 0.9% NaCl, and assessed for the maximum increase in energy expenditure observed within 1 h. The basal metabolic rates of celastrol and vehicle-treated mice housed at 30°C were assessed by averaging energy expenditure values from 4.5 to 6.5 h after light onset, a period when mice displayed the lowest daily physical activity.

GPx7 project

In global GPx7 KO and WT control mice, fat and lean mass were measured via NMR technology (EchoMRI, Houston, TX, USA). Energy expenditure, locomotor activity, respiratory exchange ratios and food intake were assessed by a combined indirect calorimetry system (TSE System, Bad Homburg, Germany), as described [56]. Mice were

acclimatized to the calorimetry system for at least 24 h before data collection for 9 d and 5 h at 23°C. Mice were fed with normal rodent chow diet before the TSE study and in the TSE system for 4 d and 6 h. Afterwards diet was switched to HFD (45% kcal from fat; table 2) and mice were monitored for 4 d and 23 h in the TSE system. For the assessment of the impact of GPx7 on maximum respiration, housing temperatures were changed to 30°C the evening before the experiment. The next morning, mice were subsequently injected with 1 µg/g BW norepinephrine in 0.9% NaCl, and assessed for the increase in energy expenditure.

2.1.4 Measurement of fasting blood glucose and HOMA-IR calculations

2.1.4.1 Measurement of fasting blood glucose

Blood glucose in Ppp3cb WT and KO mice was measured after 6 h fasting with a handheld glucometer (Freestyle freedom lite, Abbott Diabetes Care, Alameda, CA, USA).

2.1.4.2 Assessment of blood insulin and HOMA-IR calculations

Insulin content was measured from plasma of global GPx7 KO and WT mice fasted for 6 h, and 5, 15 and 60 min after the oral administration of 2 g glucose/kg BW within the oral glucose-tolerance test (oGTT). A mouse ultrasensitive insulin ELISA was performed with the plasma samples. The homeostatic model assessment-insulin resistance (HOMA-IR) was calculated by first multiplying the fasting blood glucose (mmol/l) with the fasting plasma insulin (mU/l) and by secondly dividing the product by the factor 22.5.

2.1.5 Glucose, insulin, and pyruvate tolerance tests

Celastrol project

Diet induced obese (DIO) WT and UCP1 KO and lean WT and Lep^{ob} mice were treated for 6 d with celastrol (100 µg/kg body weight) or vehicle, a glucose-tolerance test (GTT) was performed on day 7. After 6 h of fasting, 1.5 g glucose/kg body weight was injected intra peritoneal (i.p.) and tail blood glucose was measured using a handheld glucometer (Freestyle freedom Lite, Abbott Diabetes Care, Alameda, CA, USA) before (0 min) and 15, 30, 60 and 120 min after glucose injection.

GPx7 project

WT and GPx7 global KO and GPx7;Nkx2.1-Cre mice were fasted for 6 h before a GTT or a insulin tolerance test (ITT) was performed. WT and GPx7 global KO mice were subjected to over night fasting before the measurement of a pyruvate tolerance test (PTT) was performed. For the i.p. glucose tolerance test global and Nkx2.1-specific GPx7 KO mice were injected with 2 g glucose/kg body weight, except for the GTT in global GPx7 KO mice after 20 weeks of HFD feeding, where 1.5 g glucose/kg body was used, due to high body weight. For the oral glucose tolerance test 2 g glucose/kg body weight were orally applied. To test the insulin

tolerance in global and Nkx2.1-specific GPx7 KO mice 0.5 or 0.75 international units (IU) insulin/kg body weight were administered (i.p.), respectively. Pyruvate tolerance was observed by injecting (i.p.) 0.75 g pyruvate/kg body weight. In any case, tail blood glucose was measured using a handheld glucometer (Freestyle freedom lite, Abbott Diabetes Care, Alameda, CA, USA) before (0 min) and 15, 30, 60 and 120 min after glucose, insulin or pyruvate injection.

2.1.6 Acute insulin challenge

For the assessment of insulin signaling in liver, muscle and epididymal white adipose tissue (eWAT) of global GPx7 knockout and wildtype control mice 5 IU insulin/kg BW was injected (i.p.) in WT and global GPx7 KO mice. Mice were sacrificed 8 min after insulin injection. Tissues were collected and protein was extracted.

2.1.7 Isoproterenol challenge

To assess lipolysis in wildtype and global GPx7 knockout mice, mice were injected with 10 mg isoproterenol/kg BW. On the first study day, all mice were fasted for 1.5 h and were injected with saline. Five days later, after 1.5 h fasting all mice were injected with isoproterenol. Glycerol and NEFAs were measured in serum 10 min after saline or isoproterenol injections. For the assessment of the lipolytic potential in iWAT, eWAT and BAT, mice were sacrificed and organs were collected 20 min after injection of saline or of 10 mg isoproterenol/kg BW. Protein and RNA was extracted out of tissues.

2.1.8 Application of celastrol

The compound celastrol in powder was dissolved in pure Dimethyl sulfoxide (DMSO) and diluted with PBS to a final concentration of 0.02 mg/ml in 1% DMSO for injections. 100 µg/kg BW of celastrol or PBS with 1% DMSO as vehicle was injected in similar volume. DIO and lean mice were injected i.p. and UCP1 WT and KO mice, Lep^{ob} WT and KO mice and Lep^{db} WT and KO mice were injected subcutaneously (s.c.). Daily injections took place 1-2 h before the onset of the dark phase. HFD-fed mice were injected with 100 µg/kg BW celastrol or vehicle 1-2 h before sacrifice. *In vivo* experiments were performed without blinding of the investigators. All studies were based on power analyses to assure adequate sample sizes, and approved by the State of Bavaria, Germany.

2.2 Molecular biology and protein biochemistry

2.2.1 RNA extraction, cDNA synthesis and qPCR

Total RNA was extracted from tissue and equal amounts of RNA were transcribed to cDNA. Gene expression was determined with the SybrGreen or TaqMan technology. Samples were run in 384-well plates with a total reaction volume of 5 µl, containing 2.5 µl master mix, 0.25 µl water, 0.25 µl primer-mix or TaqMan assay and 2 µl diluted cDNA. Samples were run on a Viia7 cycler (Applied Biosystems/Thermo Fisher Scientific, Inc, Waltham, MA, USA). Gene expression was evaluated using the delta-delta cycle threshold (Ct) method and hypoxanthine phosphoribosyltranserase 1 (*Hprt*) was used as housekeeping gene.

2.2.2 Protein extraction and western blotting

RIPA buffer containing protease and phosphatase inhibitor cocktail and 1 mM PMSF was used for protein extraction. Proteins were transferred from the gel to nitrocellulose membranes using a Trans Blot Turbo transfer apparatus (Bio-Rad Laboratories Inc., Hercules, CA, USA). Membranes were incubated with antibodies listed in table 13 and table 14. Membranes were detected on a Li-Cor Odyseey instrument (Li-Cor Bioscience, Lincoln, NE, USA). Densitometric quantifications were performed using internal Li-Cor Odyssey software or ImageJ 1.47v software (https://imagej.nih.gov/ij/docs/guide/user-guide.pdf).

2.2.3 Immunohistochemistry

After perfusion of mice with PBS and a chilled 4% solution of PFA in 0.1 M PBS, brains were extracted and incubated in fixative overnight on a shaker at 4°C. After incubation for 24-48 h with 30% sucrose in 0.1 M tris-buffered saline (TBS) at 4°C, brains were frozen at -20°C, coronally cut in a cryostat into 30 µm sections and stored in a cryoprotectant solution. Stainings were performed with free-floating slices, and were started by applying 2-h blocking.

Celastrol project

Primary anti-phospho-STAT3 (pSTAT3) goat and anti-POMC (table 15) were diluted in blocking buffer and incubated overnight at 4°C. After several washing steps, biotin-SP-conjugated affiniPure fab fragment goat anti-mouse IgG (H+L) (table 16) was added to the slices in TBS for 1 h. After washing, strepavidin-Alexa Fluor 555 conjugate and Alexa Fluor 488 goat anti-rabbit IgG (H+L) antibodies (table 16) were added in TBS for 1 h and washed afterwards several times. Z-stack images were captured by a Leica TCS SP8 microscope (Leica Microsystems GmbH, Wetzlar, Germany). Stack and overlay pictures were created using ImageJ 1.47v software (https://imagej.nih.gov/ij/docs/guide/user-guide.pdf). The ARC was defined in each slice by orienting on DAPI and POMC staining as well as on the Allen brain atlas (http://mouse.brain-map.org/static/atlas). Green and red staining and green-red

co-localizations in the ARC were counted, and pSTAT3 and POMC double-positive cells were normalized to the total number of POMC positive cells in the ARC. Total numbers of pSTAT3 and POMC positive cells were normalized to ARC area.

Calcineurin project

GFAP and IBA1 primary antibodies (table 15) were diluted in blocking buffer and incubated over night at 4°C. Secondary anti-rabbit biotinylated antibody (table 16) was added for one hour at room temperature (RT) after several washing steps in TBS. Brains were incubated in ABC reagent for one hour at RT followed by stainings with diamino-benzdine and H_2O_2. Brain cuts were dehydrated with increasing concentrations of ethanol and were delipidated using xylene. Sections were mounted on glass slides using mounting media. Images were captured by a BZ-9000 microscope (Keyence Corporation Itasca, IL, USA).

For quantification of GFAP or IBA1 positive cells in the ARC, rectangles of equal size (0.0031 cm^2) per picture were quantified for positively stained cells. Moreover, in the respective rectangles, astrocytes were assessed for the number and length of primary projections. The areas of the DMH and VMH were assigned for each picture individually by using the mouse brain atlas (http://mouse.brain-map.org/static/atlas). Positive nuclei in the assigned areas were counted manually and normalized for the surface area. Primary projections of 15 ARC cells/picture, 10 DMH cells/picture and 2-5 VMH cells/picture were counted. The lengths of primary projections in the ARC were measured in 15 cells/picture. A total of 6 animals per group were used and a minimum of 4 technical replicates (brain hemispheres and slices) were analyzed per animal, if not indicated otherwise in the figure legend.

2.2.4 Immunocytochemistry

PFA was washed away from glass cover slips containing primary glia cells with PBS and primary antibody (table 15) was added over night as described for immunohistochemical stainings. Three PBS washing steps were performed and Alexa Fluor 488 secondary antibody (table 16) was added for 1 h, cover slips were washed again with PBS and mounted afterwards. Images were captured by a BZ-9000 microscope (Keyence Corporation Itasca, IL, USA). Total fluorescence intensity was determined with ImageJ 1.47v software (https://imagej.nih.gov/ij/docs/guide/user-guide.pdf).

2.3 Cell culture

2.3.1 Primary glia culture

Hypothalami were extracted from C57BL/6J mice at postnatal day 1 to 4 and triturated in MEM. The suspension was centrifuged and the cell pellet re-suspended in MEM containing

10% FBS. Cells were grown in T175 flasks for up to 14 days and afterwards seeded in 6-well-plates for protein extraction, or 24-well-plates or glass cover slips in 24-well-plates for immunocytochemistry. Before seeding, microglia were partially removed by heavy taping. For immunocytochemistry, 25,000 primary astrocytes were seeded on glass cover slips in a 24-well plate. Glass cover slips were pre-coated with 100 µM poly-L-lysine over night, the day before seeding and poly-L-lysine was washed away with PBS before the experiment. 225,000–350,000 cells were seeded in 6- or 12-well cell-bind-plates. One to three days after seeding, primary astrocytes were serum-fasted for 4 to 5 hours with MEM in the absence of FBS. DMSO or calcineurin inhibitor Fk506 was added in indicated concentrations and 0.5 h later 10% FBS or 10% obese serum was added. 24, 48 or 72 hours later cells were harvested for protein extraction or fixed with 4% PFA for immunocytochemistry.

2.3.2 Isolation and differentiation of primary white and brown preadipocytes

Primary murine (pre-)adipocytes were obtained from subcutaneous white adipose tissue of young (six to eight weeks old) global GPx7 knockout and C57BL/6J control mice. Fat pads were dissected and minced with spring scissors for several minutes in PBS. Minced white adipose tissue was transferred to digestion buffer containing collagenase IV (1 mg/ml), dispase II (3 U/ml) and $CaCl_2$ (0.01 mM) in PBS. Minced brown adipose tissue was transferred to digestion buffer containing collagenase II (1 mg/ml), dispase II (3 U/ml) and $CaCl_2$ (0.01 mM) in PBS. Tissues were digested by shaking at 37°C for 40-50 min. The homogenate was filtered through a 100 µm strainer. The strainer was cleared with growth media consisting of DMEM/F12 + glutaMAX™ with 10% FBS and 1% penicillin-streptomycin and was centrifuged at 500 x g for 10 min at room temperature. After removal of the supernatant the cells were re-suspended in growth media and the homogenate was filtered through a 70 µm strainer. The filter was washed with growth media and the homogenate was centrifuged at 500 x g for 10 min at RT. After removal of the supernatant the cells were re-suspended in growth media and seeded in cell culture dishes. Cells were maintained in an incubator with 10% carbon dioxide (CO_2). The day after extraction and then every other day the media was changed. Before cells reached confluence, live cells were counted and 0.15 x 10^5 cells were seeded per well in 12 well plates. One day after white pre-adipocytes reached confluence, differentiation was induced with growth media supplemented with dexamethasone (1 µM), IBMX (0.5 µM), rosiglitazone (1 µM) and insulin (5 µg/ml). Two days later, and every other day until the end of the study, media was changed to growth media supplemented with insulin (5 µg/ml). One day after brown pre-adipocytes reached confluence, differentiation was induced with growth media supplemented with dexamethasone (5 µM), IBMX (0.5 µM), indomethacine (125 µM), rosiglitazone (1 µM), insulin (0.5 µg/ml) and T3 (1 nM). Two days later, media was changed to growth media

supplemented with rosiglitazone (1 µM), insulin (0.5 µg/ml) and T3 (1 nM). Four days after the start of the induction and every other day until the end of the study, media was changed to growth media supplemented with insulin (0.5 µg/ml) and T3 (1 nM). Plates were frozen or fixed with 4% PFA before induction of differentiation (day 0) and 2, 4 and 8 days after start of the differentiation process.

The description of the method of isolation and differentiation of primary white adipocytes has been described in my recent publication named: “Dual specificity phosphatase 6 deficiency is associated with impaired systemic glucose tolerance and reversible weight retardation in mice” by Pfuhlmann K., Pfluger P.T., Schriever S.C., Müller T.D., Tschöp M.H. and Stemmer K. (2017), PLOS ONE.

2.3.3 Cell viability assay

Cell viability of primary glia cells treated with and without Fk506 was measured with MTT and Alamar assays (table 10). For the MTT assay, 0.16 x 10^5 cells were seeded per well of a 96-well plate, 7 replicates per group. Three days later astrocytes were fasted with MEM for 4 to 5 hours, Fk506 was added in different concentrations (with 0.1% DMSO) and half an hour later 10% FBS was added to the wells. One day later the MTT assay was performed. For the assay the media in the plates was changed to 100 µl fresh MEM media (10% FBS). Per condition one dead control (3 µl of 10% Triton) was used and 10% MTT (10 µl) was added to each well. Plates were placed in a normal cell culture incubator for 1 h and afterwards media was removed and 100 µl solubilization buffer (containing isopropanol, triton X-100 and HCl) was added. After 10 min, absorption was measured at wavelengths 570 nm and 650 nm. For calculations the 650 nm value was subtracted from the 570 nm value and astrocytic survival was calculated in % of DMSO treated cells. The Alamar Assay was performed according to the manufacturers protocol. Absorption was measured at wavelength 570 nm and 600 nm and the 570 nm value was normalized to the 600 nm value. Astrocytic survival was calculated in % of DMSO treated cells.

2.3.4 Oil red O staining

For Oil red O staining of the primary adipocytes the PFA (4%) used for fixation was removed, wells were washed with PBS and were air-dried. The Oil Red O stock containing 0.35 % Oil Red O powder in Isopropanol was prepared and mixed with dH_2O (v:v 6:4) and was added to the cells for 10 min. Afterwards, cells were washed multiple times with dH_2O. Water was removed and stained cells were dried. For the measurement of the absorbance, Oil Red O was eluted by adding 100% isopropanol for about 10 min. After pipetting up and down several times to assure proper mixing, staining was quantified by measurement of the optical

density (OD; 500 nm) on a PHERAstar plate reader (Bmg Labtech GmbH, Ortenberg, Germany).

2.3.5 Seahorse

The oxygen consumption rate (OCR) was determined with an extracellular flux analyzer XF96 (Seahorse Bioscience/Agilent technologies Corporation, Santa Clara, CA, USA). Primary white and brown adipocytes were seeded into a XF96-well plate at a density of 0.1 x 10^5 cells/well. Six days after the induction of the differentiation, OCR was measured in white and brown adipocytes. On the day of the experiment, cells were washed with XF-Media containing 2% BSA and 25 mM glucose and were incubated in the same media in an CO_2-free incubator at 37°C for 1 hour. Cells were treated with oligomycin (Oligo; 5 µg/ml), isoproterenol (0.5 µM), DNP (200 µM) and rotenone/antimycine A/2-deoxy-glucose (5 µM, 2 µM, 100 mM). One cycle lasted 6 min (mixing, waiting, measuring, 2 min each). For the primary white and brown adipocytes the basal measurement was performed for 4 cycles, isoproterenol or oligomycine was injected and 6 cycles were measured, followed by the injection of oligomycine or isoproterenol respectively and recordings for 6 cycles, afterwards DNP was injected and 3 cycles were measured, followed by injection of rotenone/antimycine A/2-deoxy-glucose and measurement for 4 cycles. Results were analyzed interpreted according to Divakaruni et al. [98].

2.4 Statistical analysis

Statistical analyses were performed using GraphPad Prism (GraphPad Software Inc., La Jolla, CA, USA) or SPSS (IBM, Armonk, NY, USA). Unpaired two-tailed student's t-test or two-way analysis of variances (ANOVA) with Bonferroni's post test were applied to compare differences between phenotypes or treatment groups. Combined indirect calorimetry measurements were assessed by Analysis of Co-Variance (ANCOVA), using body weight, lean mass, fat mass or food intake as covariates. P-values lower than 0.05 were considered significant. Significances levels were indicated as follows: *p < 0.05, **p < 0.01, ***p < 0.001, ****p<0.0001. All results are presented as means +/- standard error of the mean (SEM).

III Results

1 Celastrol-induced weight loss depends on leptin signaling and is independent from UCP1-mediated thermogenesis

1.1 Celastrol induces weight loss in lean and obese mice

The initial experiment aimed to confirm body weight and food intake lowering effects of celastrol in DIO mice [16, 17]. HFD (58% kcal from fat) fed DIO mice, with a mean starting body weight of 45.3 g (vehicle injected WT mice) and of 45.4 g (celastrol injected WT mice; figure 6a), significantly reduced body weight upon celastrol treatment (100 µg/kg, once daily 1 h before the start of the dark phase). Body weight losses of up to 11.2 % (0.4% BW loss in vehicle group; figure 6b) and reductions in fat mass (FM) and lean mass (LM) of 3.2 g (0.3 g FM gain in vehicle group) and 2.2 g (0.4 g LM loss in vehicle group), respectively, were

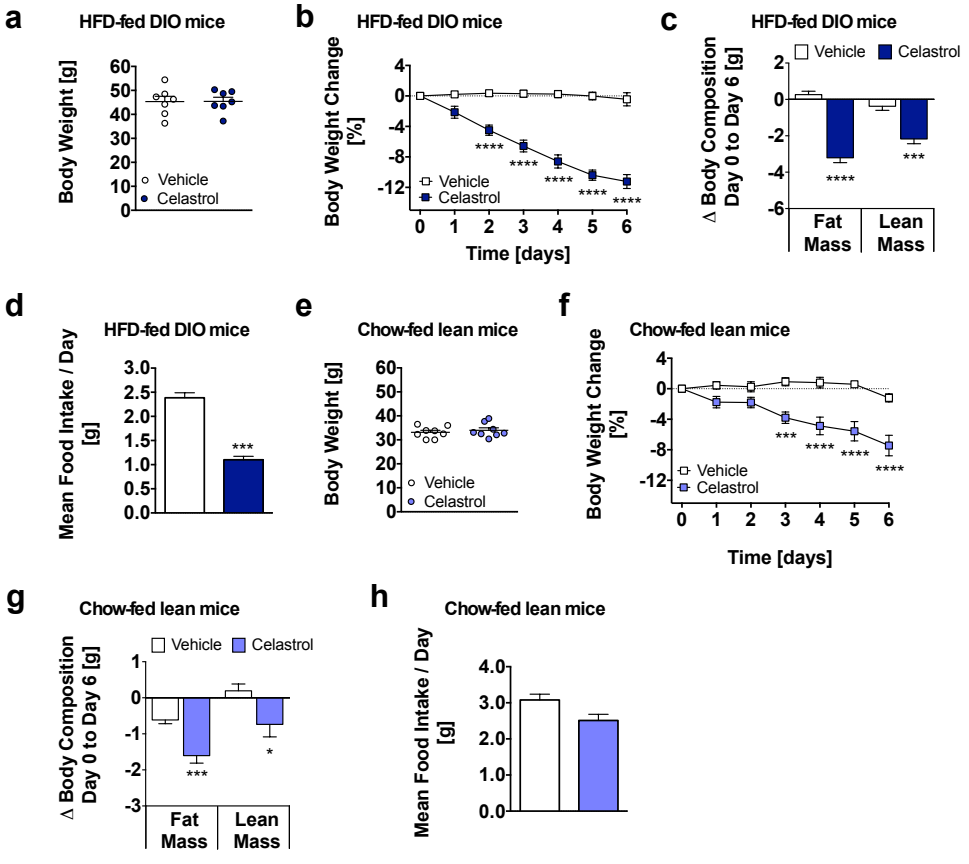

Figure 6. Celastrol induces weight loss in lean and obese mice
HFD-fed DIO **(a-d)** or chow-fed lean **(e-h)** male C57BL/6J mice were treated daily with 100 µg/kg BW celastrol or vehicle (i.p.) for 6 days. Starting body weight **(a)**, BW loss in % of day 0 **(b)**, fat and lean mass loss **(c)** and daily food intake (FI) **(d)** in DIO mice. Starting body weight **(e)**, body weight changes **(f)**, changes in body composition **(g)** and mean FI per day **(h)** in chow-fed lean mice.
Means ± SEM; n=7 per treatment group (a, b, c, d); n=8 per treatment group (e, f, g); n=2 per group (h). 2-way ANOVA: panel b, f; Unpaired two-tailed students t-test: panel a, c, d, e, g; No statistics applied due to low n number: panel h. *P<0.05; ***P<0.001; ****P<0.0001.

reached in celastrol treated mice over the study period of 6 days (figure 6c). Food intake was reduced in celastrol injected DIO mice that consumed 1.1 g HFD/day, while vehicle injected mice ate 2.4 g HFD/day, respectively (figure 6d).

Next, celastrol was administered to chow-fed lean mice that had a mean starting body weight of 33.1 g in the vehicle injected WT group and of 34.0 g in the celastrol injected WT group (figure 6e). Surprisingly, and in contrast to the data published by Liu and colleagues [16], a body weight loss of 7.4% on study day 6 (1.2% BW loss in vehicle group; figure 6f) and a reductions of both, fat and lean mass, were observed in celastrol injected lean mice on study day 6. Celastrol injected lean mice lost 1.6 g (vehicle injected mice lost 0.6 g) fat mass and 0.7 g (vehicle injected mice gained 0.2 g) lean mass (figure 6g). Food intake tended to be reduced on chow diet (figure 6h). Due to group housing only n=2 cages could be analyzed. For a final conclusion regarding differences in food intake in chow-fed lean mice, a higher number of cages would need to be studied.

1.2 Celastrol treatment leads to a delayed decrease in food intake and locomotor activity

Indirect calorimetry was applied to study the metabolic effects of celastrol on locomotor activity, respiratory exchange ratio (RER) and additionally, in more detail, on food intake.
In accordance to the observed trend towards reduced mean daily food intake in celastrol injected DIO animals, the indirect calorimetry measurements revealed a significantly reduced cumulative food intake (figure 7a). Hourly food intake was assessed over 3 days. During the day, no major difference in hourly food intake was determined (figure 7b), except for an increase in FI in celastrol injected animals 6 h after the start of the light phase. In contrast, during the dark phase significant reductions in food intake in celastrol injected mice were observed (figure 7c). A maximal reduction in food intake in celastrol injected mice was observed between 8 to 11 hours after the start of the dark cycle and therefore 9 to 12 hours after the administration of celastrol (figure 7c). Feeding efficiency was impaired in celastrol injected mice on study days 2, 3 and 4 (figure 7d). During the second half of the dark phase, decreased respiratory exchange ratios and locomotory activity patterns were observed, which temporally correlated with the reduced food intake (figure 7e, f).

1.3 Effects of celastrol on key regulators of adipose tissue and skeletal muscle metabolism in obese mice

A previous publication [17] proposed that celastrol treatment induces weight loss by increasing the thermogenic activity of skeletal muscle, white adipose tissue and brown adipose tissue. Accordingly, effects of celastrol on BAT, skeletal muscle and iWAT were

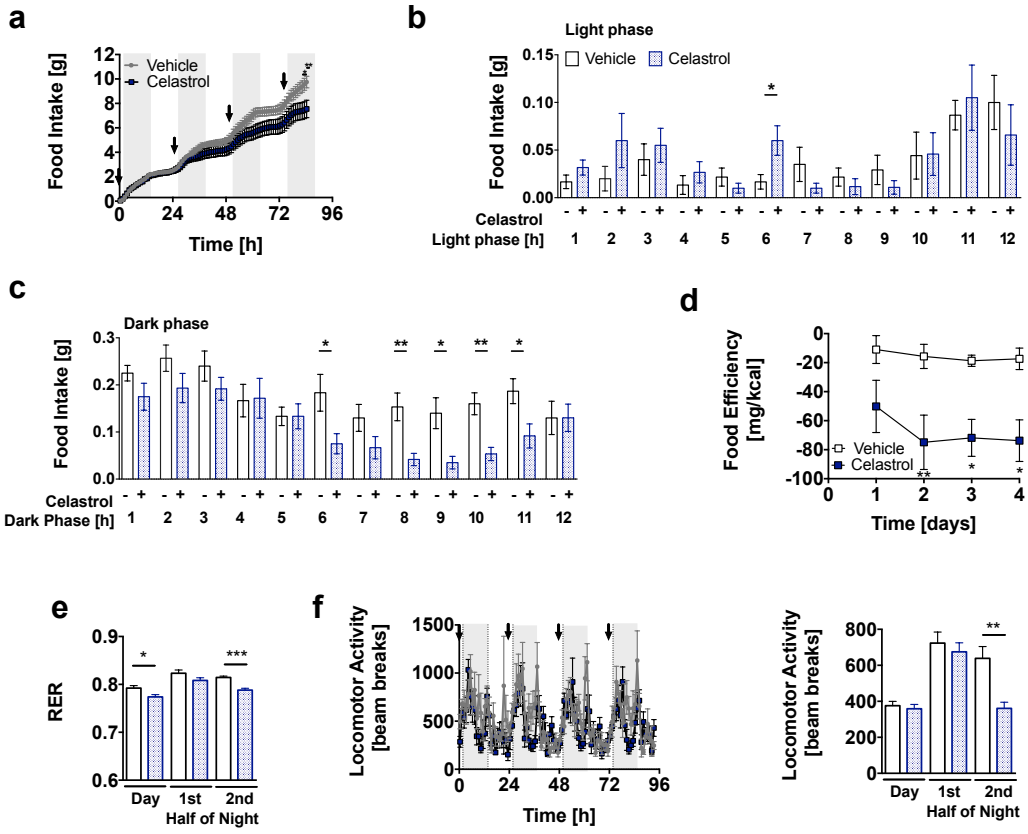

Figure 7. Celastrol treatment decreases food intake and locomotor activity specifically in the second half of the night

Cumulative food intake **(a)** and average hourly food intake in the light **(b)** and dark phase **(c)** of male DIO mice injected daily (see arrow) with 100 µg/kg BW celastrol or vehicle (i.p.) for 4 days. Food efficiency in DIO mice **(d)**. Corresponding 4-day respiratory exchange ratios **(**RER; **e)** and locomotor activity patterns **(f,** left graph**)** and average values for the light phase and the first and second half of the dark phase **(f,** right graph; 3 days and 4 nights**)** of vehicle or celastrol-treated DIO mice.

Means ± SEM; n=6 per treatment group (a, b, c, d, e); n=7 per treatment group (f); 2-way ANOVA: panel a, d; Unpaired two-tailed students t-test: panel b, c, e, f right graph. *P<0.05; **P<0.01; ***P<0.001.

assessed by qPCR and western blot in mice that had been injected with celastrol (100 µg/kg body weight (BW), once daily) or vehicle for 6 days.

Celastrol did not induce the expression of mitochondrial genes (figure 8a) or genes involved in non-shivereing thermogenesis in skeletal muscle *in vivo*, but reduced the expression of the ER-stress markers inositol 1,4,5-triphosphate receptor type 1 (*Itpr1*) and phospholamban (*Plb*) (figure 8b). In line with the publication by Ma and colleagues [17], celastrol increased mRNA levels of heat shock factor protein-1 (*Hsf1*) and *Ucp1* in iWAT (figure 8c) and of medium-chain acyl-CoA dehydrogenase (*Mcad*) and *Ucp1* in BAT (figure 8d). Upregulating effects of celastrol on *Ucp1* mRNA levels in BAT were reflected by increased UCP1 protein levels in BAT (figure 8e, f). However, transcription of *Pgc-1α* and additional thermogenic and mitochondrial genes (PR domain zinc finger protein 16 (*Prdm16*), cell death-inducing DFFA-like effector A (*Cidea*), cytochrome c (*Cyt c*), cytochrome C oxidase subunit 4 isoform 2 (*Cox4β*)) were unaffected in iWAT and BAT (figure 8c, d). Overall, the induction of *Ucp1*

mRNA and UCP1 protein levels in BAT and of *Ucp1* mRNA levels in iWAT indicate that celastrol might activate thermogenesis.

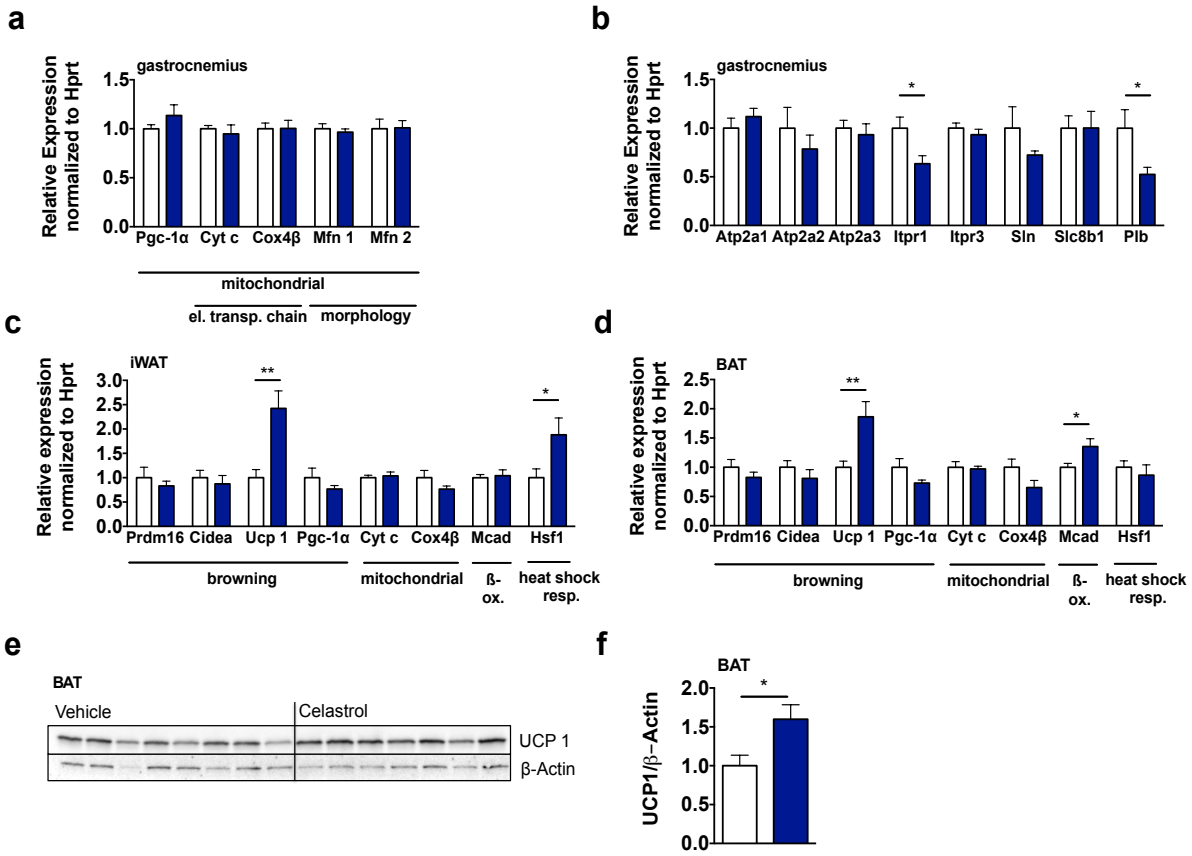

Figure 8. Effects of celastrol on key regulators of adipose tissue and skeletal muscle metabolism in obese mice

In gastrocnemii of DIO mice treated with celastrol (100 µg/kg) or vehicle (i.p.) for 6 days expression levels of genes involved in mitochondrial function (peroxisome proliferator-activated receptor gamma coactivator 1 alpha *(Pgc-1α)*, cytochrome c *(Cyt c)*, cytochrome oxidase 4 β *(Cox4β)*, mitofusin-1 (*Mfn1*) and mitofusin-2 (*Mfn2*)) **(a)** and sarcoplasmic reticulum function (ATPase sarcoplasmic/endoplasmic reticulum Ca^{2+} transporting 1 (*Atp2a1*), ATPase sarcoplasmic/endoplasmic reticulum Ca^{2+} transporting 2 (*Atp2a2*), ATPase sarcoplasmic/endoplasmic reticulum Ca^{2+} transporting 3 (*Atp2a3*), inositol 1,4,5-triphosphate receptor type 1 (*Itpr1*), inositol 1,4,5-trisphosphate receptor type 3 (*Itpr3*), sarcolipin (*Sln*), solute carrier family 8 (sodium/lithium/calcium exchanger) member B1 (*Slc8b1*) and phospholamban (*Plb*)) **(b)** were analyzed. mRNA levels of genes involved in browning (PR domain zinc finger protein 16 (*Prdm16*), cell death-inducing DFFA-Like Effector A (*Cidea*), uncoupling protein 1 (*Ucp1*), *Pgc-1α*) and mitochondrial function (*Cyt c*, *Cox4β*), β-oxidation (medium-chain-acyl-CoA-dehydrogenase (*Mcad*)) and heat shock response (heat shock factor 1 (*Hsf1*)) were measured in inguinal white adipose tissue (iWAT) **(c)** and brown adipose tissue (BAT) **(d)** of celastrol (100 µg/kg) vs. vehicle-treated (i.p.) DIO mice. Protein levels of UCP1 in brown adipose tissue of celastrol vs. vehicle-treated (i.p.) DIO mice were depicted by western blot **(e)** and densitometry analyses were performed **(f)**.

Means ± SEM; n=8 vehicle group, n=7 celastrol group (a, b, d (except for UCP1 in the vehicle group, where 1 value was identified as significant outlier by a Grubbs' test), e, f); n=8 vehicle group, n=6 celastrol group (c except for UCP1 were 7 replicates were used in the celastrol group). Unpaired two-tailed students t-test. *P<0.05; **P<0.01.

1.4 Celastrol-induced body weight loss is independent of UCP1

To evaluate whether the celastrol-induced body weight loss indeed depends on UCP1-induced thermogenesis, the compound was administered to UCP1 KO mice.

Injecting isogenic DIO WT and DIO UCP1-deficient mice for 6 days with celastrol (100 µg/kg BW) resulted in comparably decreased BW. On study day 6, celastrol injected WT mice had lost 6.3% body weight (vehicle injected control mice lost 0.7%) and celastrol injected UCP1 KO mice lost 5.1% body weight (vehicle treated UCP1 control group gained 0.4%) compared

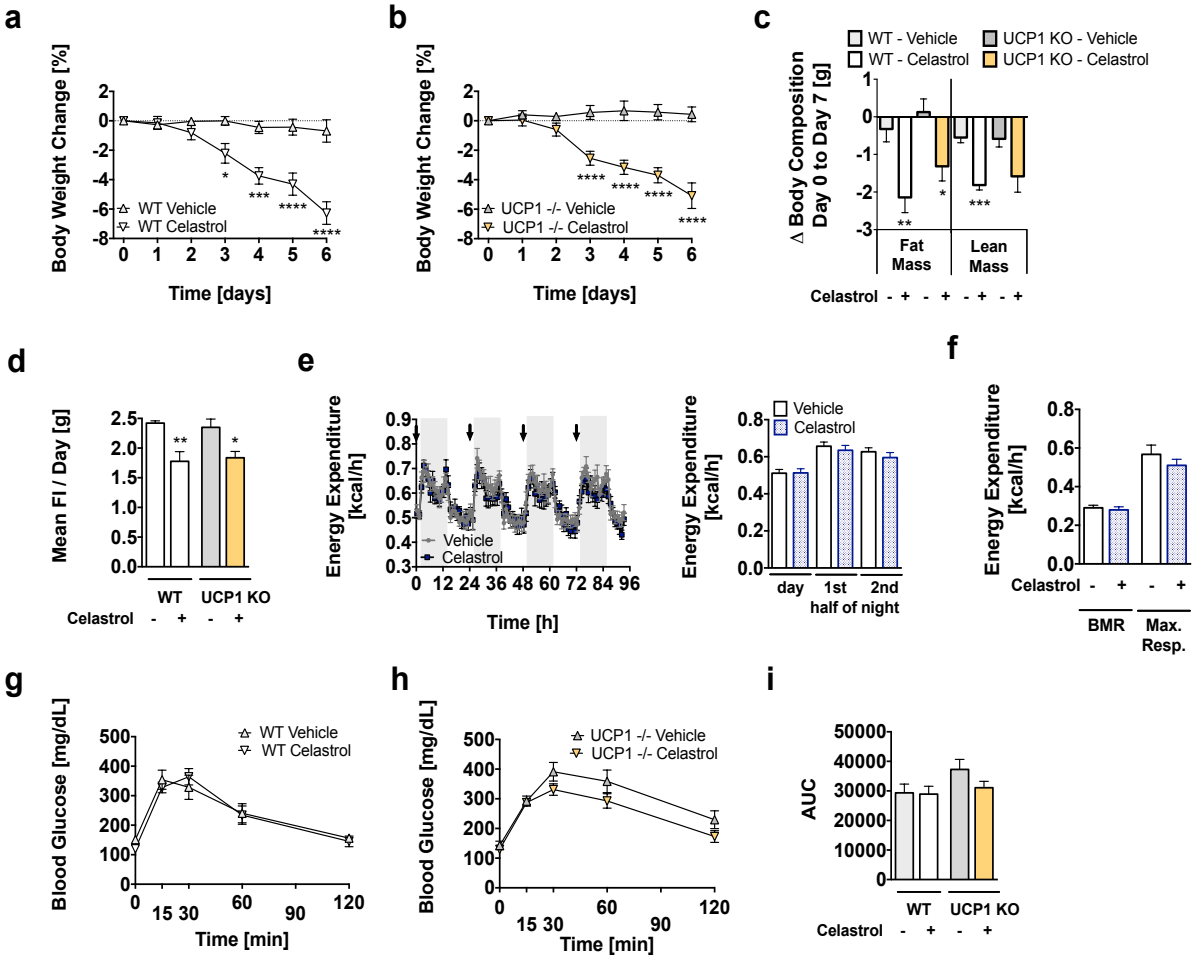

Figure 9. Celastrol decreases body weight independently of UCP1

Body weight loss of DIO WT **(a)** and UCP1 KO mice **(b)** subjected to subcutaneous (s.c.) injections of 100 µg/kg BW/d celastrol or vehicle for 6 days. Fat and lean mass loss **(c)** and daily food intake **(d)** in DIO WT and UCP1 KO mice. Energy expenditure at ambient room temperature in male DIO mice injected daily (indicated by arrows) with 100 µg/kg BW celastrol or vehicle for 4 days **(e)**. Additional indirect calorimetry measurements under thermoneutral conditions of celastrol (100 µg/kg BW/d, i.p.) and vehicle injected mice showing basal metabolic rates (BMR) and maximal respiratory capacities (Max. Resp.) after a single injection of norepinephrine (0.5 µg/g BW) **(f)**. Glucose tolerance tests (GTTs) of DIO WT **(g)** and UCP1 KO **(h)** mice treated with 100 µg/kg BW/d celastrol or vehicle (s.c.). GTTs were performed on treatment day 6 by i.p. injection of 1.5 g glucose per kg BW, depicts area under the curve (AUC) values for glucose excursions **(i)**.

Means ± SEM; n=7 per group (a, b, c, g, h, i); n=5 WT vehicle and WT celastrol, n=3 KO vehicle, n=4 KO celastrol (d); n=6 per treatment group (e); n=7 per group, except for Max. Resp. celastrol group, where one animal had to be excluded due to a failed injection (f). 2-way ANOVA: panel a, b, g, h; ANCOVA with fat and lean mass as covariate: panel e left graph; Unpaired two-tailed students t-test: sub-graphs c, d, e right panel, f, i. *P<0.05; **P<0.01; ***P<0.001; ****P<0.0001.

to their body weight at the start of the study (figure 9a, b). Fat mass was decreased in both, celastrol-treated WT and UCP1 KO mice and a significant reduction in lean mass was only observed in WT but not in UCP1 KO mice (figure 9c). According to the comparable reduction in body weight, UCP1 KO and WT mice reduced food intake to the same extent (figure 9d). Celastrol injected WT mice ate 1.8 g (vehicle injected WT mice consumed 2.4 g) and celastrol injected UCP1 KO mice also ate 1.8 g HFD (vehicle injected UCP1 KO mice consumed 2.35 g; figure 9d). Celastrol had no impact on energy expenditure under ambient housing conditions (23°C; figure 9e) nor on energy expenditure or maximal norepinephrine-induced respiration at thermoneutral conditions (30°C; figure 9f) in WT mice on HFD. Further, celastrol treatment for 6 days did not alter systemic glucose homeostasis in DIO WT (figure 9g, i) or UCP1 KO (figure 9h, i) mice. Collectively, these results strongly imply that celastrol-induced body weight reduction is not mediated by increased mitochondrial uncoupling or cellular thermogenesis via UCP1.

1.5 Celastrol-induced weight loss is leptin dependent

Recently, celastrol was postulated to have leptin sensitizing functions [16]. Leptin is a hormone secreted by adipose tissue that regulates feeding behavior by inducing satiety [99]. Leptin is secreted in proportion to adipose tissue mass and directly activates POMC neurons in the ARC that inhibit food intake and increase energy expenditure [100]. Despite high circulating leptin levels in obese humans and rodents, their leptin response is greatly diminished. This phenomenon is referred to as leptin resistance.

The aim of this sub-project was to study the leptin-sensitizing actions of celastrol by first injecting celastrol in leptin receptor deficient Lep^{db} and leptin deficient Lep^{ob} mice and by secondly assessing the regulation of classical leptin signaling molecules in the hypothalamus of leptin treated WT mice.

1.5.1 Lep^{dp} and Lep^{ob} mice are protected from celastrol induced weight loss

In the Lep^{db} study functionality of celastrol (100 µg/kg BW) was confirmed in chow-fed lean WT mice, where it reduced BW by 4.1% (vehicle injected WT mice gained 2.1%; figure 10a). Celastrol did not decrease BW in chow-fed leptin receptor-deficient Lep^{db} mice. Rather on study day 6 a BW gain of 4.6% was observed in Lep^{db} compared to vehicle injected Lep^{db} mice that gained 6.5% (figure 10b). Celastrol injected WT mice lost fat and lean mass compared to their vehicle injected controls, while celastrol injected Lep^{db} mice did not show any change in body composition (figure 10c). In line with the results obtained in the leptin receptor deficient Lep^{db} mice, celastrol action was absent in chow-fed leptin deficient Lep^{ob} mice. Daily injections of celastrol (100 µg/kg BW) did not reduce body weight in Lep^{ob} mice. At the end of the study (study day 6), celastrol treated Lep^{ob} mice lost 0.2% body weight

(vehicle treated controls gained 0.5% BW), while celastrol treated WT mice lost 6.7% (vehicle injected WT mice gained 0.1%; figure 10d, e). The reduction in fat and lean mass in WT mice was not observed in Lep^{ob} mice (figure 10f). Glucose tolerance in Lep^{ob} and lean WT control mice was tested after 6 days of celastrol treatment (100 µg/kg BW) by the injection of 1 g glucose per kg BW and was improved in WT mice (figure 10g), but no changes in glucose tolerance were detected for Lep^{ob} mice (figure 10h). Accordingly a reduction in the area under the curve (AUC) value was detected for WT but not for Lep^{ob} mice (figure 10i). The inability of celastrol to decrease body weight in Lep^{db} and Lep^{ob} mice supports the hypothesis that the weight and food intake lowering effects of celastrol are strictly leptin-dependent.

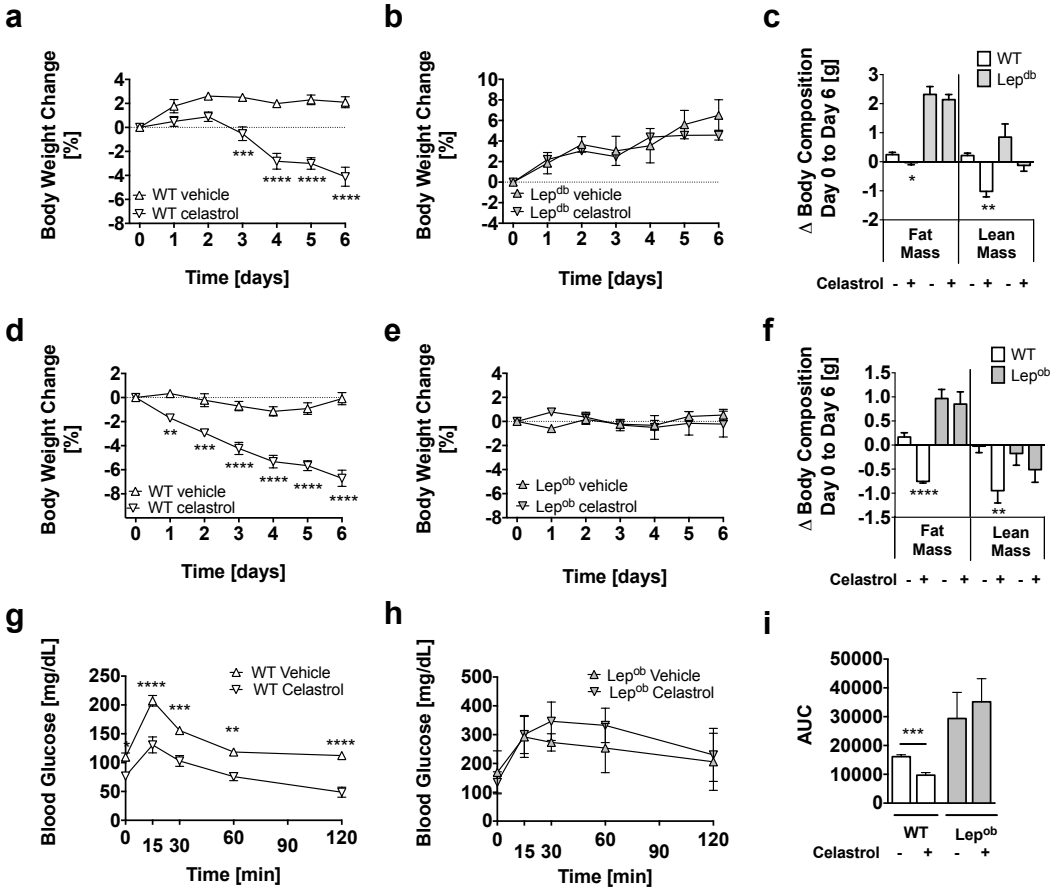

Figure 10. Celastrol-induced weight loss is leptin dependent
BW changes in age-matched male C57BL/6J control mice **(a)** and leptin receptor-deficient Lep^{db} mice **(b)** fed with chow diet and treated with celastrol (100 µg/kg BW/d, s.c.) or vehicle for 6 days. Changes in body composition in celastrol or vehicle-injected WT and Lep^{db} mice **(c)**. BW changes in male chow-fed WT **(d)** and leptin-deficient Lep^{ob} mice **(e)** treated with celastrol (100 µg/kg BW/d; s.c.) or vehicle for 6 days. Changes in body composition in WT and Lep^{ob} mice injected for 6 days with celastrol or vehicle **(f)**. Glucose tolerance tests (GTTs) of lean WT **(g)** and obese Lep^{ob} mice **(h)** treated with 100 µg/kg BW/d celastrol or vehicle (s.c.). GTTs were performed on treatment day 6 by i.p. injection of 1 g glucose per kg BW, depicts area under the curve (AUC) values for glucose excursions **(i)**.
Means ± SEM; n=4 per group (a, b, c); n=8 per group (d); n=5 vehicle injected mice, n=6 celastrol injected mice (e); n=8 for vehicle and celastrol injected WT mice, n=5 for vehicle injected Lep^{ob} mice, n=6 for celastrol injected Lep^{ob} mice (f); n=5 per group (g); n=4 per group (h); n=5 per WT group, n=4 per Lep^{ob} group (i). 2-way ANOVA: sub-graphs a, b, d, e, g, h; Unpaired two-tailed students t-test: sub-graphs c, f, i. *P<0.05; **P<0.01; ***P<0.001; ****P<0.0001.

1.5.2 Celastrol augments phospho-STAT3, total STAT3 and STAT5 levels in the hypothalamus of obese mice

To delineate celastrol's first-order targets, key hypothalamic signaling networks that orchestrate glucose and energy homeostasis, including leptin signaling partners, were assessed *ex vivo* in hypothalami of celastrol treated DIO mice.

Celastrol treatment for 6 days significantly increased *AgRP* mRNA expression while having no effect on mRNA expression of *Pomc*, Cocaine- and amphetamine-regulated transcript (*Cart*) and *Npy* (figure 11a). No effects of celastrol on components of the leptin and melanocortin signalling network namely *Mc3r*, *Mc4r*, leptin receptor (*LepR*), *Stat3*, forkhead box O1 (*FoxO1*), suppressor-of-cytokine signaling-3 (*Socs3*), protein tyrosine phosphatase 1B (*Ptp1b*), t-cell protein tyrosine phosphatase (*Tcptp*) and Src-homology 2 domain-containing phosphatase 2 (*Shp2*; figure 11b) were observed in obese mice. The ER-stress protein heat shock protein family A (Hsp70) member 5 (*Bip*) was up-regulated in celastrol treated mice. Celastrol had no impact on ER-stress- and inflammatory-regulators spliced form of X-box binding protein 1 (*sXbp1*), *Xbp1*, activating transcription factor 4 (*Atf4*), CCAAT/enhancer-binding protein homologous protein (*Chop*), endoplasmic reticulum-localized DnaJ4 (*Erdj4*) or on the inflammatory genes interleukin-1 beta (*Il-1β*), interleukin-6 (*Il-6*) and *Tnf* (figure 11c). Phosphorylation levels of leptin target STAT3 (figure 11d, e) and basal STAT3 and STAT5 protein levels were elevated in the hypothalami of celastrol-injected mice (figure 11d, f). However, the number of pSTAT3-positive POMC neurons remained unchanged (figure 11g, h) and POMC and pSTAT3 positive cells in the ARC exhibit equal numbers (figure 11g, i).

Overall, these data, showing ineffective celastrol action in Lep^{db} and Lep^{ob} mice and enhanced basal STAT5, STAT3 and pSTAT3 protein levels in the hypothalamus of celastrol injected DIO mice, might indicate that the negative leptin feedback signalling by inhibitory regulators of JAK-STAT such as PTP1B, TCPTP or SOCS3 might be ameliorated by celastrol treatment [101].

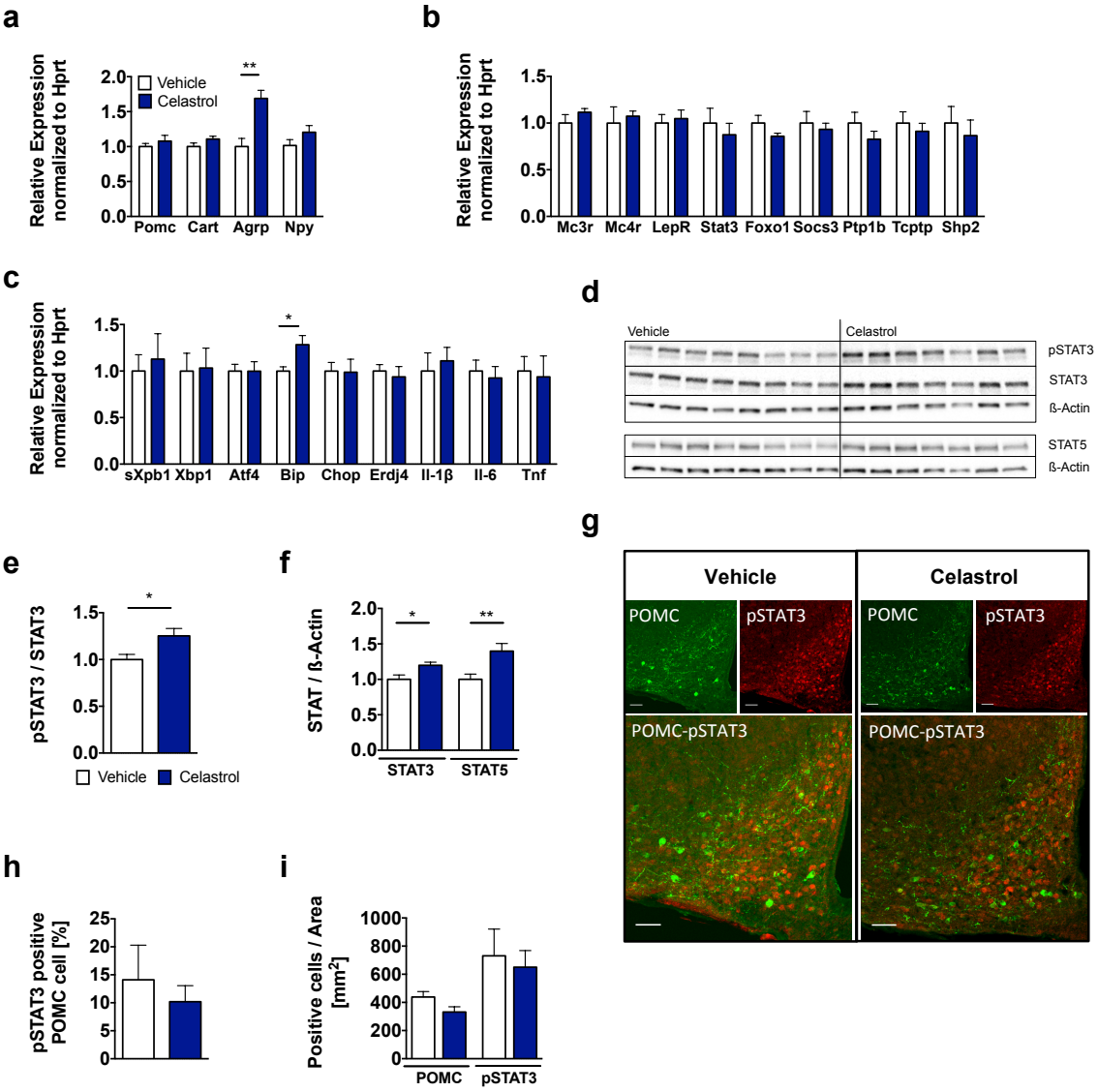

Figure 11. Celastrol augments STAT3 and STAT5 protein levels in the hypothalamus
Impact of celastrol (100 µg/kg BW/d for 6 days, i.p., DIO mice) on hypothalamic expression levels of genes involved in orexigenic/anorexigenic signaling (pro-opiomelanocortin (*Pomc*), cocaine- and amphetamine-regulated transcript (*Cart*), agouti-related protein (*Agrp*) and neuropeptide Y (*Npy*)) **(a)**, or in melanocortin and leptin-signaling (melanocortin receptor 3 (*Mc3r*), melanocortin receptor 4 (*Mc4r*), leptin receptor (*LepR*), signal-transducer-and-activator of transcription-3 (*Stat3*), forkhead box O1 (*Foxo1*), suppressor-of-cytokine signaling-3 (*Socs3*), protein tyrosine phosphatase 1B (*Ptp1b*), t-cell protein tyrosine phosphatase (*Tcptp*) and Src-homology 2 domain-containing phosphatase 2 (*Shp2*)) **(b)**. Hypothalamic expression levels of genes involved in endoplasmatic reticulum (ER) stress (spliced form of X-box binding protein 1 (*sXbp1*), *Xbp1*, activating transcription factor 4 (*Atf4*), heat shock protein family A (Hsp70) member 5 (*Bip*), CCAAT/enhancer-binding protein homologous protein (*Chop*), endoplasmic reticulum-localized DnaJ4 (*Erdj4*)) and inflammation (interleukin-1 beta (*Il-1β*), interleukin-6 (*Il-6*) and tumor necrosis factor (*Tnf*)) **(c)**. Western blot **(d)** and densitometric analyses of phosphorylated signal-transducer-and-activator of transcription-3 (pSTAT3, normalized to total STAT3) **(e)** or basal STAT3 and STAT5 (normalized to β-Actin) protein levels **(f)** in hypothalami of celastrol (100 µg/kg BW/d) or vehicle treated mice (i.p.). Hypothalamic slices of male C57BL/6J mice injected with 100 µg/kg BW/d celastrol or vehicle for 6 d (i.p.) were subjected to immunostaining with anti-POMC and anti-pSTAT3 antibody (scale bar 50 µm) **(g)** and assessed for the percentage of pSTAT3-positive POMC cells **(h)** or the number of POMC or pSTAT3-positive cells per area **(i)**.
Means ± SEM; n=8 per vehicle treated group, n=7 per celastrol treated group (a, b, c, d, e, f); n=5 mice in vehicle treated group, n=6 mice in celastrol treated group, 2 hemispheres were analyzed for each mouse (h, i). Unpaired two-tailed students t-test. *P<0.05; **P<0.01.

2 Calcineurin Aβ deficiency ameliorates HFD-induced hypothalamic astrocytosis in mice

2.1 Ppp3cb deficiency decreases astrocytosis in the arcuate, ventromedial and dorsomedial nucleus of the hypothalamus of HFD-fed mice

We recently showed protection from diet-induced obesity in Ppp3cb KO mice [56]. Here, I aimed to assess whether calcineurin ablation affects the activation of hypothalamic astrocytes in mice chronically exposed to HFD.

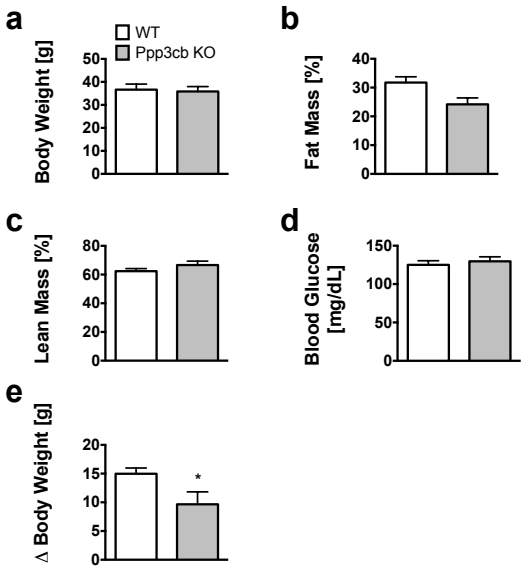

Figure 12. A sub-cohort, selected from a large cohort of Ppp3cb WT and KO mice exhibited no difference in body weight, body composition and blood glucose but a lower body weight gain

Subgroups of WT and Ppp3cb KO mice matched for body weight **(a)**, fat mass **(b)**, lean mass **(c)** and blood glucose levels after 5h of fasting **(d)** were selected from a larger cohort of WT and Ppp3cb KO mice that were exposed to HFD for 16 weeks. The selected Ppp3cb KO mice nevertheless showed a decreased body weight gain over the period of HFD feeding when compared to their selected WT controls **(e)**. Means ± SEM; n=6. Unpaired two-tailed students t-test. *p<0.05.

Body weight matched Ppp3cb WT and KO mice were selected from a large cohort of HFD-fed mice to account for the impact of body weight as covariate for HFD-induced astrocytosis (figure 12a). The sub-selection of BW-matched Ppp3cb WT and KO mice assured similar fat (figure 12b) and lean mass (figure 12c) as well as blood glucose levels (figure 12d) between genotypes. HFD-fed Ppp3cb KO mice nevertheless retained their partial protection from DIO compared to WT mice, which was demonstrated by lower body weight gain in the 16 weeks of HFD feeding (figure 12e).

Reactive astrocytosis in HFD-fed weight-matched Ppp3cb WT and KO mice was determined by immunohistochemical staining for GFAP (figure 13a, b). Stainings were quantified in the arcuate nucleus of the hypothalamus (ARC), ventromedial nucleus of the hypothalamus (VMH) and in the dorsomedial nucleus of the hypothalamus (DMH), which are important centers for the regulation of food intake and body weight [102]. In the ARC, DMH and VMH of HFD-fed Ppp3cb KO mice, less GFAP-positive astrocytes compared to their WT controls were found (figure 13c, d, e). Analyses of astrocyte morphology revealed unchanged lengths of primary projections in the ARC (figure 13f), but decreased overall numbers of primary projections in the ARC of Ppp3cb KOs (figure 13g). A strong tendency towards a decrease in the number of primary projections was observed in the DMH (p=0.057; figure 13h) but not in the VMH of Ppp3cb

KO mice (figure 13i). Overall, this data suggests the involvement of Ppp3cb in HFD-induced astrocytosis.

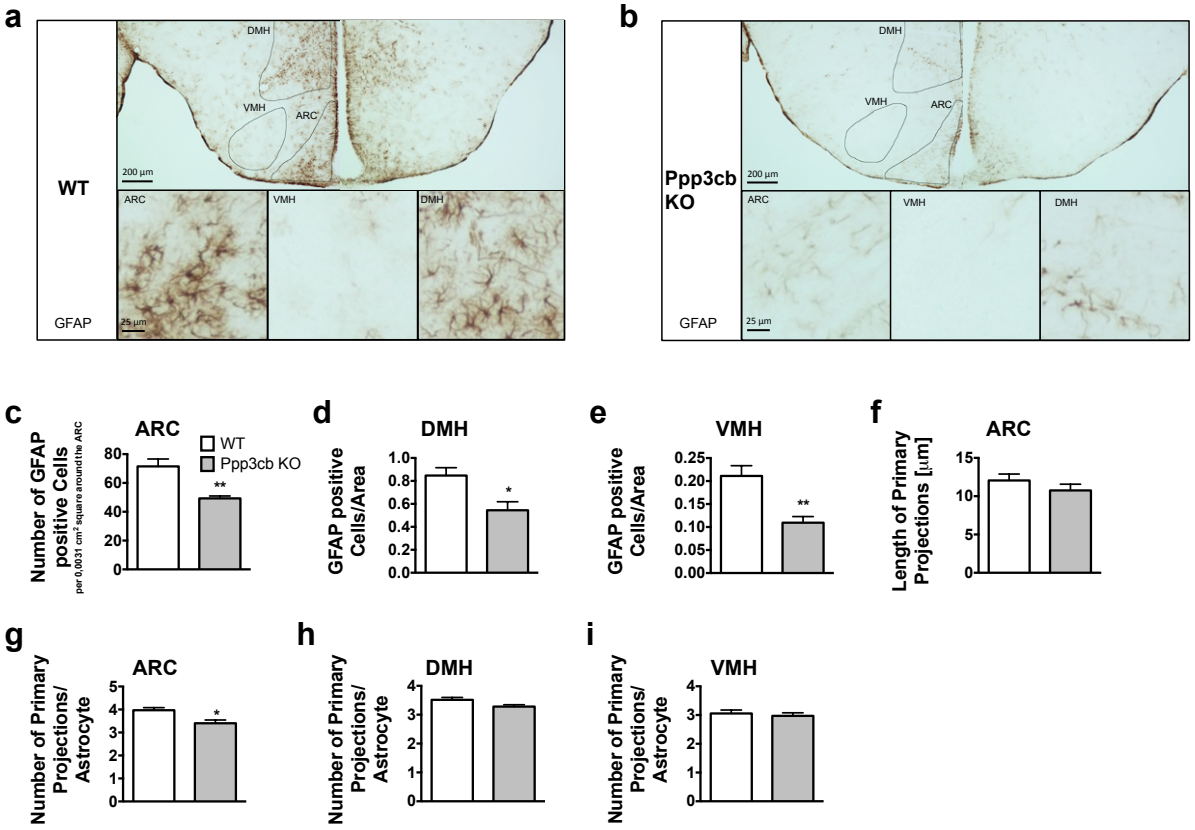

Figure 13. Deletion of Ppp3cb decreases the number of glial fibrillary acidic protein (GFAP) positive cells in the ARC, DMH and VMH and the number of primary projections in the ARC
Immunohistochemical staining for GFAP in the arcuate nucleus (ARC), dorsomedial hypothalamus (DMH) and ventromedial hypothalamus (VMH) of Ppp3cb WT and KO mice. Representative images of the mediobasal hypothalamus **(a,b, upper pictures)** and of astrocytes in the ARC, DMH, VMH **(a,b, lower pictures)** of HFD-fed Ppp3cb WT and KO mice. Numbers of GFAP-positive cells in the ARC **(c)**, DMH **(d)**, VMH **(e)**; Length of primary projections in the ARC of Ppp3cb KO and WT mice **(f)**. Numbers of primary projection per astrocyte in the ARC **(g)**, DMH **(h)** and VMH **(i)**.
Means ± SEM; n=6 biological replicates per genotype (4 pictures per biological replicate were quantified) except for d, where only 5 KO brains could be used, and f where length could be measured only in 4 KO brains. Unpaired two-tailed students t-test. *P<0.05, **P<0.01.

2.2 Ppp3cb deficiency decreases microglia numbers in the VMH of HFD-fed mice

Changes in the number of GFAP positive astrocytes are often associated with changes in the number of microglia. HFD feeding was shown to simultaneously increase the expression of GFAP and of microglia markers [48]. Furthermore, it was reported that microglia activation is responsible for the activation of a subset of astrocytes [50].

In this thesis hypothalami of BW-matched HFD-fed Ppp3cb WT and KO mice were stained for the microglia marker IBA1 (figure 14a, b). In contrast to a decrease in astrocytosis in HFD-fed Ppp3cb KO mice, I did not observe differences in the numbers of IBA1-positive

microglia between genotypes in the ARC (figure 14c) and in the DMH (figure 14d). In the VMH, a decrease in IBA1 positive cells in Ppp3cb KO mice was detected compared to their WT control mice (figure 14e). Accordingly, these data suggest that Ppp3cb is only involved in HFD induced microgliosis in selected areas of the hypothalamus.

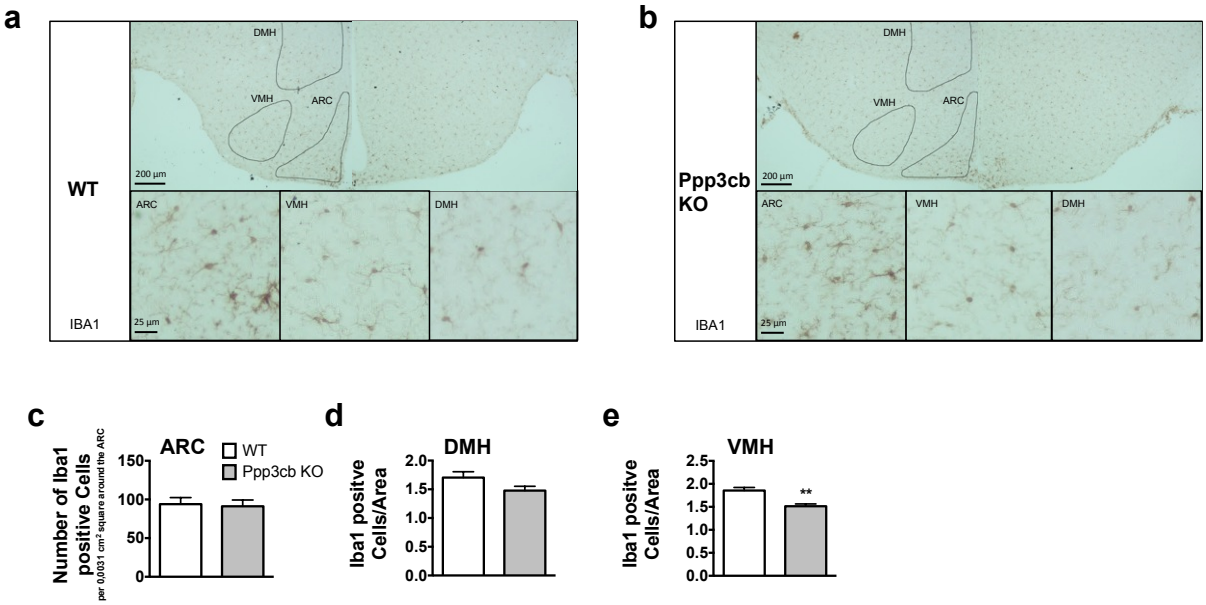

Figure 14. Deletion of Ppp3cb decreases the number of IBA1 positive cells in the VMH
Immunohistochemical staining for IBA1 in the ARC, DMH and VMH of Ppp3cb WT **(a)** and KO **(b)** mice and quantitative analysis of IBA1 positive microglia **(c-e)** in the ARC **(c)**, DMH **(d)** and VMH **(e)**.
Means ± SEM; n=6 WT and 5 KO mice (c); n=6 mice per genotype (d, e). 4 pictures per biological replicate were quantified. Unpaired two-tailed students t-test. **P<0.01.

2.3 Unperturbed astrocyte morphology or GFAP protein levels in primary astrocytes treated with the calcineurin inhibitor Fk506

Next, it was aimed to translate the *in vivo* findings into an *in vitro* system to facilitate mechanistic studies. I hypothesized a decrease in GFAP protein levels after treatment of primary astrocytes with the calcineurin inhibitor Fk506. Specifically, it was aimed to assess whether treatment with obese serum affects GFAP levels in the absence or presence of calcineurin inhibitor Fk506. I chose primary murine hypothalamic astrocytes isolated from 1 to 4 days old male pups as model system, and used treatment with 10% serum generated from blood of obese mice as surrogate for HFD feeding [51]. Exposure of primary astrocytes with 10% obese serum for 24, 48 and 72 h induced changes in morphology towards a more reactive phenotype, characterized by a distinct prolongation of astrocytic projections compared to FBS-treated astrocytes (figure 15a-c, left pictures). However, no obvious changes in the morphology of primary astrocytes after the addition of 2 or 5 µM of Fk506 were found, regardless of the supplementation of media with 10% normal FBS or with 10% obese serum to mimic an obesogenic environment (figure 15a-c, middle and right pictures).

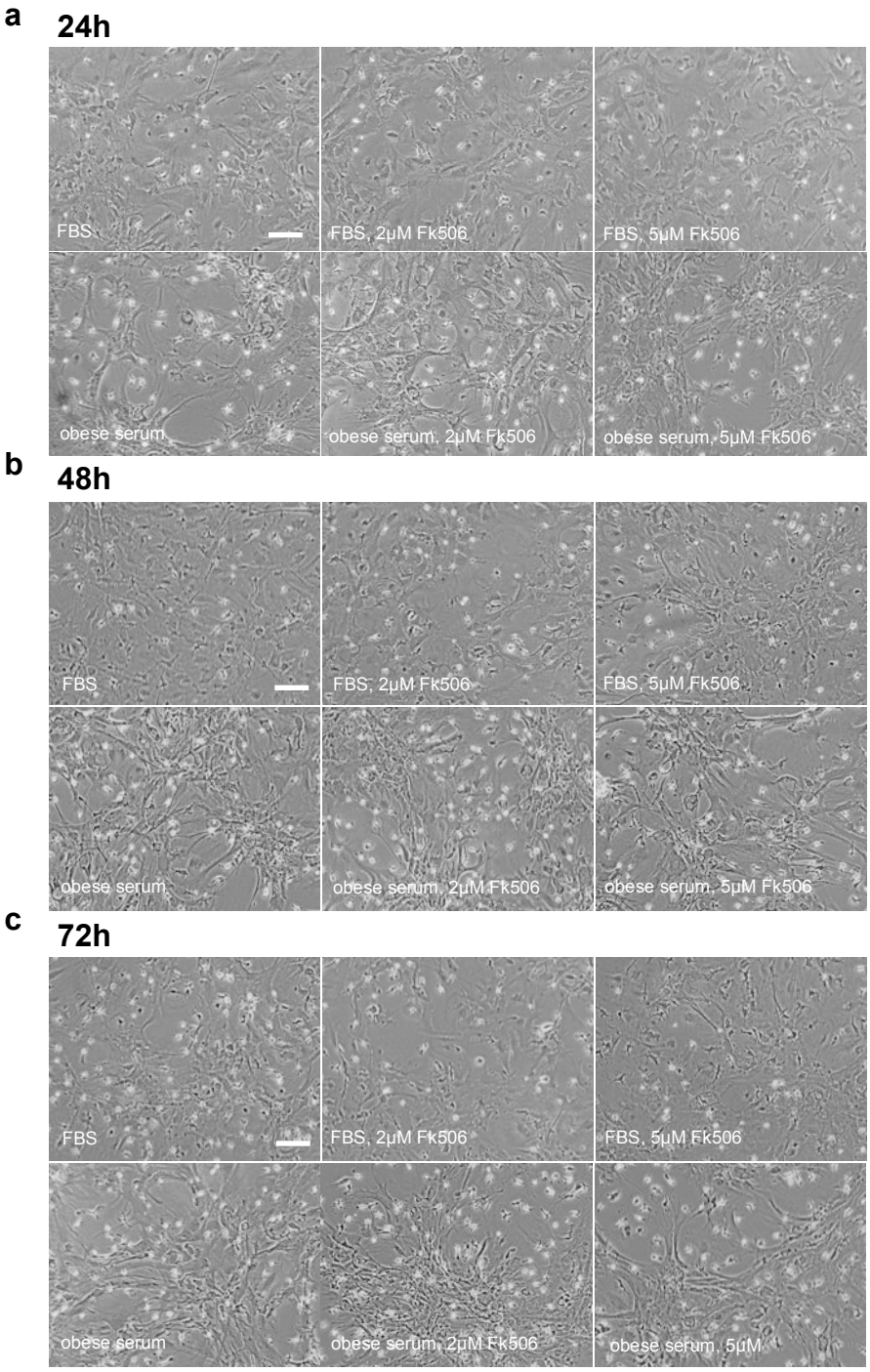

Figure 15. Glial morphology after treatment with fetal bovine serum (FBS) or obese serum and/or Fk506
Representative light microcopy images of primary astrocytes and co-isolated microglia treated with 10% FBS or 10% obese serum, and 2 µM or 5 µM Fk506 for 24 h **(a)**, 48 h **(b)** and 72 h **(c)**, respectively. Scale: 100 µm.

Morphological changes in astrocytes were not associated with an increase in protein levels of GFAP and vimentin, detected by western blotting (figure 16a). Treatment of primary astrocytes with 10% obese serum for 48 h did not increase basal GFAP and vimentin protein levels compared to treatment with 10% FBS (figure 16a). Similarly, unchanged levels of GFAP and vimentin protein after the treatment with 2 or 5 µM Fk506 in primary astrocytes

that grew in media with normal FBS were observed (figure 16a). Further supplementation with 10% obese serum as an additional stimulant had no additional effect. Importantly, I confirmed calcineurin inhibition by Fk506 by showing hyperphosphorylation of NFAT, indicated by a shift in the band towards a higher molecular weight (figure 16a). Additionally, I showed that treatment of primary astrocytes with Fk506 in concentrations from 1 µM up to 30 µM had no effect on astrocytic cell survival (figure 16b). The lack of induction of GFAP by Fk506 was corroborated by immunocytochemical stainings for GFAP in primary glia cultures, which revealed similar GFAP fluorescence intensity upon treatment with 5 or 10 µM Fk506 (figure 16c, d).

Last, treatment of glial cultures with 2 or 5 µM Fk506 ± obese serum did not change the number of microglia present in the primary culture (figure 15a-c). In contrast, the addition of obese serum to primary astrocytes increased the number of microglia that were co-isolated with primary astrocytes. This increase in microglia number was detectable 24 h after the addition of the obese serum (figure 15a, left pictures) and became more apparent with prolonged exposure to obese serum (48h: figure 15b, left pictures; 72h: figure 15c, left pictures). Overall, my data indicate that primary astrocyte cultures are not a suitable tool to study astrocytosis under obesogenic conditions in the context of calcineurin inhibition.

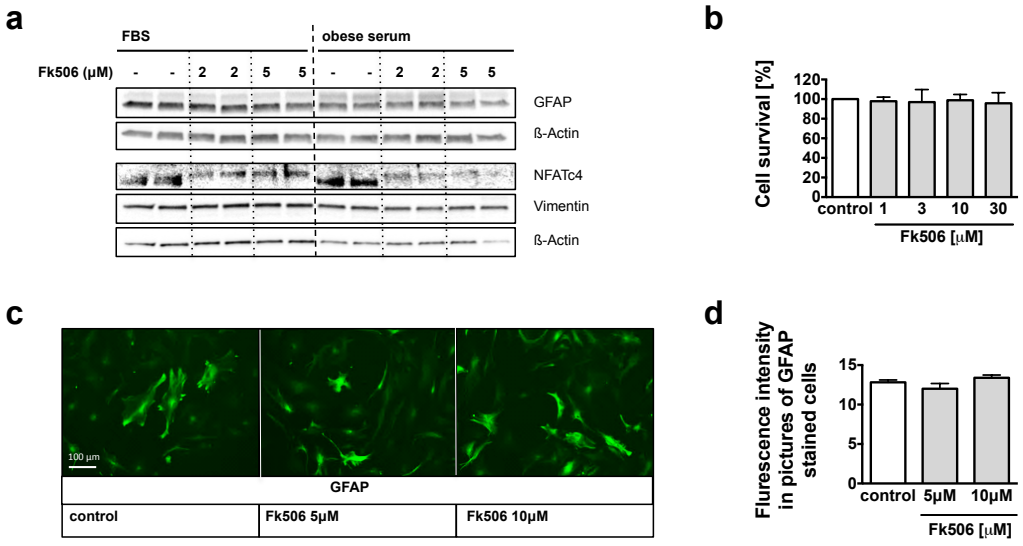

Figure 16. Effect of Fk506 treatment on GFAP and vimentin levels and on cell survival
Representative Western blot of GFAP and vimentin protein levels **(a)** after treatment of the primary glia cultures with 10% FBS, 10% obese serum, and/or Fk506 (2 µM or 5 µM); calcineurin inhibition was corroborated by revealing an Fk506-mediated decrease in nuclear factor of activated T-cells 4 (NFATc4) protein levels; β-Actin was used as housekeeping protein. Cell survival assay **(b)** showing cells treated with increasing concentrations of Fk506 for 48 h. Representative pictures of immunocytochemical stainings **(c)** and fluorescence intensities **(d)** for GFAP in untreated, 5 µM Fk506 and 10 µM Fk506 treated primary astrocytes.
Means ± SEM; n=2 biological replicates; calcineurin inhibition was confirmed once with NFATc4 (a); n=3 biological replicates (b); quantification of GFAP staining was done in 10 - 11 pictures/ treatment group (c, d). Unpaired two-tailed students t-test was applied to sub-graph b.

3 Hypothalamic deletion of GPx7 induces diet-induced glucose intolerance

3.1 Global depletion of GPx7 results in a decreased birth ratio of male KO mice

The first interesting observation made with the global GPx7 KO mice was a shift in the birth ratio towards less GPx7 KO offspring out of heterozygous GPx7 breeding pairs. Pup ratios to be expected from matings with heterozygous (+/-) parents are 50% (25% male, 25% female mice) heterozygous, 25% (12.5% male, 12.5% female mice) wildtype and 25% (12.5% male, 12.5% female mice) knockout mice.

In our mouse facilities, a total number of six heterozygous GPx7 global KO breeding pairs were setup. Four breeding pairs contained one male and one female mouse and two were matings with one male and two female breeders. Each female received one first litter and four of eight females received a second litter and one female mouse even a third, leading to a total number of 90 mice, when the first, second and third litter were combined.

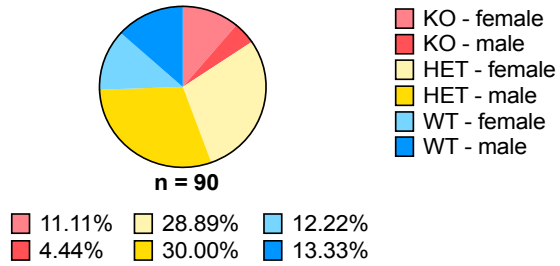

Figure 17. Decreased birth ratio of male mice globally ablated for GPx7
Genotypes and sex of pups generated within six independent matings of male GPx7$^{+/-}$ and female GPx7$^{+/-}$ mice. Figure shows first, second and third litters. Four of the six breeding pairs received a second litter and one of the four a third one.
N=90. No statistics applied.

The total ratio for obtained WT mice was 25.6% and therefore very close to the calculated ratio of 25%. Approximately the same numbers of WT male and female mice were obtained and mice numbers with 12.2% for the females and 13.3% for the males were very close to the expected ratios. Notably the total number of KO mice was with 15.6% lower than expected. Surprisingly only 4.4% GPx7 KO male mice were obtained, a considerable lower number. The ratio of female GPx7 KO mice with 11.1% was close to the calculated ratio. In total 58.9% of all mice were heterozygous and female heterozygous mice with 28.9% and male heterozygous mice with 30% were close to expected ratios (figure 17). Overall, a clear impairment in male KO output as well as a general lower number of KO mice was observed.

3.2 GPx7 ablation affects body weight and glucose homeostasis

3.2.1 Global deletion of GPx7 increases percentage body weight gain in male mice fed chow diet

As a sensor for ER-stress, GPx7 is involved in mediating stress signals to down-stream proteins via transmission of disulfide bonds to effector proteins. As a result, oxidized effector

proteins such as PDI or GRP78 can more efficiently exert functions like protein re-folding. The knockout of GPx7 was shown to increase ER-stress [61, 80]. As a side-product of this catalytic reaction ROS e.g. H_2O_2 become detoxified and split up to H_2O and O_2. ROS are linked to obesity and the co-development of insulin resistance and type 2 diabetes [103-105].

It was hypothesized that deletion of the ER-stress sensor/regulator GPx7 might lead to impairment in stress signal transmission and to an increase in reactive oxygen species, finally resulting in obesity and insulin resistance in mice.

The hypothesis was first tested in lean global GPx7 KO mice fed with normal rodent chow diet. Body weight gain in gram was not different between genotypes (figure 18a) but body weight gain in percent was significantly higher in GPx7 global knockout mice (figure 18b).

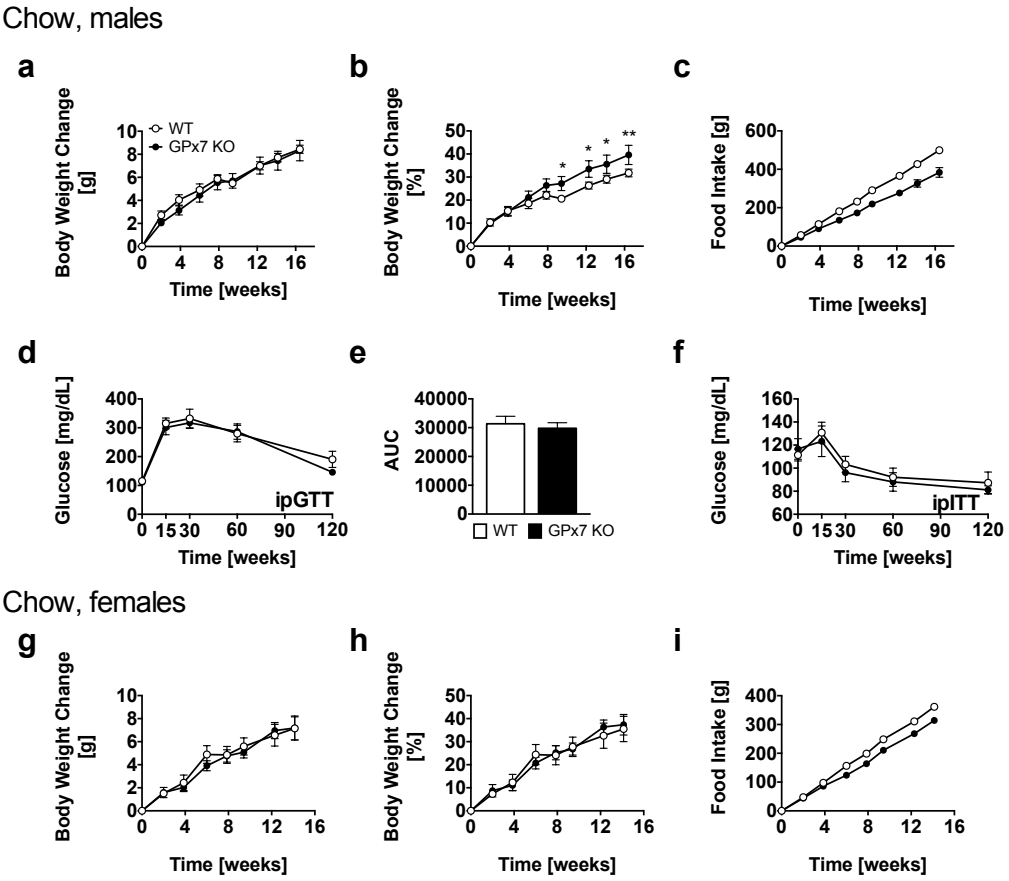

Figure 18. Global deletion of GPx7 increases body weight in lean male but not in lean female mice and has no effect on glucose homeostasis in lean mice
Male **(a-f)** and female **(g-i)** whole body GPx7 KO and WT mice on a C57Bl/6J background were fed regular rodent chow diet. The biweekly monitoring of body weight gain in gram **(a)** and percent **(b)** as well as food intake **(c)** were started in 8-weeks-old mice over a period of 16 weeks. At an age of 30 weeks mice were subjected to glucose tolerance tests **(**i.p., 2 g/kg body weight; **d, e)**, revealing similar glucose excursions **(d)** and area under the curve values **(**AUC; **e)**. Insulin tolerance tests **(**i.p., 0.5 IU/kg body weight; **f)** were conducted in mice aged 31 weeks. In 8-week-old females body weight gain in gram **(g)** and percent **(h)** and food intake **(i)** were monitored over a period of 14 weeks.
Mean +/- SEM; n=8 (a, b, d, e, f, g, h); n=2 (c, i). 2-way ANOVA: panel a, b, d, f, g, h; Unpaired two-tailed students t-test: panel e; No statistics were applied for sub-graphs c and i due to low n-number (group housing was mandated by animal ethics). *P<0.05; **P<0.01.

The higher body weight gain in global GPx7 male mice in percent compared to the graph where body weight gain is shown in gram, is due to the difference in starting body weight. GPx7 global KO mice started with a mean body weight of 21 g, while the WT mice were heavier and started with 26.7 g (data not shown). Food intake tended to be lower in GPx7 knockout mice compared to its wildtype control mice (figure 18c). However more detailed observations are necessary, due to group housing of mice only two cages per genotype were studied. Glucose tolerance was observed by injections of 2 g/kg body weight glucose. Blood glucose values before and after injection of glucose as well as the area under the curve were not different at any time point between GPx7 KO and WT mice (figure 18d, e). To assess insulin tolerance GPx7 KO and WT mice were injected with 0.5 IU/kg BW Insulin. No difference in insulin tolerance 15, 30, 60 and 120 min after insulin injections was observed (figure 18f). In female global GPx7 KO mice the body weight was similar when compared to the WT control mice (figure 18g, h) but a tendency towards a decrease in FI (figure 18i) was observed. Also here group housing of mice was the reason for the low n number of two for the FI measurement. For reliable results, food intake of more cages needs to be measured.

3.2.2 Global deletion of GPx7 increases body weight and impairs glucose tolerance in HFD-fed male mice

HFD feeding is a broadly used challenge to expose protective or harmful effects of genes in weight control in mice, and is known to be an additional stressor to trigger hypothalamic inflammation. Depletion of the stress sensor GPx7 is known to lead to higher ROS levels in tissues. Accordingly, an increase in body weight upon HFD feeding in GPx7 globally depleted mice was hypothesized.

Higher BW in male global GPx7 knockout mice compared to their wildtype controls could be observed in two independent cohorts fed with HFD (45% kcal from fat; figure 19a, b). GPx7 knockout mice displayed similar FI compared to their respective control mice (figure 19c), but for a final statement more cages would need to be included to increase the number. Impaired glucose tolerance was observed in male GPx7 global KO mice after 8 weeks of HFD feeding (figure 19d) with a corresponding higher area under the curve value (figure 19e). After 20 weeks of HFD feeding in GPx7 KO and WT mice glucose tolerance was impaired to a similar extent (figure 19f) and area under the curve values did not differ (figure 19h left bars). The possible importance of differentially regulated gut hormones in GPx7 KO mice was tested with an oral glucose tolerance test after 20 weeks of HFD feeding. Similar glucose tolerance with similar area under the curve values was observed in GPx7 KO and WT mice (figure 19g, h right bars). Insulin values, measured in the context of the oGTT tended to be higher in GPx7 knockout mice at time points 0 and 60 min after an oral glucose challenge ($p=0.055$, $p=0.053$; figure 19i), but no differences in HOMA-IR values were observed (figure 19j).

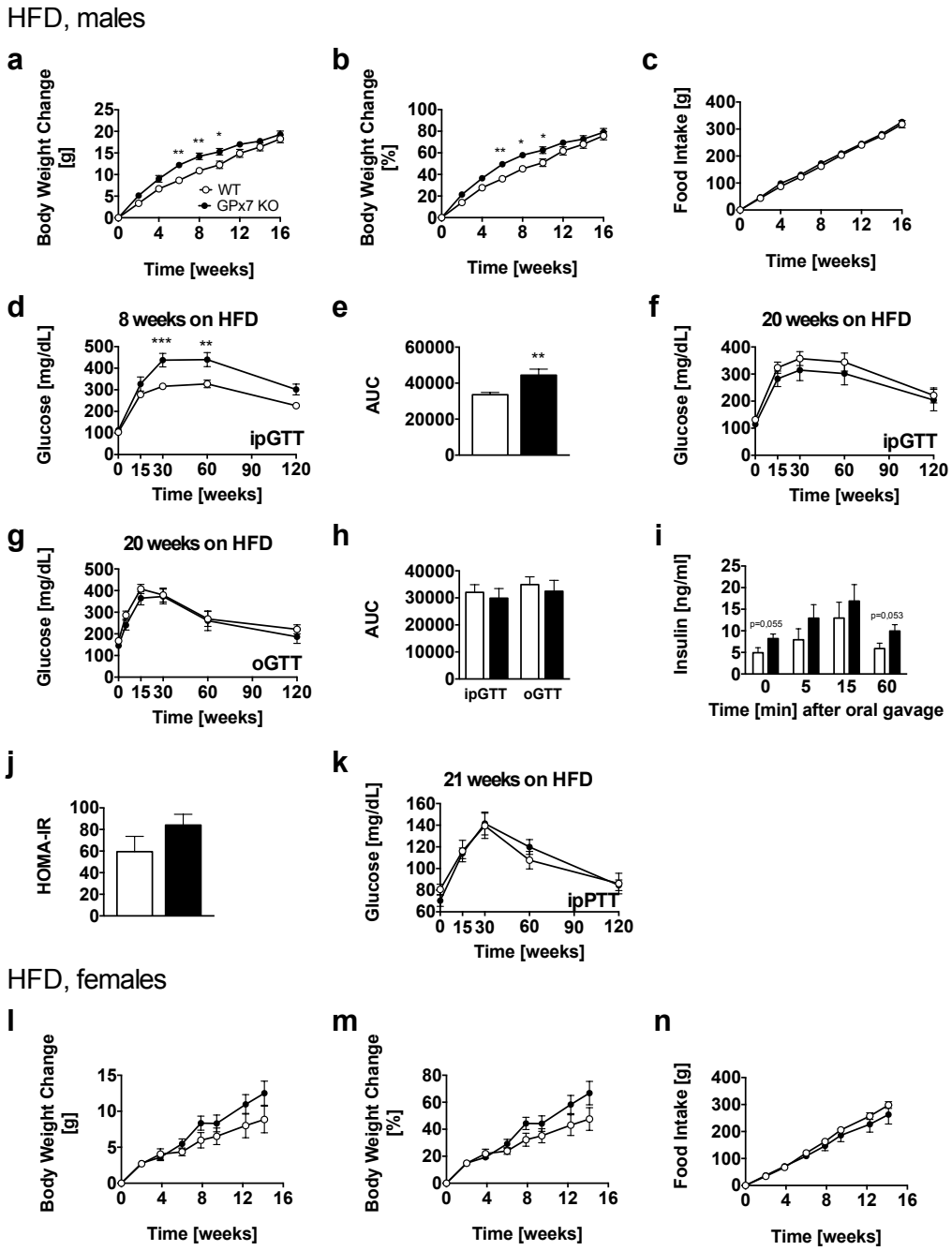

Figure 19. Global GPx7 ablation increases body weight and impairs glucose tolerance upon high fat diet feeding in male mice

Male **(a-k)** and female **(l-n)** whole body GPx7 KO and WT C57BL/6J control mice were fed with HFD for the indicated time periods. Body weight gain was assessed in gram **(a)** and percent **(b)** and food intake was measured in a sub-cohort **(c)**. Glucose tolerance tests were performed 8 weeks **(**i.p., 2 g/kg body weight; **d)** and 20 weeks **(**i.p., 1.5 g/kg body weight; **f)** after the start of HFD feeding. Corresponding area under the curve plots are shown in panels **(e, h** left bars**)**. Oral glucose tolerance tests (oGTT) were performed in a cohort fed for 20 weeks with HFD **(**2 g/kg body weight; **g)**. The corresponding AUC plot is shown in panel **(h,** right bars**)**. Plasma insulin was measured before and 5, 15 and 60 min after the oral administration of glucose within the oGTT **(i)**. Fasting glucose and insulin levels from panels (g, i) were used to calculate the HOMA-IR **(j)**. Glucose levels were measured after a pyruvate tolerance test (PTT) in a sub-cohort of mice **(**i.p., 0,75 g/kg BW pyruvate, **k)**. In female mice fed with HFD for 14 weeks, body weight in gram **(l)** and percent **(m)** and food intake **(n)** were assessed.

Mean +/- SEM; n=32 WT, 28 KO mice (a, b); n=3 WT, 2 KO (c); n=8 WT, 7 KO (d, e); n=10 WT, 7 KO (f, h left panel); n=8 WT, 8 KO (g, h right panel); n=8 WT, 8 KO except for the time point 15 min, were 1 WT and 1 KO animal could not be measured within the range of the ELISA and therefore had to be excluded (i); n=8 WT, 8 KO (j); n=7 WT, 8 KO (fasting glucose levels of one mouse were extremely high and the value was identified as a significant outlier by the Grubbs' test, thus the mouse was excluded) (k); n=12 WT, 11 KO (l, m); n=4 WT, 4 KO (n). 2-way ANOVA: panel a, b, d, f, g, k, l, m, n; unpaired two-tailed students t-test: panel e, h, i, j; no statistics were applied for sub-graph c due to low n-number. *P<0.05; **P<0.01; ***P<0.001.

Pyruvate tolerance did not differ between genotypes (figure 19k). HFD-fed female GPx7 KO and WT mice showed the same propensity to develop obesity (figure 19l, m) and displayed no difference in food intake (figure 19n).

3.3 GPx7 ablation decreases energy expenditure in mice fed with high fat diet

Changes in energy expenditure or locomotor activity may translate into changes in body weight. Indirect calorimetric measurements were applied to chow and HFD-fed GPx7 wildtype and knockout mice to assess whether a decrease in energy expenditure and/or in locomotor activity contribute to the higher body weight in GPx7 knockout mice on HFD. In parallel, food intake was assessed by scales integrated into the calorimetry cages.

Overall cumulative food intake did not differ between genotypes (data not shown). During chow diet feeding, decreased food intake in the light phase in GPx7 global KO mice was observed, while no changes in feeding behavior in the night were detected. HFD feeding resulted in no changes in food intake in the light and in the dark phase (figure 20a, b). ANCOVA analysis with body weight as covariate showed a tendency towards lower food intake ($F = 4.505$, $p = 0.055$; supplementary table 1) in the light phase when mice were fed with chow diet. HFD feeding resulted in a significantly lower food intake during the day ($F = 4.838$, $p = 0.048$; supplementary table 1) and a significant higher food intake during the night ($F = 25.373$, $p \leq 0.0005$; supplementary table 1) in GPx7 knockout animals when tested with ANCOVA and when body weight was chosen as a covariate.

The RER is calculated by dividing the carbon dioxide production (VCO_2) by the oxygen consumption (VO_2) and is an indirect measurement of the body's substrate preference. The VCO_2/VO_2 ratios differ for carbohydrates, lipids and proteins. RER values close to 1 show evidence that carbohydrates are used as preferred substrates, while values close to 0.7 confirm the gain of energy from fat [106]. In living animals, food intake, body weight and body composition also matter for the outcome of the RER value. Similar RER values were observed for global GPx7 knockout and wildtype mice when day and night were considered together on chow diet and on high fat diet (figure 20c), if body weight, lean mass or FI were used as covariates (supplementary table 1). No difference in the RER value in the dark and light phase on chow and HFD could be detected between genotypes when a t-test was applied (figure 20d). ANCOVA analysis displayed unchanged RER values in chow fed animals in the dark and light phase (supplementary table 1). However, ANCOVA analysis revealed a significantly higher RER value for GPx7 global knockout mice on HFD during the night when body weight or lean mass were used as covariates ($F = 14.537$, $p = 0.002$; $F = 4.851$, $p = 0.048$; supplementary table 1). The absolute mean RER HFD value was 0.90 in GPx7 knockout mice and 0.88 in wildtype mice in the night, which points towards slightly

higher energy utilization from glucose compared to fat in GPx7 knockout animals. RER values for HFD fed KO animals during the day tended to be lower when body weight was used as a covariate (F = 4.096, p = 0.066; supplementary table 1).

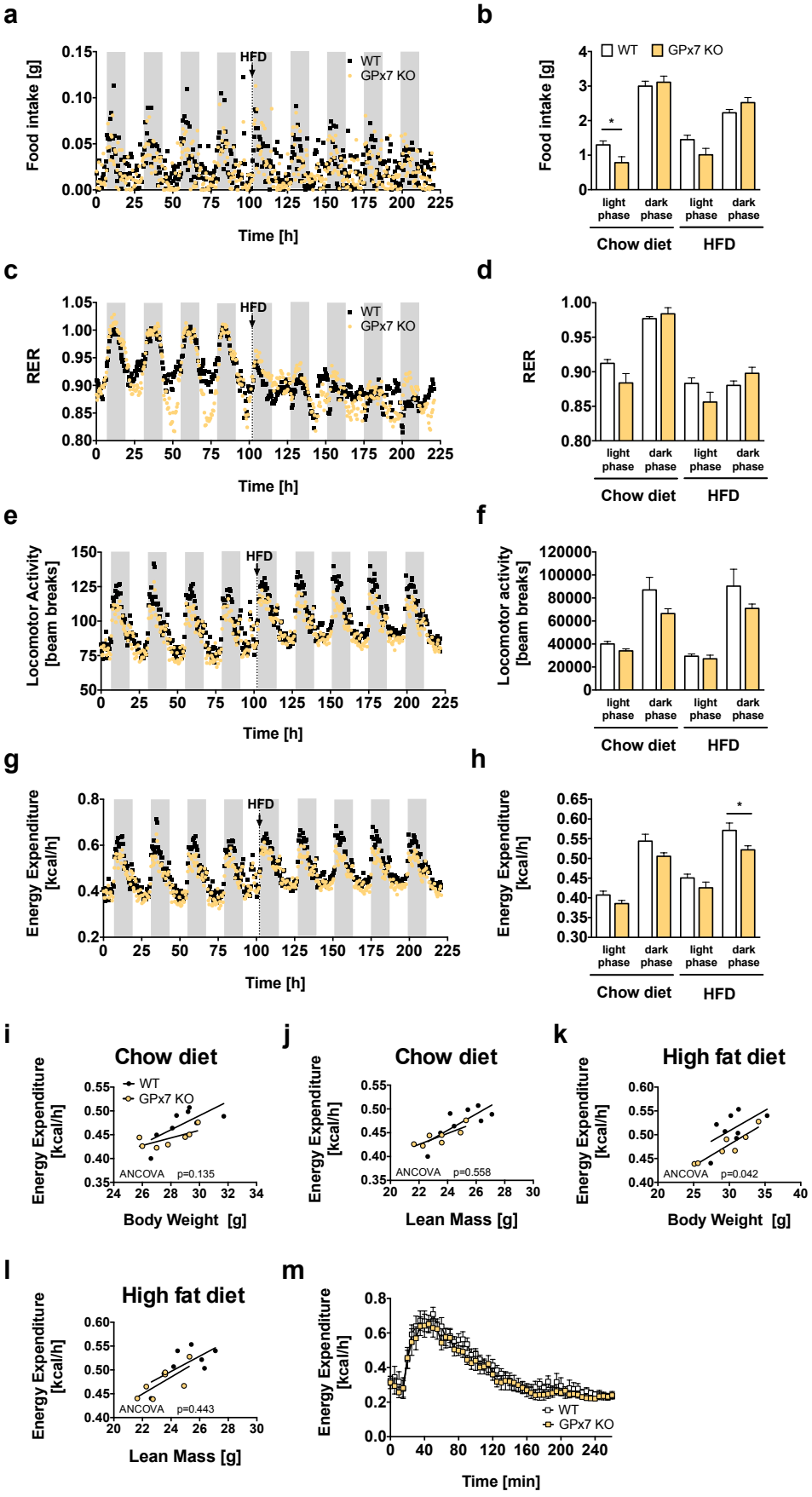

Figure 20. Decreased energy expenditure in global Gpx7 KO mice after a switch from chow to HFD
In indirect calorimetric chambers food intake **(a, b)**, respiratory exchange ratio (RER) **(c, d)**, locomotor activity **(e, f)**, and energy expenditure **(g, h)** were measured on chow (4.25 days) and 45% high fat diet (5 days). Panels a, c, e, g display values over time, panels b, d, f, h represent mean values of the light and dark phase for chow and HFD feeding. Mice were allowed 1 day acclimatization to the HFD before mean values were recorded. Average energy expenditure values were plotted against body weight **(i, k)** or lean mass **(j, l)**. Energy expenditure was measured after injection of 1 µg/g BW norepinephrine at 30°C **(m)**.
Mean +/- SEM; n=8 WT, 7 KO mice (one KO had to be excluded due to sensor error) (a-l); n=6 WT, 7 KO mice (two WT mice had to be excluded due to failed injection) (m). ANCOVA: sub-graphs a, c, e, g, i, j, k, l; 2-way ANOVA: sub-graph m; unpaired two-tailed students t-test: sub-graphs b, d, f, h. Detailed information about p-values and covariates of the ANCOVA can be found in supplementary table 1 (page 79). *P<0.05.

No difference in total locomotor activity between global GPx7 knockout and wildtype mice was observed when body weight or lean mass were used as a covariates, regardless of the diet used (figure 20e, supplementary table 1). Locomotor activity during the day and during the night was similar between genotypes on chow and on HFD when tested with t-test (figure 20f) or ANCOVA (supplementary table 1).

Similar energy expenditure was found for global GPx7 knockout and wildtype mice during the day and during the night on chow diet when tested with t-test (figure 20g, h) and when body weight (figure 20i, supplementary table 1) or lean mass (figure 20j, supplementary table 1) were used as covariates. Interestingly, HFD feeding resulted in a decrease in energy expenditure when body weight was used as a covariate ($F = 5.191$, $p = 0.042$; figure 20k, supplementary table 1), but not if lean mass was used (figure 20l, supplementary table 1). A significant decrease in mean average energy expenditure per night on high fat diet was observed in GPx7 knockout animals when tested with t-test ($p = 0.045$; figure 20h). The decrease in energy expenditure in GPx7 knockout mice may at least in part account for the higher body weight observed in knockout animals. Maximal energy expenditure was measured by injection of 1 µg/g BW norepinephrine and did not differ between genotypes (figure 20m).

3.4 GPx7 ablation affects lipolysis and adipogenesis in white but not brown adipose tissue of global Gpx7 KO mice

3.4.1 Higher adipogenesis, cellular respiration and isoproterenol induced glycerol release in white adipocytes of global Gpx7 KO mice

Higher body weight in GPx7 global knockout mice upon HFD feeding prompted me to measure lipolysis in white adipose tissue. Lipolysis is the catabolic process leading to the breakdown of triglycerides stored in fat cells and to the release of fatty acids and glycerol.

The release of non-esterified free fatty acids (NEFAs) and of glycerol was measured in the serum of GPx7 global knockout and wildtype control mice before and 10 min after the

injection of isoproterenol. Basal and isoproterenol stimulated NEFA levels were identical in both genotypes (p=0.62; p=0.89; figure 21a). Non-stimulated glycerol serum levels displayed no difference between wildtype and knockout mice (p=0.36), while higher glycerol serum levels were observed in GPx7 knockout mice compared to control mice after isoproterenol stimulation (p=0.033; figure 21b).

Glycerol arises from triglycerides, the main form of stored fat. Triacylglycerol (TG) is converted to diacylglycerol (DG), then to monoacylglycerol (MG) and last to glycerol. Glycerol is released into the blood stream and is mostly taken up by the liver, where it is utilized for glycolytic or gluconeogenic pathways. Hormone sensitive lipase (HSL) is a key enzyme in the process of lipolysis. It is able to convert TGs to DGs and more efficiently DGs to MGs [107].

Next, western blotting was applied using antibodies against HSL and phospho-HSL to test whether higher glycerol levels in GPx7 knockout mice are due to an increased activity of HSL. Phosphorylated HSL was up-regulated 20 min after isoproterenol injections in BAT of both WT and GPx7 KO mice (figure 21c, d) and in iWAT of GPx7 KO mice (figure 21f, g), confirming the functionality of the isoproterenol challenge itself. In epididymal WAT phosphorylation of HSL was similar in isoproterenol injected and saline injected mice (figure 21h, i), suggesting that either eWAT is unresponsive to catecholamines, or that the kinetics of catecholamine-induced lipolysis are different to iWAT and BAT. Nevertheless, eWAT featured a significant up-regulation of CCAAT/enhancer binding protein beta (*Cebpb*) after isoproterenol stimulation in GPx7 knockout mice (p=0.035) and basal levels of the beta adrenergic receptor 2 (*A2*) tended to be up-regulated in GPx7 KO mice (p=0.071; figure 21j). In BAT, no clear basal (saline injected) and isoproterenol-stimulated difference in pHSL and HSL protein levels could be detected between genotypes (figure 21c, d). In the iWAT isoproterenol stimulated phosphorylation of HSL tended to be lower in GPx7 knockout mice compared to wildtype isoproterenol stimulated samples but no clear difference could be detected (figure 21f, g). In the eWAT no clear difference in the phosphorylation of HSL was observed between genotypes (figure 21h, i). BAT is a highly thermogenic organ that utilizes free fatty acids (FFAs) from triglycerides as primary substrate for the production of heat. Moreover, FFAs were shown to induce an up-regulation of UCP1 in BAT [108-110]. Significantly up-regulated expression of thermogenic genes *Pgc-1α* (p=0.012) and *Ucp1* (p=0.039) in isoproterenol stimulated GPx7 knockout samples compared to un-stimulated knockout samples was observed. However, enhanced expression did not translate into difference in UCP1 protein levels in KO saline vs. isoproterenol-injected mice. Rather, a decrease in basal UCP1 protein levels (figure 21c, e), and lower basal *Ucp1* mRNA levels were detected in GPx7 knockout mice compared to wildtype controls (p=0.010; figure 21k).

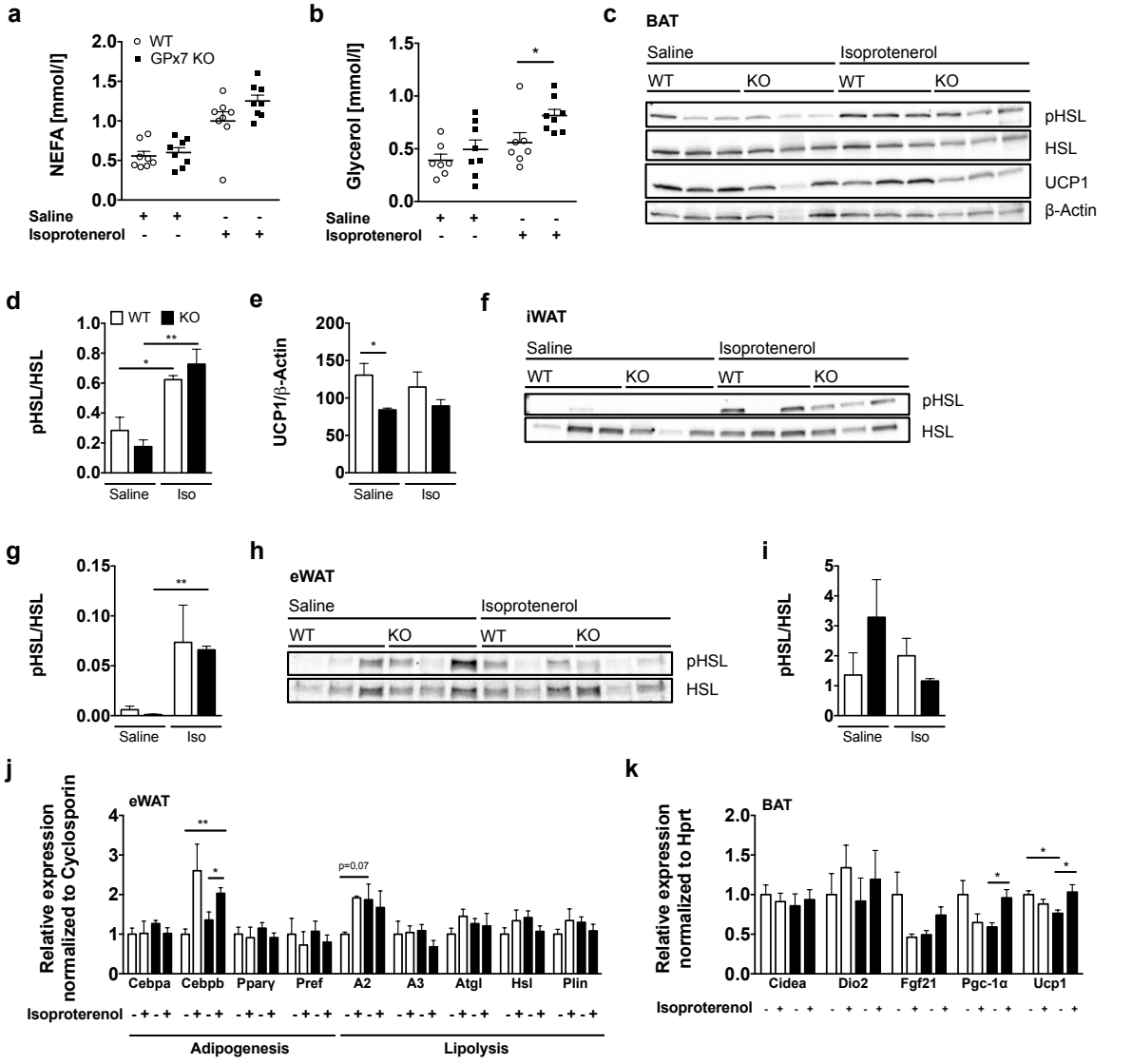

Figure 21. GPx7 ablation enhances isoproterenol stimulated glycerol release

Global GPx7 KO and WT mice were injected with 10 mg/kg BW isoproterenol (Iso) or saline. Non-esterified free fatty acids (NEFAs) **(a)** and glycerol **(b)** were measured in the blood 10 min after injection. 20 min after isoproterenol or saline injections protein levels were assessed. Phospho-HSL (pHSL), total HSL, UCP1 and β-Actin were measured in BAT **(c-e)**. pHSL and HSL were determined in iWAT **(f, g)** and eWAT **(h, i).** Adipogenic and lipolytic genes were assessed in eWAT **(j)** and thermogenic genes in BAT **(k)** of isoproterenol or saline injected mice 20 min after injection.

CCAAT/Enhancer binding protein alpha (*Cebpa*), CCAAT/Enhancer binding protein beta (*Cebpb*), Peroxisome proliferator activated receptor gamma (*Pparγ*), Preadipocyte factor 1 (*Pref*), Beta-2 adrenergic receptor (*A2*), Beta-3 adrenergic receptor (*A3*), Adipocyte triglyceride lipase (*Atgl*), Hormone sensitive lipase (*Hsl*), Perilipin (*Plin*), Cell death-inducing DFFA-like effector A (*Cidea*), Deiodinase, Iodothyronine, Type II (*Dio2*), Fibroblast growth factor 21 (*Fgf21*), Peroxisome proliferator-activated receptor gamma coactivator 1 alpha (*Pgc-1α*), Uncoupling Protein 1 (*Ucp1*).

Mean +/- SEM; n=8 WT, 8 KO (a); n=7 WT, 8 KO (b); n=3 WT saline, 3 KO saline, 3 WT iso, 3 KO iso (c-i); n=4 WT saline, 4 KO saline, 4 WT iso, 4 KO iso, except for *Cebpb* (1 sample in WT iso group had to be excluded), *Pref* (2 samples in the WT saline, 1 sample in the WT iso and 1 sample in the KO saline group had to be excluded), *A2* (2 samples in the WT iso group were excluded), *Atgl* (1 sample in the KO saline group was excluded). Excluded samples were identified as significant outliers with a Grubbs' test (j); n=4 WT saline, 4 KO saline, 4 WT iso, 4 KO iso samples (k). Unpaired two-tailed students t-test: panel a, b, j, k; In graphs d, e, g, i saline WT vs. saline KO, iso WT vs. iso KO, saline WT vs. iso WT and saline KO vs. iso KO were tested with an unpaired two-tailed students t-test. No statistics were applied to the mRNA data set of *A2* WT iso injected group in sub-graph j due to low n number. *P<0.05; **P<0.01.

The higher body weight in GPx7 knockout mice prompted me to clarify whether this was due to increased adipogenesis and changes in cellular respiration. Higher lipid content in primary GPx7 deficient white adipocytes was detected with Oil red O staining on differentiation day 8 (figure 22a, b). No obvious changes in the general morphology of differentiated adipocytes were detected (figure 22c). Peroxisome proliferator activated receptor gamma (PPARγ) protein levels increased with the differentiation in wildtype and knockout cells. However, PPARγ levels in GPx7 depleted cells tended to be higher, especially at days 4, 6 and 8 of differentiation (figure 22d). Notably, GPx7 protein decreases throughout the process of differentiation in primary adipocytes of wildtype mice, and was absent in GPx7 knockout adipocytes (figure 22d). Preliminary Seahorse mitochondrial bioenergetics measurements revealed higher differentiation rates in knockout cells due to higher oxygen consumption rate (OCR) in differentiated GPx7 knockout adipocytes (figure 22e). Moreover, higher isoproterenol-stimulated, ATP-linked and proton leak respiration, and lower coupling efficiency (CE) was observed in GPx7 knockout primary white adipocytes (figure 22f). Overall, these data, although preliminary in nature, indicate that less nutrient energy is converted into ATP and that the energy release into heat is increased in primary white fat GPx7 knockout cells. The higher respiratory capacity in white GPx7 knockout fat cells might be an indication for higher UCP1 levels.

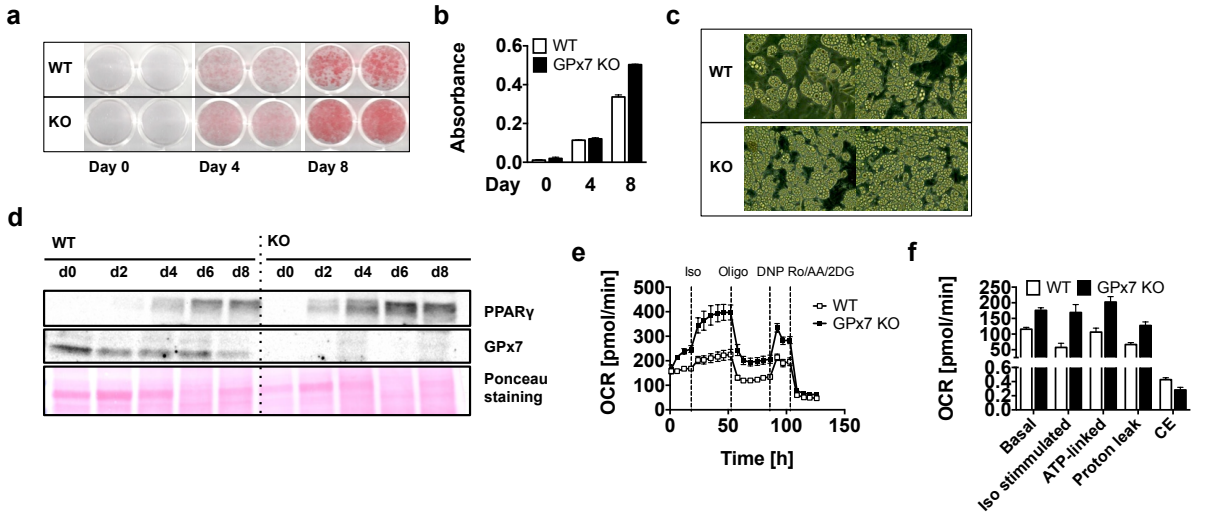

Figure 22. Increased adipogenesis in GPx7 deficient primary white adipocytes
Oil red O staining of primary white adipocytes before (day 0) and 4 and 8 days after the start of the differentiation **(a)**. Oil red O stainings were quantified by measuring the absorbance at 500 nm **(b)**, and the morphology of fully differentiated white subcutaneous wildtype and GPx7 knockout adipocytes were recorded by light microscopy **(c)**. Western blot showing PPARγ and GPx7 protein levels and ponceau staining of undifferentiated (day 0) and differentiated (day 2, 4, 6 and 8) white wildtype and GPx7 knockout subcutaneous adipocytes **(d)**. Oxygen consumption rates (OCRs, time resolved, averaged) in 6-days-differentiated white adipocytes using the XF96 extracellular flux analyzer. OCRs were initially measured under basal conditions, followed by stimulation with isoprotenerol (Iso), oligomycin (Oligo) to block the ATP synthase. Addition of dinitrophenol (DNP) revealed maximum uncoupling capacity, whereas the addition of Rotenone/Antimycine A/2-Deoxy-glucose revealed non-mitochondrial respiration. Coupling efficiency (CE) was calculated as ATP-linked respiration/basal respiration **(e, f)**.
Mean +/- SEM of n=2 technical replicates for WT and GPx7 KO (b); n=1 biological replicate per genotype (d); n=5 technical replicates for WT and KO mice (e, f). No statistical analyses were applied due to low n numbers.

3.4.2 Unimpaired adipogenesis and cellular respiration in brown adipocytes

In contrast to white adipocytes, no differences in differentiation rates between the genotypes in brown adipocytes could be observed. Oil red O staining confirmed similar lipid content in both GPx7 knockout and wildtype cells (figure 23a, b). Similar cell morphologies (figure 23c) and similar PPARγ protein levels were observed during differentiation of wildtype and knockout primary brown adipocytes (figure 23d). Similar to primary white adipocytes, GPx7 protein levels in wildtype cells decreased during the process of differentiation (figure 23d). A seahorse experiment confirmed functional mitochondrial respiration in GPx7 knockout primary brown adipocytes. Unchanged basal respiration corroborated identical differentiation rates in WT and GPx7 KO primary brown adipocytes (figure 23e, f). Decreased ATP linked respiration and a tendency towards higher protein leak respiration as well as a decrease in coupling efficiency could be detected for GPx7 depleted primary brown adipocytes (figure 23e, f). Notably, UCP1 protein levels (figure 23d) were increased in GPx7 knockout cells. Whether this implies that less nutrient energy is converted into ATP in GPx7 deficient cells, thereby allowing more energy to be released as heat, needs to be assessed in independent Seahorse replication experiments.

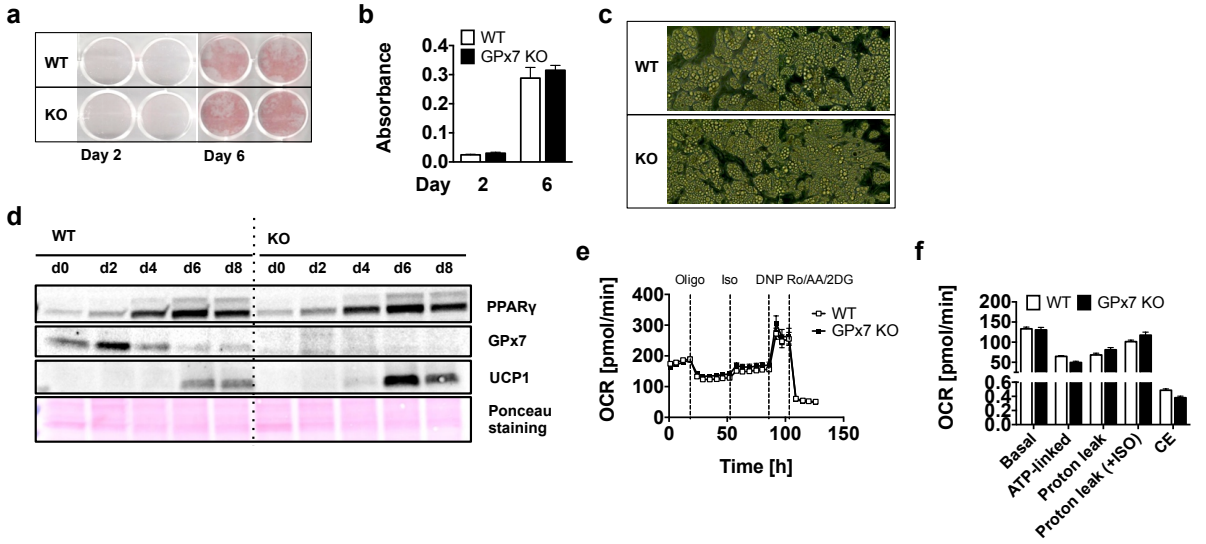

Figure 23. Unimpaired adipogenesis in primary brown GPx7 ablated adipocytes
Oil red O staining of primary brown adipocytes 2 and 6 days after the start of the differentiation **(a)**. Oil red O staining was quantified by measuring the absorbance at 500 nm **(b)**. Morphology of fully differentiated brown adipocytes from global GPx7 KO and WT mice **(c)**. Western blot showing PPARγ, GPx7 and UCP1 protein levels and ponceau staining of undifferentiated (day 0) and differentiated (days 2, 4, 6 and 8) brown adipocytes from WT or GPx7 KO mice **(d)**. Oxygen consumption measurement (time resolved, averaged) in brown, day 6 differentiated adipocytes using the XF96 extracellular flux analyzer. OCRs were initially measured under basal conditions, followed by stimulation with oligomycin (Oligo) to block the ATP synthase and stimulation with isoprotenerol (Iso). Addition of dinitrophenol (DNP) revealed maximum uncoupling capacity, whereas the addition of Rotenone/Antimycine A/2-Deoxy-glucose revealed non-mitochondrial respiration. Coupling efficiency (CE) was calculated as ATP-linked respiration/basal respiration **(e, f)**.
Mean +/- SEM; n=2 technical replicates for WT and KO (b); n=2 biological replicates (d); n=5 technical replicates for WT and KO mice (f; g). No statistics applied.

3.5 Distinct phosphorylation of insulin signaling proteins in soleus, eWAT and liver in GPx7 KO and WT mice after acute stimulation with insulin

Diabetes is mostly accompanied with impairments in insulin signaling. I here applied an acute insulin challenge to DIO GPx7 WT and KO mice to determine whether GPx7 deficiency affects the regulation of proteins involved in insulin signaling.

5 IU/kg BW insulin were injected in WT and GPx7 deficient mice and tissues were collected 8 min later. In liver tissue, regardless of the genotype, a general up-regulation of phospho-protein kinase B alpha (pAKT; Ser473) and phospho-S6 (Ser235/236) could be detected in insulin-injected mice (figure 24a). A tendency, although not significant, towards a reduction in phosphorylated AKT (Ser473) was detected in insulin-injected GPx7 KO mice compared to their WT insulin-injected controls (p=0.195), while phospho-S6 (Ser235/236) samples remained unchanged between genotypes (figure 24a-c). In the soleus, which consists mainly of red muscle fibers, a general induction of pAKT (Ser473) was observed in WT and GPx7 KO mice upon insulin injection, but no difference between genotypes could be detected (figure 24d, e) and no induction of phospho-ribosomal protein S6 (pS6) (Ser235/236) after insulin injection was observed (figure 24d, f). Different timing might be necessary to detect insulin-induced changes in phosphorylation profiles for S6. In the eWAT phosphorylation of AKT (Ser473) was increased in insulin treated WT and GPx7 KO mice samples (figure 24g), but no difference between genotypes could be detected (figure 24g, h).

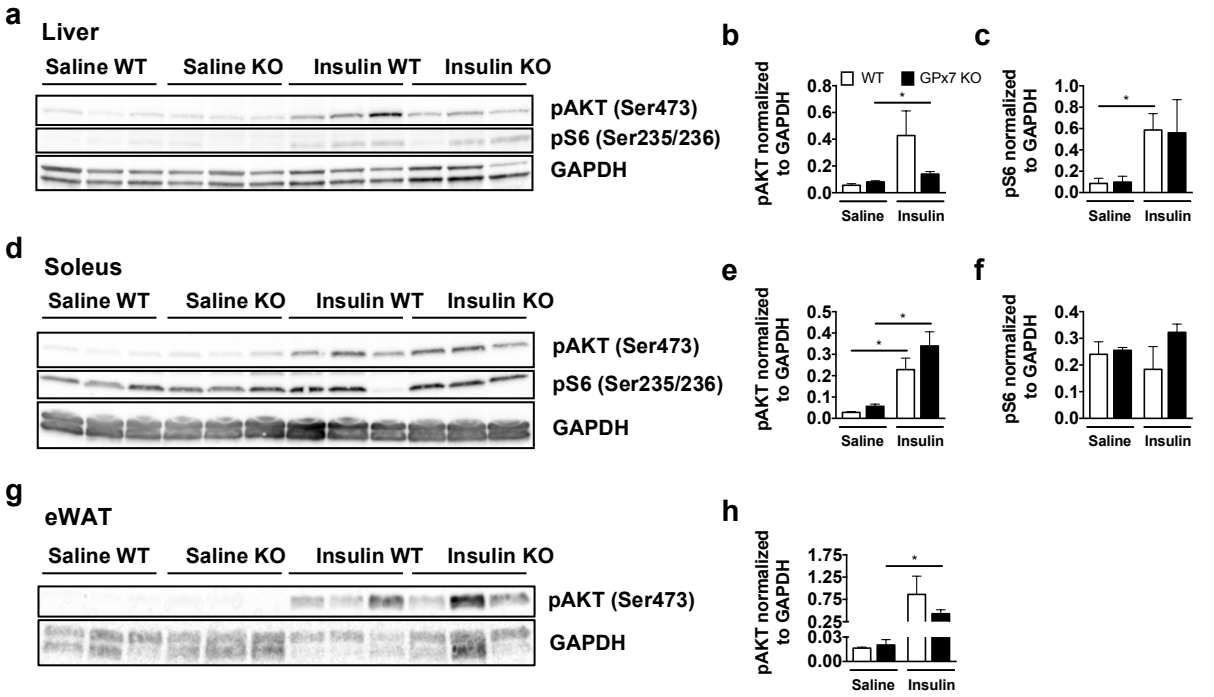

Figure 24. Disparate effects of acute insulin treatment on liver, soleus and eWAT in GPx7 KO mice
Insulin signaling was assessed by i.p. injections of 5 IU insulin/kg body weight in mice fed with HFD (45% kcal from fat) for 29 weeks. Mice were sacrificed 8 min after injection. Phosphorylation of Akt (Ser473) and of S6 (Ser235/236) were measured in liver **(a-c)** and soleus **(d-f)**. In eWAT phospho-Akt (Ser473) **(g, h)** was determined. Glyeraldehyde 3-phosphate dehydrogenase (GAPDH) was used as a housekeeping gene. Quantification of western blots is shown in panels b, c: liver, e, f: soleus, h: eWAT.
Mean +/- SEM; n=3 WT saline, 3 WT insulin, 3 KO saline, 3 KO insulin samples. Unpaired two-tailed students t-test was applied to the sub-graphs b, c, e, f, h; WT or KO saline vs. insulin and saline or insulin WT vs. KO were statistically tested.

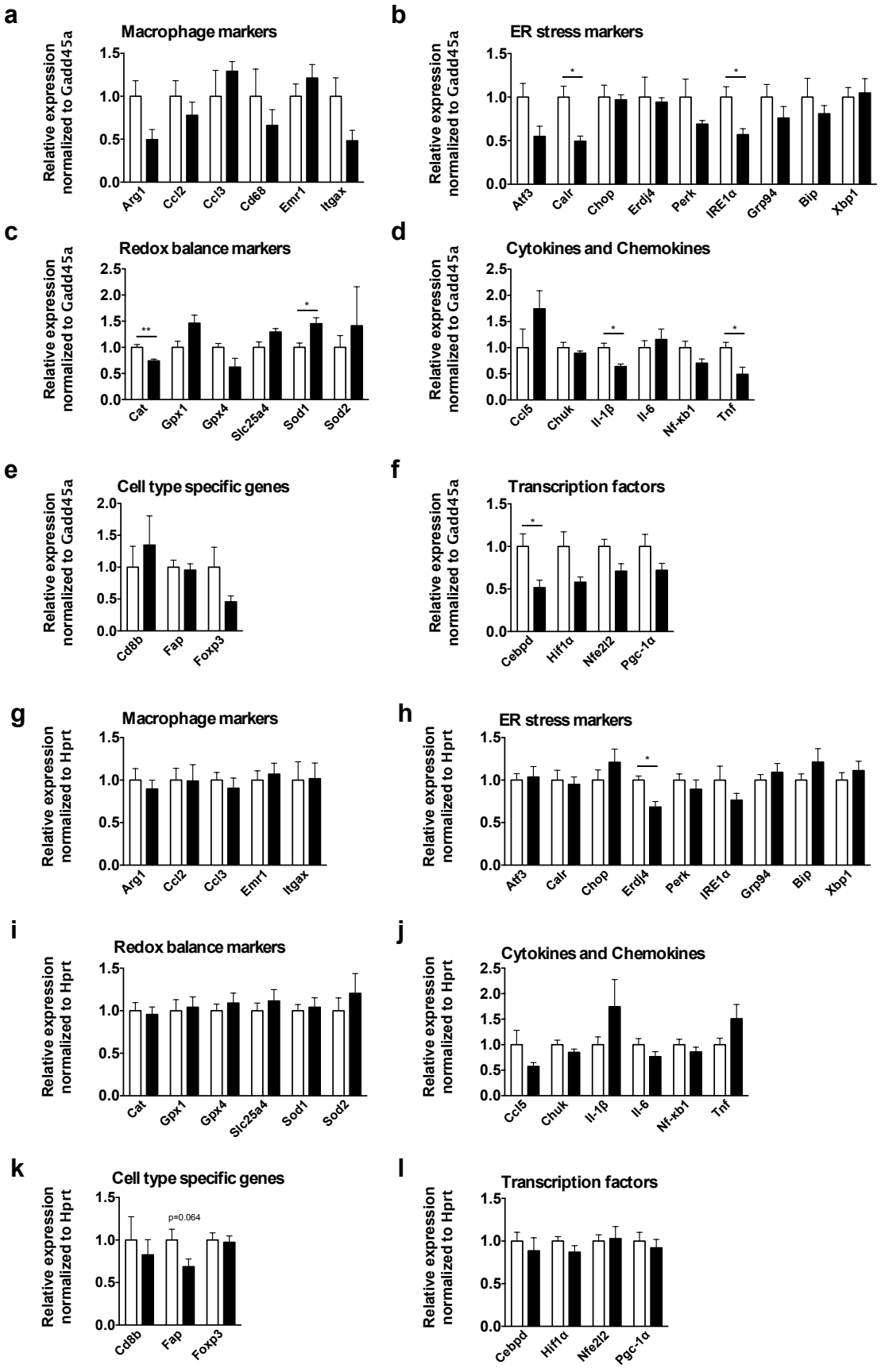
a
Macrophage markers
Relative expression normalized to Gadd45a
Arg1
Ccl2
Ccl3
Cd68
Emr1
Itgax
b
ER stress markers
Atf3
Calr
Chop
Erdj4
Perk
IRE1α
Grp94
Bip
Xbp1
c
Redox balance markers
Cat
Gpx1
Gpx4
Slc25a4
Sod1
Sod2
d
Cytokines and Chemokines
Ccl5
Chuk
Il-1β
Il-6
Nf-κb1
Tnf
e
Cell type specific genes
Cd8b
Fap
Foxp3
f
Transcription factors
Cebpd
Hif1α
Nfe2l2
Pgc-1α
g
Macrophage markers
Relative expression normalized to Hprt
h
ER stress markers
i
Redox balance markers
j
Cytokines and Chemokines
k
Cell type specific genes
p=0.064
l
Transcription factors

Figure 25. Regulation of genes in hypothalami of lean and obese GPx7 global KO and WT mice
Sets of genes were measured in the hypothalami of 10-month-old global GPx7 KO and WT mice fed with normal rodent chow diet **(a-f)** or high fat diet **(g-l)**. The **macrophage markers**, arginase 1 (*Arg1*), chemokine (C-C motif) ligand 2 (*Ccl2*), chemokine (C-C motif) ligand 3 (*Ccl3*), scavenger receptor class D, member 1 (*Cd68*), EGF-like module-containing mucin-like hormone receptor-like 1 (*Emr1*), integrin subunit alpha X (*Itgax*) were measured with qPCR **(a, g)**. The following **ER-stress markers** were measured: Activating transcription factor 3 (*Atf3*), calreticulin (*Calr*), CCAAT/enhancer-binding protein homologous protein (*Chop*), endoplasmic reticulum-localized DnaJ 4 (*Erdj4*), eukaryotic translation initiation factor 2 alpha kinase 3 (Perk), inositol-requiring enzyme 1 α (*Ire1α*), glucose-regulated protein, 94 kDa (*Grp94*), heat shock protein family A (Hsp70) member 5 (*Bip*), X-box binding protein 1 (*Xbp1*) **(b, h)**. The following **redox balance markers** were analyzed: Catalase (*Cat*), glutathione peroxidase 1 (*GPx1*), glutathione peroxidase 4 (*GPx4*), solute carrier family 25 member 4 (*Slc25a4*), superoxide dismutase 1 (*Sod1*), superoxide dismutase 2 (*Sod2*) **(c, i)**. The following **cytokine and chemokine markers** were assessed: C-C motif chemokine ligand 5 (*Ccl5*), conserved helix-loop-helix ubiquitous kinase (*Chuk*), interleukin-1 beta (*Il-1β*), interleukin 6 (*Il-6*), nuclear factor kappa B subunit 1 (*Nf-κb1*), tumor necrosis factor (*Tnf*) **(d, j)**. The following **cell type specific genes** were measured: T lymphocyte surface glycoprotein beta chain (*Cd8b*), fibroblast activation protein alpha (*Fap*), forkhead box p3 (*Foxp3*) **(e, k)**. The following **transcription factors** were assessed: CCAAT/Enhancer binding protein delta (*Cebpd*), hypoxia inducible factor 1 alpha subunit (*Hif1α*), nuclear factor, erythroid 2 like 2 (*Nfe2l2*), peroxisome proliferator-activated receptor gamma, coactivator 1 alpha (*Pgc-1α*) **(f, l)**.
Genes with Ct-values higher than 32,5 were excluded. Genes with Ct-values between 30 and 32,5 were: for chow diet samples: *Arg1*, *Ccl2*, *Ccl3*, *Cd68*, *Cd8b*, *Fap*, *Foxp3*, *Il-1β*, *Il-6*, *Itgax*, *Tnf*. Ct-values between 30 and 32,5 in hypothalami of HFD fed mice were detected for the following genes: *Arg1*, *Cd8b*, *Fap*, *Foxp3*, *Il-1β*, *Il-6*, *Itgax*, *Tnf*.
Mean +/- SEM; n=4 WT, 4 KO mice, except for *Cd68* panel a, one WT animal had to be excluded (a-f); n=8 WT, 8 KO mice, except for *Ccl2* panel g, one WT and one KO mouse had to be excluded; for *Sod2* panel i, one WT animal had to be excluded (g-l). Excluded animals were defined as significant outliers using the Grubbs' test. Unpaired two-tailed students t-test. *P<0.05; **P<0.01.

3.6 Differential regulation of key hypothalamic regulators of energy and glucose homeostasis

3.6.1 Regulation of mRNA levels of key hypothalamic regulators in chow-fed mice

To assess the involvement of GPx7 in the hypothalamic control of energy and glucose homeostasis, macrophage-, ER-stress- and redox balance- markers, cytokines and chemokines, cell type specific genes and transcription factors were measured in the hypothalamus of global GPx7 knockout vs. wildtype mice. Markers were first tested in lean mice fed with normal rodent chow diet (figure 25a-f). Differential expression profiles, in this case down regulation, could be detected for the ER-stress markers calrediculin (*Calr*) as well as of inositol-requiring enzyme 1 α (*Ire1α*) (figure 25b). The redox balance marker catalase (*Cat*) was down-regulated and superoxide dismutase 1 (*Sod1*) up-regulated (figure 25c) in GPx7 depleted hypothalami. Down-regulation was observed in the cytokines *Il-1β* and *Tnf* (figure 25d) as well as for the transcription factor CCAAT/Enhancer Binding Protein Delta (*Cebpd*) (figure 25f). None of the observed macrophage markers (figure 25a) and cell type specific genes (figure 25e) were regulated.

3.6.2 Regulation of mRNA levels of key hypothalamic regulators in HFD-fed mice

In the hypothalami of obese mice fed with HFD (45% kcal from fat) for 29 weeks, no differences in marcrophage- and redox balance markers, cytokines, chemokines and transcription factors was observed between genotypes (figure 25g, i, j, l). The ER-stress marker *Erdj4* was significantly down-regulated in hypothalami of GPx7 knockout mice (figure 25h) and a strong tendency towards down-regulated fibroblast activation protein alpha (*Fap*; p=0.064), a cell surface bound glycoprotein, was observed in GPx7 knockout mice (figure 25k).

3.7 GPx7 ablation in the hypothalamus leads to impaired glucose tolerance and hypothalamic inflammation

Next, it was assessed whether the increase in body weight in GPx7 knockout mice is mediated via the hypothalamus by generating mice lacking GPx7 specifically in Nkx2.1 expressing cells. Mice containing a loxP-flanked GPx7 sequence were crossed with the Nkx2.1-Cre line, resulting in deletion of the floxed (fl) GPx7 alleles in brain interneuron progenitors and pituitary as well as in peripheral Nkx2.1 expressing cells of the developing lung and thyroid gland [111]. Nkx2.1 was shown to be broadly expressed in $GABA^+$, NPY^+, $POMC^+$ and tyrosine hydroxylase (TH^+) cells as well as in tanycytes in the ARC [112].

No difference in body weight between GPx7;Nkx2.1-Cre KO mice and WT control mice was observed in 10 weeks old male mice on chow diet (figure 26a). A tendency towards an increase in body weight of GPx7;Nkx2.1 KO mice compared to WT mice was detected when mice were fed with HFD (45% kcal from fat; figure 26b, c). Fat and lean mass were not different before HFD feeding, but a strong tendency towards lower percentage lean (p=0.096) and higher percentage fat mass (p=0.071) in GPx7;Nkx2.1-Cre KO mice was observed when mice were fed for 21 weeks with HFD (figure 26d). Food intake was not different between genotypes (figure 26e), but higher n numbers are needed for a final assessment. A strong impairment of glucose tolerance in GPx7;Nkx2.1 KO mice especially 60 min after the injection of glucose was observed (figure 26f). The corresponding area under the curve value was significantly increased in GPx7;Nkx2.1 KO mice, respectively (figure 26g). Results of the insulin tolerance test were determined by higher basal fasting blood glucose levels observed in knockout animals (figure 26h, i). No differences, although close to significance, in insulin tolerance could be detected, when basal fasting glucose values were normalized to 1 (p=0.065, figure 26j, k). Fasting blood glucose levels were significantly increased 8 and 10 weeks after high fat diet feeding in GPx7;Nkx2.1 KO mice, but differences disappeared after 14 weeks of HFD feeding due to wildtype mice increasing

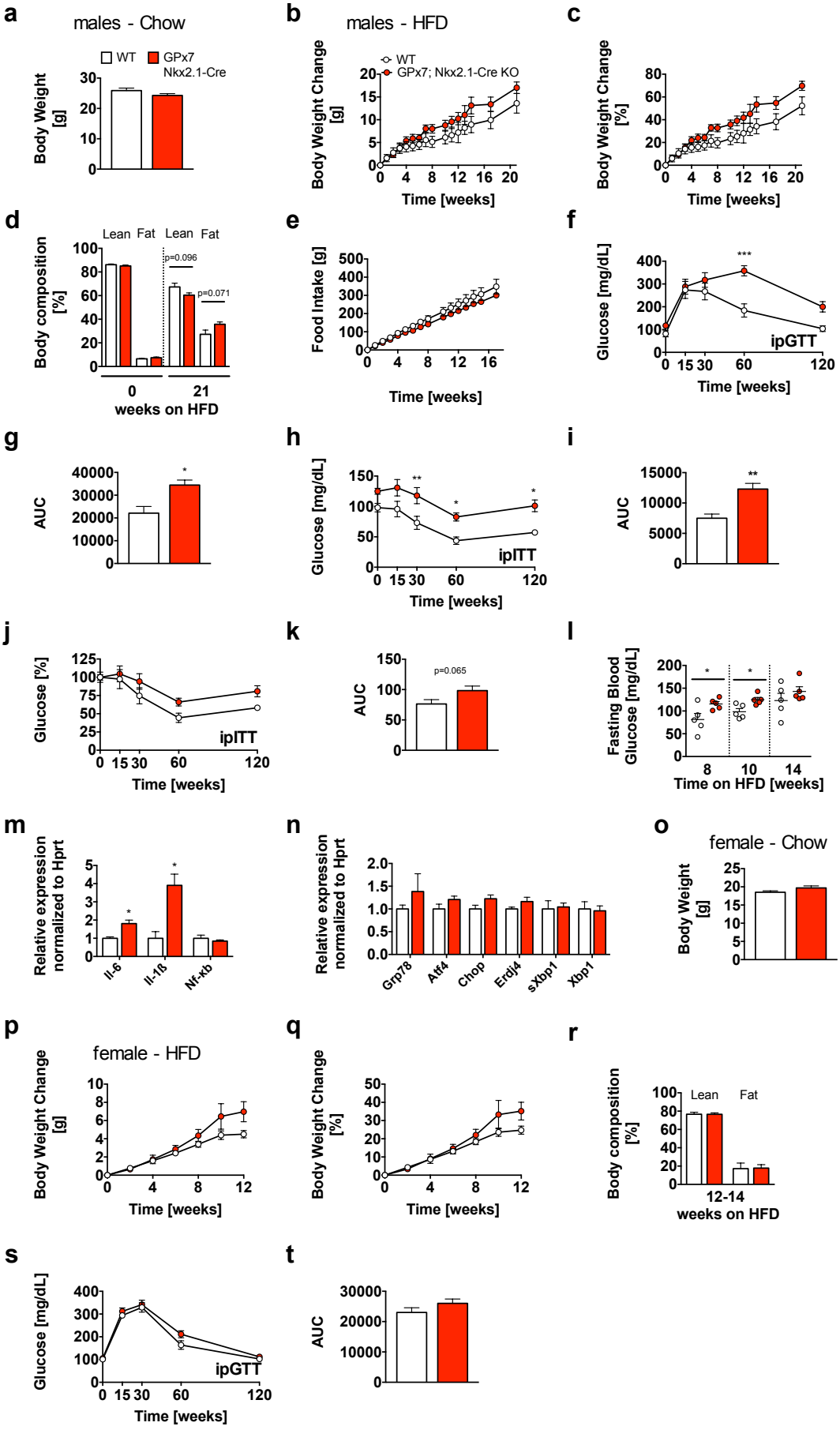
a
males - Chow
WT
GPx7 Nkx2.1-Cre
Body Weight [g]
b
males - HFD
WT
GPx7; Nkx2.1-Cre KO
Body Weight Change [g]
Time [weeks]
c
Body Weight Change [%]
Time [weeks]
d
Lean Fat Lean Fat
p=0.096
p=0.071
Body composition [%]
0
21
weeks on HFD
e
Food Intake [g]
Time [weeks]
f
Glucose [mg/dL]
ipGTT
Time [weeks]
g
AUC
h
Glucose [mg/dL]
ipITT
Time [weeks]
i
AUC
j
Glucose [%]
ipITT
Time [weeks]
k
AUC
p=0.065
l
Fasting Blood Glucose [mg/dL]
Time on HFD [weeks]
m
Relative expression normalized to Hprt
Il-6
Il-1ß
Nf-κb
n
Relative expression normalized to Hprt
Grp78
Atf4
Chop
Erdj4
sXbp1
Xbp1
o
female - Chow
Body Weight [g]
p
female - HFD
Body Weight Change [g]
Time [weeks]
q
Body Weight Change [%]
Time [weeks]
r
Lean
Fat
Body composition [%]
12-14
weeks on HFD
s
Glucose [mg/dL]
ipGTT
Time [weeks]
t
AUC

Figure 26. GPx7;Nkx2.1-Cre KO mice display impaired glucose tolerance
Body weight of male GPx7;Nkx2.1 knockout mice and their respective controls at the age of 10 weeks on chow diet **(a)**. HFD (45% kcal from fat) feeding was started at an age of 10 weeks, lasting for 21 weeks. Body weight changes in gram **(b)** and percent **(c)**, body composition before and after 21 weeks of HFD feeding **(d)** and food intake **(e)**. Glucose tolerance tests **(**2 g/kg body weight glucose, i.p.; **f)** were performed after 8 weeks of HFD feeding; corresponding area under the curve (AUC) plot **(g)**. Insulin tolerance test **(**ITT; 0.75 IU/kg body weight insulin, i.p.; **h)** were conducted after 10 weeks of HFD feeding; corresponding AUC plot **(i)**. Blood glucose levels of the insulin tolerance test shown in panel g were baseline corrected **(j)**; corresponding AUC plot **(k)**. 6-h fasting blood glucose levels after 8 (within the GTT, data shown in panel e), 10 (within the ITT, data shown in panel g) and 14 weeks of HFD feeding **(l)**. Inflammatory **(m)** and ER-stress markers **(n)** were measured in male GPx7;Nkx2.1-Cre and WT mice 21 weeks after the start of the HFD feeding: Interleukin 6 (*Il-6*), interleukin-1 beta (*Il-1β*), nuclear factor kappa B subunit 1 (*Nf-κb1*), glucose-regulated protein, 78 kDa (*Grp78*), activation transcription factor 4 (*Atf4*), CCAAT/enhancer-binding protein homologous protein (*Chop*), endoplasmic reticulum DNA J domain-containing protein 4 (*Erdj4*), Spliced X-box-binding protein 1 (*sXBP1*), X-box-binding protein 1 (*Xbp1*). Body weight of female GPx7;Nkx2.1-Cre and WT mice at the age of 8 weeks on chow diet **(o)**. HFD (45% kcal from fat) feeding was started in the age of 8 weeks. Body weight change in gram **(p)** and percent **(q)** and body composition 12-14 weeks after the start of HFD feeding **(r)**. A GTT was performed in HFD-fed female mice (2 g/kg body weight glucose i.p.; **s**); corresponding AUC plot **(t)**.
Mean +/- SEM; n=5 WT, 5 KO animals (a, b, c, d, f, g, h, i, j, k, l); n=2 WT, 2 KO animals (e); n=3-4 WT, 5 KO animals (m, n); n=12 WT, 7 KO mice (o, p, q); n=7 WT, 5 KO (r); n=10 WT, 7 KO mice (s, t); 2-way ANOVA – panels b, c, f, h, j, p, q, s; unpaired two-tailed students t-test - panels a, d, g, i, k, m, n, o, r, t. No statistics were applied to panel e due to low n number. *P<0.05; **P<0.01; *** P<0.001.

their fasting glucose levels to the levels observed in GPx7;Nkx2.1 knockout mice (figure 26l). qPCR analysis in the hypothalamus of male WT and GPx7 KO mice revealed hypothalamic inflammation, i.e. an up-regulation of *Il-6* and *Il-1β* in GPx7 deficient mice (figure 26m), but unchanged levels of key regulators of ER-stress (figure 26n). Female GPx7;Nkx2.1 KO mice displayed the same tendency for increased diet-induced obesity compared to WT mice (figure 26p, q), and unperturbed body composition (figure 26r). Glucose excursions in a GTT, and AUC levels were similar between genotypes for female mice on HFD (figure 26s, t).

IV Discussion

The unabated obesity and type 2 diabetes pandemic demands a better understanding of mechanistic underpinnings underlying deregulated metabolic control and, built upon this, novel therapeutic intervention strategies.

Data generated in the first project of this thesis adds fundamental and novel results to the field of medical obesity treatment, by proving evidence that the natural compound celastrol does not decrease body weight in mice by activating thermogenesis via UCP1. Furthermore it is shown in this thesis that functional signaling of the hunger- and satiety regulating hormone leptin is necessary for the weight lowering potential of celastrol. However, the exact signaling pathways for celastrol action remain unknown and further research is warranted.

The second and third project of the thesis add novel insights to the field of diabetes and obesity research by focusing on the impact of single proteins on aspects of diabetes and obesity development. Consumption of diets with high fat content leads to inflammation as well as to changes in astrocytic number and morphology in the hypothalamus, which is a center for the regulation of food intake and energy expenditure. This thesis provides novel evidence that the absence or presence of the protein calcineurin impacts astrocytic numbers in the hypothalamus. Calcineurin deficient mice were shown to not gain body weight when fed with a diet containing high amounts of fat. Future studies build upon my thesis should delineate whether the lack of HFD-induced astrocytosis in calcineurin deficient mice is causally linked with the protection of diet-induced obesity.

With a third project, the thesis uncovers an important role for GPx7 in the regulation of energy and glucose homeostasis. The impact of hypothalamic GPx7 deletion appears to specifically affect glucose homeostasis, whereas peripheral GPx7 deletion appears to drive body adiposity via decreased energy expenditure and increased adipogenesis. Future studies should expand the characterization of GPx7 tissue-specific mouse models in metabolically active tissues to dissect the distinct roles of GPx7 as putative oxidative stress sensor in neuronal subpopulations and/or tissues such as brown adipose tissue, muscle or liver.

In the following, results of the three projects will be discussed in detail.

1 Impact of celastrol on body weight and pathways, governing glucose and energy homeostasis

1.1 Celastrol drives body weight loss via a reduction in food consumption

My data clearly shows that celastrol drives body weight loss via a reduction in food consumption. Interestingly, the decrease in food intake after celastrol administration accompanied by diminished locomotor activity was time-delayed, i.e. occurring 7 to 12 hours after celastrol administration in the second half of the dark phase. Decreased food intake in the last hours of the night was further accompanied by diminished locomotor activity. At present, little is known on the phamacokinetic properties and mechanistic roles of celastrol that could explain the time shift in its efficacy. Celastrol action may require degradation of the parent compound to an active metabolite. The time-delayed efficacy of celastrol may also indicate slow transport kinetics into the CNS. Alternatively, celastrol may require a time-shifted induction of extensive gene programs or secretion of hormones responsible for satiety or gastric emptying. Last, celastrol may also target proteins with a circadian expression pattern that are most active in the second half of the night.

1.2 Celastrol-induced body weight loss is independent of UCP1

Substantial amounts of energy can be burned by BAT via UCP1-mediated thermogenesis. In addition, BAT's high capacity for insulin-stimulated glucose uptake makes it an interesting target for anti-obesity and anti-diabetes drugs [113]. Celastrol was recently shown to induce the transcriptional regulators PGC-1α and HSF1, ultimately leading to UCP1-induced BAT activity and iWAT browning as well as enhanced expression of mitochondrial genes in skeletal muscle [17]. In line with Ma and colleagues, in my studies I detected up-regulation of *Ucp1* mRNA levels in BAT and increased *Hsf1* and *Ucp1* expression in iWAT of obese mice upon celastrol treatment. However, treatment of UCP1 KO mice with celastrol showed comparable BW loss in KO and WT mice, indicating that UCP1 is not involved in the body weight-lowering effects of celastrol. Increased *Ucp1* expression in our mice may rather result from elevated levels of reactive oxygen species [114], which were shown to be induced by celastrol treatment [115-119]. In contrast to my observation of elevated *Ucp1* mRNA levels and to data reported by Ma *et al.* [17], I found no differences in expression for *Pgc-1α* and genes involved in mitochondrial function and fatty acid oxidation in BAT, iWAT and skeletal muscle, respectively. I further revealed unchanged mRNA levels for sarcolipin and sarco-/endoplasmatic reticulum Ca^{2+} ATPase (SERCA), two key players in skeletal muscle non-shivering thermogenesis that uncouple calcium transport from ATP hydrolysis [120]. These data are in line with my indirect calorimetry findings, which revealed unperturbed energy

expenditure at ambient temperature and unperturbed basal metabolic rates and maximal respiratory capacities at thermoneutrality.

Collectively, my work corroborate several findings reported by Ma *et al.* [17], such as the decrease in body weight after celastrol treatment, the induction of *Hsf1* and *Ucp1* in iWAT, and elevated UCP1 levels in BAT. However, my data also suggest that celastrol does not mediate weight loss via non-shivering energy expenditure from skeletal muscle or via UCP1-mediated uncoupling from iWAT or BAT. Reasons for the discrepant findings between the studies by Ma *et al.* [17] and my findings might be due to the route, dose and duration of celastrol administration. Celastrol was injected subcutaneously or intraperitoneally for one week in DIO mice in my studies, revealing similar body weight lowering efficacy; Ma *et al.* administered celastrol via the food for up to 8 weeks and HFD feeding was started on the same day as celastrol treatment was started, which may induce alternative celastrol actions. Furthermore, if UCP1 is indeed a functional target of celastrol, was not tested in UCP1 KO mice by Ma *et al.* [17].

1.3 Effects of celastrol on glucose tolerance

In line with Liu *et al.* [16] my data reveal an improvement in glucose tolerance in lean chow-fed mice and no improvement in glucose tolerance in obese chow-fed Lep^{ob} mice after one week of celastrol treatment. However, contrary results were observed in obese mice. Liu and colleagues published an improvement in glucose tolerance in DIO mice after one week of celastrol treatment, whereas in this thesis glucose tolerance was not improved in celastrol treated HFD-fed obese WT and UCP1 KO mice. Notably, the efficiency of celastrol in the studies performed by Liu and colleagues was substantially higher compared to my studies and celastrol treated mice had lower body weights when GTTs were performed. Specifically, mice treated by Liu *et al.* lost around 15% of body weight after one week of celastrol treatment and had a body weight of approximately 38 g [16]. In my studies, DIO WT mice lost about 6% and had a body weight of 48 g when GTTs were performed. I speculate that the celastrol-induced weight loss in my studies was not sufficient to improve the serious glucose intolerance in DIO mice. Long-term celastrol treatment might lead to higher body weight loss in DIO mice and might therefore also improve glucose tolerance. Overall, celastrol-mediated improvements in glucose tolerance may be secondary to a reduction in body weight and fat mass.

1.4 Effects of celastrol on central anorexigenic and orexigenic proteins and on leptin signaling

In line with Liu and colleagues, I show here the up-regulation of *AgRP* mRNA in the hypothalami of celastrol-treated mice. AgRP is a neuropeptide secreted from AgRP neurons that is diminished upon exogenous leptin administration [121]. When AgRP is administered intracerebroventricularly at high doses, animals display massive hyperphagia [122] and white adipose tissue (WAT) lipogenesis [123] via inverse agonism at melanocortin 3 and 4 receptors. However, physiological effects of endogenous AgRP appear less potent, as evidenced by unperturbed metabolism in global AgRP KO mice [124]. Certainly, increased AgRP expression in my celastrol-treated mice stands in stark contrast to the observed reduction in food intake, which suggests prevailing anorexigenic signals as major drivers for celastrol actions on food intake.

In the past, celastrol was shown to induce weight loss and improve glucose homeostasis in diabetic leptin receptor deficient Lep^{db} mice [18, 30]. These results are contradictory to my work and findings by Liu *et al.* [16], which reveal a complete lack of weight loss in celastrol-treated Lep^{ob} and Lep^{db} mice. Importantly, mice received different doses of celastrol for varying durations. For instance, Kim and colleagues intraperitoneally injected 1 mg/kg BW celastrol for 2 months whereas Liu treated Lep^{db} mice with 10 mg celastrol/kg BW by oral gavage or with 0.1 mg/kg BW by injections (i.p.) for 21 days and while I injected my Lep^{db} mice subcutaneously for six days with 0.1 mg/kg celastrol. Weisberg and colleagues used one single i.p. injection of 3 mg/kg BW celastrol in Lep^{db} mice and saw an improvement in non fasting blood glucose levels and insulin sensitivity as well as an improved insulin production [30]. In contrast, Liu and colleagues treated Lep^{db} mice for 3 weeks with 100 µg/kg BW celastrol and saw no improvements in fasting blood glucose or insulin levels and systemic glucose tolerance as well as insulin sensitivity. Next to the divergent duration and dosing of celastrol action, different genetic backgrounds and ages for the Lep^{ob} or Lep^{db} mice may further complicate a direct comparison of the studies. In summary, low-dose effects of celastrol on body weight seem to require a functional leptin signaling axis.

Leptin binding to its receptor activates STAT3 [125, 126], which is a major regulator of food intake and body weight within anorexogenic POMC-neurons in the hypothalamus. In this thesis unchanged levels for several components of the leptin signaling cascade, such as *LepR*, *FoxO1*, *Mc3r* and *Mc4r,* were observed. Moreover, expression levels for *Pomc* and *Cart*, two direct targets of leptin signaling in the arcuate nucleus, were unchanged in celastrol-treated mice. The importance of leptin signaling for celastrol action was nevertheless corroborated by my observation of enhanced basal STAT5, STAT3 and pSTAT3 levels in the hypothalamus. This finding might indicate aberrant negative leptin

feedback signaling by inhibitory regulators of the JAK-STAT pathway such as PTP1B, TCPTP or SOCS3 [101]. Protein tyrosine phosphatases (PTPs) are known anti-obesity drug targets [127] and PTP1B and TCPTP exhibit synergistic roles in insulin and leptin signaling [128, 129]. A recent publication reported an increase in insulin and leptin signaling in POMC neurons and a protection from diet-induced obesity due to increased iWAT browning as a result of PTP1B and TCPTP deletion [130]. Nonetheless, unchanged *Ptp1b*, *Tcptp*, or *Socs3* expression in celastrol-treated mice does not suggest a negative feedback inhibition at the level of gene expression. However, within the scope of a collaboration with Eleni Kyriakou and Ana Messias from Michael Sattler's Lab, Institute for Structural Biology, Helmholtz-Zentrum Munich, binding of celastrol to PTP1B and TCPTP in the low micro-molar range could be confirmed. Furthermore, they show celastrol induced reversible non-competitive inhibition of the both phosphatases. To prove functional importance of PTP1B and TCPTP inhibition *in vivo*, a second collaboration with Stephanie Simonds and Michael Cowley from the Monash University, Victoria, Australia, who generated triple-floxed $Ptpn1^{fl/fl}$ $PTPn2^{fl/fl}$ $Socs3^{fl/fl}$ mice, was started. Bilateral injections of adeno-associated-virus (AAV; cre virus) directly in the ARC subsequently led to knock down of PTP1B, TCPTP and SOCS3 in the ARC and blocked the reduction in body weight and food intake induced by celastrol treatment. Results of these studies done by my collaboration partners strongly imply binding of celastrol to and inhibition of PTP1B and TCPTP. Overall, we show strong evidence that celastrol induces inhibition of the leptin signaling negative feedback regulators PTP1B and TCPTP to facilitate JAK-STAT signaling and leptin sensitivity.

1.5 Effects of celastrol on ER-stress markers

Liu and colleagues reported that celastrol treatment reduces ER-stress by decreasing eukaryotic translation initiation factor 2 alpha kinase 3 (PERK) phosphorylation in the hypothalamus. They further showed that celastrol does not change the transcription of common ER-stress genes such as *sXbp1* and *Chop* [16]. In line with Liu *et al.*, I observed unchanged expression for both markers, but revealed increased gene expression for Hsp70 protein *Bip*. Elevated heat shock proteins after celastrol treatment have already been described and linked with potentially cytotoxic celastrol action [131]. Cytotoxic effects of celastrol are indeed considered as novel therapeutic modality against several cancer types [132-134]. In line with potential cytotoxic effects of celastrol, attention needs to be drawn towards the observed lean mass loss after celastrol treatment in most of my studies. Lean mass loss can be a normal physiological consequence of an animal undergoing a chronically negative energy balance. Lean mass loss may however also be a sign for possible negative effects of celastrol, which warrants further studies.

1.6 Conclusion and outlook

Overall, I demonstrate that celastrol administration decreases body weight, an effect that is not due to enhanced energy expenditure and UCP1 mediated thermogenic activity from iWAT or BAT. Celastrol decreases food consumption, which is most prominent in the second half of the dark phase. The inability of celastrol to lower body weight in Lep^{ob} and Lep^{db} mice demonstrates that functional leptin signaling is necessary for celastrol action. Mechanistically, my finding of enhanced basal STAT3 and STAT5 protein levels suggests a model whereby celastrol activates downstream leptin circuitry. Nevertheless, leptin appears to be required, as indicated by a lack of efficacy in leptin-deficient Lep^{ob} mice.

Future studies should delineate the exact molecular mechanisms of celastrol action, with an emphasis on further studies of negative feedback inhibitors such as PTP1B or TCPTP. Additionally, the observed lean mass loss after celastrol administration should be addressed. Further, attention should be drawn towards the type of neuronal populations in the ARC that mediate celastrol's catabolic actions. Furthermore, the impact of celastrol action on neurocircuitry outside the ARC would be interesting to study.

2 High fat diet induced astrocytosis and the role of calcineurin

The results of the thesis show for the first time that Ppp3cb deficiency in mice protects from HFD-induced astrocytosis in the arcuate-, dorsomedial-, and ventromedial nucleus of the hypothalamus. Findings of this thesis extend a number of reports on calcineurin as mediator of astrocytosis in various models of brain insult [54, 55, 135-137], indicating that hypothalamic calcineurin may play a role in metabolic dysfunction.

2.1 Regulatory role of HFD induced astrocytosis for hypothalamic CNS circuitry and energy and glucose metabolism

Astrocytosis as a response to chronic exposure of mice and humans to an obesogenic diet has been reported by various authors [42, 48, 138]. However, the role of HFD-induced astrocytosis for astrocyte function and survival, as well as for surrounding nerve tissue and for the hypothalamic control of metabolism remains largely unknown. Nevertheless, a number of reports point towards an important function of astrocytes in feeding behavior. Recently, my lab reported glial activation in response to chronic leptin exposure and central leptin resistance [138], potentially induced by higher reactive oxygen release from POMC neurons [139]. Loss of astrocytic leptin receptor signaling was linked with alterations in hypothalamic synaptic function and CNS control of feeding behavior [140]. My institute further showed that insulin signaling in hypothalamic astrocytes co-controlled CNS glucose sensing and systemic glucose metabolism via regulating glucose uptake at the level of the

blood brain barrier [42]. Astrocyte-specific ablation of leptin and insulin signaling effector STAT3 protected from local astrocytosis and the spreading of inflammatory cells in response to experimental injury to the spinal cord [141]. Overall, these reports indicate that a regulatory role of HFD-induced reactive astrocytes for hypothalamic CNS circuitry and energy and glucose metabolism appears likely. However, to date solid evidence is missing. Future studies on the impact of HFD-induced astrocytosis for systemic metabolism are thus warranted. Such studies should entail research on the potential physiological impact of astrocytic calcineurin Aβ ablation.

2.2 The importance of calcineurin in astrocytosis

To date, reports on positive versus negative effects of calcineurin for astrocytic activation and recovery of injured neurons are often contradictory [54, 55, 142-146]. Murine models of aging and Alzheimers disease displayed high calcineurin immunoreactivity in activated astrocytes located in the hippocampus and neocortex, but undetectable immunoreactivity in non-activated normal astrocytes [54]. Follow-up reports suggest that Ppp3cb activation increases neuronal dysfuntion and that inhibition in astrocytes may serve as crucial step in protecting nerve tissue from traumatic brain insults. Proteolytic activation of calcineurin in activated astrocytes exacerbated neural dysfunction during neurodegenerative disease and injury [142]. Regulation of calcineurin by insulin-like growth factor I and interaction with the transcription factor Forkhead box O3 (FOXO3) were recently identified as prime drivers for inflammation in Alzheimers disease [55, 144], and blockade of calcineurin-forkhead box O (FOXO) binding decreased neuropathologies in murine models of Alzheimers disease [145]. Virally mediated inhibition of calcineurin signaling in astrocytes was shown to normalize hippocampal synaptic function and plasticity in rats undergoing traumatic brain injury. Notably, such neuroprotective functions of astrocytic calcineurin inhibition were found despite the presence of GFAP activation [143]. Contrary to the above listed publications, a recent report demonstrated that mice with Ppp3cb deficiency were unable to cope with brain injury, displaying a significant increase in cerebral damage due to the lack of unfolded protein response [146]. Astrocyte size and GFAP expression were decreased in the brain of Ppp3cb KO mice following brain injury. Mechanistically, calcineurin A beta was directly linked with non-enzymatic activation of PERK - eukaryotic translation initiation factor 2 subunit alpha (eIF2α) signaling and the UPR, which facilitated astrocytosis as a function of increased astrocyte survival and protection from cerebral damage [146].

Based on the present literature, the impact of astrocytic Ppp3cb ablation on metabolic homeostasis is hard to predict. Both exacerbation and protection from metabolic diseases appears possible. Experiments in Ppp3cb KO mice conducted by Chen and colleagues [146],

suggest similar effects of calcineurin ablation on astrocyte activity for cerebral brain damage as I observed in my HFD mouse model.

2.3 *In vitro* studies of astrocytosis in primary glia cultures

Previous *in vitro* studies linked astrocytic calcineurin with free radical production and cellular damage in the presence of high calcium [147]. Inhibition of calcineurin by Fk506 protected cultured astrocytes from Ca^{2+} paradox like injury [147] and inhibited astrocyte proliferation and induced apoptosis [148], a process potentially involving inhibition of arachidonic acid release by cytosolic phospholipase A2 [149], increased mitogen activated protein (MAP) kinase ERK1/2 and AKT signaling [150] and/or the prevention of glutamate toxicity [151]. *In vitro*, adenoviral overexpression of calcineurin was linked with morphologic changes and gene expression profiles that mimicked the *in vivo* activation phenotype [54]. Furthermore, adenoviral inhibition of astrocytic calcineurin activity reduced neuroinflammatory IL-1 signaling and neuronal death in co-cultures of neurons and glia cells [137].

Data of this thesis indicate that *in vitro* experiments in isolated primary hypothalamic astrocytes are of limited value to address the role of calcineurin for HFD-induced astrocytosis or metabolic dysfunction. I was unable to corroborate the protective role of calcineurin A beta from HFD-induced astrocytosis observed *in vivo* in Ppp3cb knockout mice. Rather, I found unchanged GFAP protein levels and unchanged general GFAP fluorescence intensity upon calcineurin inhibition by Fk506 treatment *in vitro* in primary astrocytes. After treating primary astrocytes with obese serum, I observed unchanged GFAP expression but a shift towards a more reactive morphology, which could not be blocked by calcineurin inhibition. Similarly and consistent with previous reports on increased IBA1 positive microglia in the ARC of HFD fed mice [48, 51], I found increased microglia numbers in primary cultures treated with serum obtained from obese mice, regardless of the presence or absence of calcineurin inhibitior Fk506.

Data of this thesis show that hypothalamic astrocytes *in vitro* behave differently compared to hypothalamic astrocytes *in vivo*. Hypothalamic astrocytes might need the network with other cells, especially with neurons, where they can exert their actual functions. Differential astrocytic phenotypes *in vitro* may further result from subtle differences in culture conditions such as serum and cell confluency, which can exert profound effects on astrocytic calcineurin (CN)/NFAT signaling [152]. Moreover, hypothalamic astrocytes, or subpopulations thereof, may differ greatly from astrocytes isolated from other brain regions. Putative differences in the function of calcineurin in distinct astrocytic subpopulations further complicate comparisons between studies, highlighting the plurality of astrocyte biology and function.

2.4 Conclusion and outlook

In summary, these data demonstrate decreased astrocytosis in the hypothalamus of Ppp3cb KO mice chronically exposed to HFD, compared to weight-matched WT controls. In contrast, equal numbers of reactive microglia in HFD-fed WT and Ppp3cb KO mice in the ARC and DMH, but a decrease in the number in the VMH were observed. Data generated *in vivo* could not be found *in vitro*. Inhibition of calcineurin with Fk506 in primary hypothalamic astrocytes did not result in changes in morphology and in GFAP or vimentin protein levels and changes in fluorescence intensity, independent from the supplementation with normal FBS or obese serum. However, treatment of primary hypothalamic astrocytes with obese serum resulted in a more reactive astrocytic phenotype, characterized by longer projections and a higher total microglia number. To date, the significance of these findings remains to be tested.

To completely discover the role of Ppp3cb in astrocytes, more experiments are necessary. First of all it would be of interest to perform GFAP and IBA1 stainings in brains of chow fed lean Ppp3cb KO mice to determine whether changes in astrocyte and microglia number, as well as of number and length of primary projections, already exist under basal conditions. Furthermore, it would be of importance to specifically delete Ppp3cb in astrocytes and to perform a through metabolic characterization of lean and DIO mice. Moreover, such studies should further entail specific ablation of calcineurin activity from sub-populations of astrocytes e.g. in the hypothalamus to help delineating the complexity and heterogeneity of astrocyte activation during injury and disease. Besides that, future studies should focus on the effect of astrocytic Ppp3cb ablation on neuronal function and possible impairments in brain development. Astrocyte specific restoration of calcineurin function in Ppp3cb KO mice, would further help to study the impact of astrocytic calcinurin on the phenotype [56].

3 Effects of global and hypothalamic deletion of GPx7 on glucose and energy metabolism

Here evidence is provided that global GPx7 depletion leads to higher body weight in lean and obese male, but not in female mice. Male GPx7 KO mice displayed impaired glucose tolerance after 8 weeks of HFD feeding, compared to HFD-fed WT controls. After 20 weeks of HFD exposure, glucose tolerance was equally impaired in WT and KO mice. The higher propensity for body weight gain in HFD-fed KO mice was not due to an increase in food intake or changes in locomotor activity, but rather due to a decrease in energy expenditure and higher adipogenesis. Hypothalamus-specific GPx7 depletion led to an impairment of glucose tolerance and tended to result in higher fat mass in male mice. These studies strongly imply the importance of GPx7 in the hypothalamus. Since the obese phenotype

observed in global GPx7 KO mice was not clearly detected in male Nkx2.1-Cre specific GPx7 KO mice, it is still possible that GPx7 also exerts important functions in other tissue.

3.1 GPx7 ablation shifts birth ratio towards female offspring

A shift in the sex-birth ratio towards female GPx7 global KO mice was observed. The in general lower number of GPx7 knockout pups compared to wildtype pups, which is mostly due to the decrease in GPx7 knockout male pups, might be due to a general disadvantage of carrying a knockout of GPx7 in the genome compared to a wildtype genome. Disadvantages might occur before the fertilization, the fertilization might be less successful or a spontaneous abort of embryos during the 21-d gestation period might occur [153]. In general it is possible that the motility or fertilization ability of sperm of one sex is affected differentially by the reproductive tract milieu [154] such as vaginal pH or viscosity of cervical mucus. Furthermore the selective loss of the conceptus either before or after implantation [155] might affect the embryonic development of one sex over the other differentially [154]. Other reasons for the shift in birth ratio can be the physiological conditions of the parents and also environmental factors can play an important role. According to Triver and Willard, females in poor physiological condition give birth to more female offspring [156]. Goundie and colleagues proposed that for white footed-mice, more male offspring are born in spring where mothers were heavier and more female offspring in fall, where mothers were in a poorer nutritional state [157]. Studies on the influence of diet on the birth ratios towards one sex, showed that diets with lower fat content influenced birth ratio towards more female mice, while a diet with a higher fat content led to a higher ratio in male pups [155]. However $GPx7^{+/-}$ female and male breeders were all fed with the same standard chow diet and all breeding pairs were set up in spring and pups were born from beginning of April to end of May. Importantly, the obtained data set is based on only six independent breeding pairs and more independent breeding pairs would need to be studied at different time points during the year to rule out serendipity for the differences in birth rates.

3.2 GPx7 deletion promotes an obesogenic phenotype

A higher body weight in male global GPx7 knockout mice on high fat diet was shown here. In 2013 Chang and colleagues reported that GPx7 deficiency promotes diet-induced obesity, accompanied with a markedly increased fat mass and adipocyte hypertrophy when fed with high fat diet (60% calories from fat). In contrast to my observation, Chang and co-authors did not study male mice, but reported obesity in female mice. In my studies a higher body weight in GPx7 depleted female mice was not detected, which might be due to the general higher body weight variations in female mice, compared to male mice. Cohorts of female mice with a higher n number might need to be studied in future experiments. Another reason might be

the feeding of different high-fat diets: while my mice were fed with 45% HFD, Chang and colleagues used 60% HFD. Higher percentage body weight gain in lean GPx7 knockout mice fed chow diet compared to their wildtype controls was shown in my studies, while Chang and colleagues reported no difference [78]. Here, the type and composition of chow diets also differed between the two studies. Moreover, different propensities of obesity might also be explained by different microbiomes due to housing of mice in different housing facilities [158].

I claim, that the higher body weight in male GPx7 global KO mice is due to a decrease in energy expenditure on HFD. These findings are in line with already published data by Chang and co-workers [78]. Similar to results of this thesis, Chang *et al.* report no difference in the energy expenditure in lean mice between the genotypes. Further data in line with Chang and colleagues are normal fasting blood glucose and no difference in overall food intake in GPx7 knockout mice, a decrease in GPx7 expression in white primary adipocytes during adipogenesis and in general higher adipogenesis in primary subcutaneous adipocytes of GPx7 KO mice. Higher body weight in GPx7 depleted mice is also in line with human data, where SNPs near the GPx7 gene were associated with lower GPx7 expression and increased adiposity in several populations [78]. Accordingly, data of this thesis corroborate and extend reports by Chang and colleagues, and suggest that GPx7 is an important component of adipogenesis, energy expenditure and weight control also in male mice fed chow or high fat diet.

3.3 Effect of GPx7 on ER-stress and insulin signaling

Earlier studies report up-regulated expression of ER-stress markers *Grp78*, *Chop*, *Atf4* and of the spliced form of *Xbp1* in liver, kidney, spleen and heart of 10-month-old GPx7 KO mice [80]. In this study peripheral organs were not tested, but the focus was on hypothalamic ER-stress. Accordingly, a direct comparison between studies is not possible. Nevertheless, in my studies I observed hypothalamic down-regulation of *Calr* and *Ire1α* in lean mice and of *Erdj4* in DIO (29 weeks of HFD feeding) mice globally deleted for GPx7, suggesting a negative impact of GPx7 in ER-stress. Moreover, hypothalamic *Grp78*, *Chop* and *Xbp1* mRNA levels remained unaltered in GPx7 WT and global KO mice fed chow or high fat diet. Specific deletion of GPx7 in Nkx2.1 expressing cells did not alter hypothalamic ER-stress markers in mice fed for 21 weeks with HFD. These data thus suggest that GPx7 deficiency might lead to a differential regulation of ER-stress for different organs.

In the liver of GPx7 KO mice, a trend towards impaired insulin signaling, reflected by a strong tendency towards decreased phospho-AKT levels was detected. Considering liver, kidney, spleen and heart, the liver was shown to be the first organ that is affected from GPx7 induced ER-stress [80]. Long term ER-stress was shown to affect insulin signaling in the liver

cells by the induction of e.g. the expression of tribbles-related protein 3 (*Trb3*) leading to the inhibition of Akt activation by insulin [159, 160]. Possible impairments in insulin signaling may be explained by increased ER-stress in GPx7 deficient mice. To confirm this assumption, further studies with a focus on ER-stress and insulin signaling molecules are mandated.

3.4 Effect of GPx7 deletion on UCP1 protein levels

UCP1 protein levels in primary brown GPx7 deficient adipocytes were up-regulated compared to their wildtype control cells. Higher UCP1 expression could be a result of higher ROS levels [114] in GPx7 KO cells. However, up-regulation of UCP1 protein could not be detected in brown adipose tissue of GPx7 KO animals. In contrast, UCP1 protein in BAT was down-regulated in global GPx7 knockout mice. Isolated primary brown adipocytes are differentiated out of pre-adipocytes from new-born mice, and lack exogenous signals such as sympathetic nervous system input or hormones such as fibroblast growth factor 21 (FGF21) [161, 162]. Differences in UCP1 protein expression in primary brown adipocytes and in brown adipose tissue may arise from these differences in exogenous input. Moreover, brown fat adipocytes from new-born mice cultured *in vitro* may behave differently compared to aged brown adipocytes *in vivo*, which lose their BAT activity [163].

3.5 The function of hypothalamic GPx7

Hypothalamus-specific deletion of GPx7 increases hypothalamic inflammation and impairs glucose tolerance, underlining the importance of GPx7 in the hypothalamus. However, GPx7;Nkx2.1-Cre WT and KO mice did not differ in body weight or adiposity. Interestingly, there was a trend towards increased fat mass and decreased lean mass in hypothalamic GPx7 specific knockout mice. Impaired glucose tolerance was also found for global GPx7 KO mice after 8 weeks of high fat diet feeding. Notably, inflammatory markers were unaffected in hypothalami of global HFD-fed GPx7 KO mice compared to WT controls, but global Gpx7 KO mice displayed increased body weight and body adiposity. Based on these data and data by Chang *et al.* [78], GPx7 deficiency in tissues such as adipose tissue appear to more likely explain the obesogenic phenotype, which may be driven by higher adipogenesis and lower energy expenditure. Overall, the data suggests that hypothalamic GPx7 plays a direct role in the regulation of glucose homeostasis, which is independent from the regulation of body weight. Future studies should delineate whether increased hypothalamic inflammation is causally linked with the impairment of glucose tolerance in HFD-fed GPx7;Nkx2.1-Cre KO mice.

3.6 Conclusion and outlook

The present experiments demonstrate the importance of GPx7 in body weight regulation and glucose homeostasis. Global depletion of GPx7 led to a significant increase in weight gain in chow fed lean male mice and in male mice exposed to high fat diet feeding. Higher body weight in GPx7 depleted mice fed with high fat diet is not a consequence of higher food intake or lower locomotor activity, but rather a result of lower energy expenditure and of increased adipogenesis in white adipose tissue. Importantly, increased weight gain and adiposity are not observed in hypothalamus specific GPx7 KO mice, which point towards non-hypothalamic brain areas, and/or peripheral tissues as culprits for the obese phenotype of global GPx7 KO mice. Glucose tolerance after eight weeks of high fat diet feeding was impaired in globally deleted GPx7 knockout mice and might be linked with hepatic insulin resistance. Importantly, follow-up studies in hypothalamus-specific GPx7 KO mice revealed a direct central glucose regulatory function of GPx7 that was independent of body weight or adiposity. Specifically, higher fasting glucose levels eight and ten weeks after the start of high fat diet feeding were observed, and an impairment of glucose tolerance in GPx7;Nkx2.1-Cre KO mice was detected. Whether increased hypothalamic mRNA levels of inflammatory markers in GPx7 deficient mice are causally linked with the observed glucose intolerance remains to be tested. Future studies should further entail a thorough monitoring of birth ratios in global and tissue specific GPx7 KO models to assess a putative embryonal and/or postnatal lethality in male KO mice, and the in-depth characterization of neuronal subpopulation-specific as well as tissue-specific mouse models for GPx7 deficiency in metabolically active tissues such as the brown adipose tissue, muscle or liver.

Supplementary material

Supplementary table 1: Results of the ANCOVA analysis of GPx7 global KO and WT mice in the indirect calorimetry system.
P- and F-values are listed for the food intake (FI), respiratory exchange ratio (RER), locomotor activity and energy expenditure. Body weight or lean mass or FI (for RER) were used as covariates. N=8 WT, 7 KO mice.

	Covariate body weight				Covariate lean mass				Covariate food intake			
	p-value geno-type	F-value geno-type	p-value co-variate	F-value co-variate	p-value geno-type	F-value geno-type	p-value co-variate	F-value co-variate	p-value geno-type	F-value geno-type	p-value co-variate	F-value co-variate
FI (daily) total Chow	0.217	1.697	0.029	6.148	0.574	0.335	0.021	7.106				
FI (daily) day Chow	0.055	4.505	0.148	2.393	0.110	2.975	0.325	1.054				
FI (daily) night Chow	0.499	0.485	0.456	0.592	0.294	1.206	0.212	1.738				
FI (daily) total HFD	0.497	0.490	≤0.0005	118.381	0.479	0.533	0.038	5.449				
FI (daily) day HFD	**0.048**	4.838	0.001	19.035	0.254	1.435	0.302	1.164				
FI (daily) night HFD	**≤0.0005**	25.373	≤0.0005	50.794	**0.002**	16.022	0.003	14.329				
RER total Chow	0.355	0.925	0.079	3.678	0.687	0.171	0.069	4.003	0.781	0.081	0.009	9.846
RER day Chow	0.138	2.521	0.035	5.612	0.337	1.00	0.73	3.867	0.984	≤0.0005	0.001	20.576
RER night Chow	0.51	0.462	0.854	0.035	0.414	0.715	0.729	0.126	0.562	0.356	0.006	11.106
RER total HFD	0.595	0.299	≤0.0005	44.386	0.621	0.257	0.125	2.723	0.825	0.051	≤0.0005	130.459
RER day HFD	0.066	4.096	≤0.0005	31.551	0.459	0.585	0.129	2.658	0.818	0.055	≤0.0005	62.884
RER night HFD	**0.002**	14.537	≤0.0005	28.286	**0.048**	4.851	0.171	2.119	0.722	0.133	0.001	22.123
Locomotor activity total Chow	0.125	2.725	0.472	0.551	0.246	1.488	0.317	1.092				
Locomotor activity day Chow	0.13	2.646	0.217	1.701	0.23	1.602	0.310	1.123				
Locomotor activity night Chow	0.189	1.943	0.627	0.249	0.336	1.005	0.404	0.747				
Locomotor activity total HFD	0.259	1.403	0.764	0.095	0.612	0.271	0.213	1.727				
Locomotor activity day HFD	0.784	0.079	0.027	6.350	0.779	0.082	0.619	0.261				
Locomotor activity night HFD	0.269	1.344	0.895	0.018	0.652	0.214	0.247	1.478				
Energy expenditure total Chow	0.135	2.572	0.008	10.117	0.558	0.362	0.001	17.326				
Energy expenditure day Chow	0.272	1.327	0.008	10.213	0.721	0.134	0.11	9.030				
Energy expenditure night Chow	0.183	1.997	0.046	4.969	0.599	0.292	0.005	11.405				
Energy expenditure total HFD	**0.042**	5.191	0.002	14.580	0.443	0.63	0.005	12.121				
Energy expenditure day HFD	0.116	2.867	≤0.0005	38.622	0.74	0.115	0.042	5.167				
Energy expenditure night HFD	0.063	4.214	0.063	4.208	0.377	0.843	0.006	11.312				

Abbreviations

°C	-	Degree Celsius
A2	-	Adrenoceptor beta 2
A3	-	Adrenoceptor beta 3
AAV	-	Adeno-associated-virus
Agrp	-	Agouti-related peptide
AMPK	-	AMP-activated protein kinase
ANCOVA	-	Analysis of covariance
ANOVA	-	Analysis of variance
ARC	-	Arcuate nucleus
Arg1	-	Arginase 1
Atf3	-	Activating transcription factor 3
Atf4	-	Activating transcription factor 4
Atgl	-	Adipocyte triglyceride lipase
ATP	-	Adenosine triphosphate
Atp2a1	-	ATPase sarcoplasmic/endoplasmic reticulum Ca^{2+} transporting 1
Atp2a2	-	ATPase sarcoplasmic/endoplasmic reticulum Ca^{2+} transporting 2
Atp2a3	-	ATPase sarcoplasmic/endoplasmic reticulum Ca^{2+} transporting 3
AUC	-	Area under the curve
BAT	-	Brown adipose tissue
Bip	-	Heat shock protein family A (Hsp70) member 5; glucose-regulated protein, 78kDa
BMI	-	Body mass index
bp	-	Base pairs
BW	-	Body weight
CA	-	California
Ca^{2+}	-	Calcium
$CaCl_2$	-	Calcium chloride
Calr	-	Calreticulin
Cart	-	Cocaine- and amphetamine-regulated transcript
Cat	-	Catalase
Cb1	-	Cannabinoid receptor type 1
CCK	-	Cholecystokinin
Ccl2	-	Chemokine (C-C motiv) ligand 2
Ccl3	-	Chemokine (C-C motiv) ligand 3
Ccl5	-	Chemokine (C-C motiv) ligand 5
Cd68	-	Scavenger receptor class D, member 1
Cd8b	-	T lymphocyte surface glycoprotein beta chain
Cdc37	-	Cell division cycle 37
cDNA	-	Complementary DNA
CE	-	Coupling efficiency
Cebpa	-	CCAAT/enhancer binding protein alpha
Cebpb	-	C/EBPβ, CCAAT/enhancer binding protein beta
Cebpd	-	CCAAT/Enhancer binding protein delta
Chop	-	CCAAT/enhancer-binding protein homologous protein
Chuk	-	Conserved helix-loop-helix ubiquitous kinase
Cidea	-	Cell death-inducing DFFA-like effector A

cm^2	-	Square centimeter
Cn	-	Calcineurin
CNS	-	Central nervous system
CO_2	-	Carbon dioxide
Cox4β	-	Cytochrome C oxidase subunit 4 isoform 2
C_P	-	Peroxidatic Cys
Cpeb2	-	Cytoplasmic polyadenylation element binding protein 2
C_R	-	resolving Cys
Ct	-	Cycle threshold
Cys	-	Cysteine
Cyt c	-	Cytochrome c
d	-	Day
DAB	-	3,3'-Diaminobenzidine
DG	-	Diacylglycerol
DIO	-	Diet induced obese
Dio2	-	Deiodinase, iodothyronine, type II
DMEM	-	Dulbecco's modified eagle medium
DMH	-	Dorsomedial (nucleus of the) hypothalamus
DMSO	-	Dimethyl sulfoxide
DNA	-	Desoxyribonucleic acid
DNP	-	2,4-Dinitrophenol
dNTP	-	Deoxynucleotide
EDTA	-	Ethylenediaminetetraacetic acid
eIF2α	-	Eukaryotic translation initiation factor 2 subunit alpha
ELISA	-	Enzyme-linked immunosorbent assay
Emr1	-	EGF-like module-containing mucin-like hormone receptor-like 1
ER	-	Endoplasmic reticulum
Erdj4	-	Endoplasmic reticulum DNA J domain-containing protein 4
Erk	-	Extracellular signal-regulated kinase
Ero1α	-	Endoplasmic reticulum oxidoreductase 1 alpha
et al.	-	Et alii, and others
eWAT	-	Epididymial white adipose tissue
Fap	-	Fibroblast activation protein alpha
FBS	-	Fetal bovine serum
FDA	-	Food and drug administration
Fen-Phen	-	Fenfluramine/phentermine
FFA	-	Free fatty acid
Fgf21	-	Fibroblast growth factor 21
FI	-	Food intake
fl	-	Floxed
FM	-	Fat mass
FoxO	-	Forkhead box O
FoxO1	-	Forkhead box O1
FoxO3	-	Forkhead box O3
Foxp3	-	Forkhead box P3
fwd	-	Forward
g	-	Gram
Gaba	-	Gamma-aminobutyric acid

Gadd45a	-	Growth arrest and DNA damage inducible alpha
Gapdh	-	Glyeraldehyde 3-phosphate dehydrogenase
Gfap	-	Glial fibrillary acidic protein
Glp-1	-	Glucagon-like peptide 1
Gpx	-	Glutathione peroxidase
Gpx7 $^{+/-}$	-	Heterozygous for GPx7
Grp78	-	Glucose-regulated protein, 78 kDa
Grp94	-	Glucose-regulated protein, 94 kDa
GSH	-	Glutathione
GTT	-	Glucose tolerance test
h	-	Hour
H_2O	-	Dihydrogen oxide, water
H_2O_2	-	Hydrogen peroxide
HCl	-	Hydrogen chloride
HFD	-	High fat diet
Hif1α	-	Hypoxia inducible factor 1 alpha subunit
HIV	-	Human immunodeficiency virus
HOMA-IR	-	Homeostatic model assessment - insulin resistance
Hprt	-	Hypoxanthine phosphoribosyltranserase 1
HRP	-	Horseradish peroxidase
Hsf1	-	Heat shock transcription factor 1
Hsl	-	Hormone sensitive lipase
i.e.	-	id est, that is to say
i.p.	-	Intra peritoneal
Iba1	-	Ionized calcium binding adaptor molecule 1
IBMX	-	3-isobutyl-1-methylxanthine
IDO	-	Institute for diabetes and obesity
IgG	-	Immunoglobulin G
IL	-	Illinois
Il-1β	-	Interleukin-1β
Il-6	-	Interleukin-6
IRS	-	Insulin receptor substrate
Iso	-	Isoproterenol
Itgax	-	Integrin subunit alpha X
Itpr1	-	Inositol 1,4,5-trisphosphate receptor type 1
Itpr3	-	Inositol 1,4,5-trisphosphate receptor type 3
ITT	-	Insulin tolerance test
IU	-	International unit
iWAT	-	Inguinal white adipose tissue
Jak	-	Janus kinase
Jnk	-	C-jun N-terminal kinase
kcal	-	Kilocalories
kDa	-	Kilo Dalton
KDEL	-	Amino acid sequence: Lysine, aspartic acid, glutamic acid, leucine
kg	-	Kilogram
KO	-	Knockout
Lep^{db}	-	Leptin receptor deficient mice
Lep^{ob}	-	Leptin deficient mice

LepR	-	Leptin receptor
LH	-	Lateral hypothalamus
LM	-	Lean mass
loxP	-	Locus of X-over P1
m	-	Milli
M	-	Molar
MA	-	Massachusetts
Map	-	Mitogen activated protein
Mc3r	-	Melanocortin receptor 3
Mc4r	-	Melanocortin receptor 4
Mcad	-	Medium-chain-acyl-CoA-dehydrogenase
ME	-	Maine
MEM	-	Minimum essential medium
Mfn1	-	Mitofusin-1
Mfn-2	-	Mitofusin-2
MG	-	Monoacylglycerol
$MgCl_2$	-	Magnesium chloride
min	-	Minutes
MO	-	Missouri
mQTL	-	Methylation quantitative trait loci
mRNA	-	Messenger RNA
MTT	-	3-(4,5-Dimethylthiazol-2-yl)-2,5-diphenyltetrazolium bromide
n	-	Nano
NaCl	-	Sodium chloride
NE	-	Nebraska
NEFA	-	Non-esterified free fatty acid
NF-κB	-	Nuclear factor kappa B
Nfatc4	-	Nuclear factor of activated T-cells 4
Nfe2l2	-	Nuclear factor, erythroid 2 like 2
NH	-	New Hampshire
NJ	-	New Jersey
Nkx2.1	-	NK2 Homeobox 1
NMR	-	Nuclear magnetic resonance
Npgpx	-	Non-selenocysteine containing phospholipid hydroperoxide glutathione peroxidase
Npy	-	Neuropeptide Y
NT-siRNA	-	Non-target siRNA
NY	-	New York
O_2	-	Oxygen
OCR	-	Oxygen consumption rate
OD	-	Optical density
oGTT	-	Oral glucose tolerance test
Oligo	-	Oligomycine
p23	-	Prostaglandin E synthase 3
PA	-	Pennsylvania
pAkt	-	Phospho-protein kinase B alpha
PBS	-	Phosphate buffered saline
PCR	-	Polymerase chain reaction

Pdi	-	Protein disulfide isomerase
Perk	-	Eukaryotic translation initiation factor 2 alpha kinase 3
PFA	-	Paraformaldehyde
PGC-1α	-	Peroxisome proliferator-activated receptor gamma coactivator 1 alpha
Phen-Top	-	Phentermine-topiramate
pHsl	-	Phospho-HSL
PI3K	-	Phosphoinositide 3-kinase
Plb	-	Phospholamban
Plin	-	Perilipin
PMSF	-	Phenylmethane sulfonyl fluoride
Pomc	-	Pro-opiomelanocortin
Pparγ	-	Peroxisome proliferator activated receptor gamma
Ppp3	-	Protein phosphatase 3
Ppp3c	-	Protein phosphatase 3 catalytic subunit
Ppp3ca	-	Protein phosphatase 3 catalytic subunit alpha
Ppp3cb	-	Protein phosphatase 3 catalytic subunit beta, Calcineurin A beta
Ppp3cc	-	Protein phosphatase 3 catalytic subunit gamma
Ppp3r	-	Protein phosphatase 3 regulatory subunit B
Ppp3r1	-	Protein phosphatase 3 regulatory subunit B, alpha
Ppp3r2	-	Protein phosphatase 3 regulatory subunit B, beta
Prdm16	-	PR domain zinc finger protein 16
Pref	-	Preadipocyte factor 1
pS6	-	Phospho-ribosomal protein S6
pStat3	-	Phospho-STAT3
Ptp	-	Protein tyrosine phosphatase
Ptp1b	-	Protein tyrosine phosphatase 1B
Ptpn1	-	Protein tyrosine phosphatase 1B
Ptpn2	-	Protein tyrosine phosphatase, non-receptor type 2, Tcptp
PTT	-	Pyruvate tolerance test
PVN	-	Paraventricular hypothalamic nucleus
PYY	-	Peptide YY
qPCR	-	Quantitative PCR
RER	-	Respiratory exchange ratio
rev	-	Reverse
RIPA	-	Radioimmunoprecipitation assay buffer
RNA	-	Ribonucleic acid
ROS	-	Reactive oxygen species
RT	-	Room temperature
s.c.	-	Subcutaneous
sec	-	Second
Sec	-	Selenocysteine
SEM	-	Standard error of the mean
SERCA	-	Sarcolipin and sarco-/endoplasmatic reticulum Ca^{2+} ATPase
Shp2	-	Protein tyrosine phosphatase, non-receptor type 11
Sirt1	-	Sirtuin 1
Slc25a4	-	Solute carrier family 25 member 4
Slc8b1	-	Solute carrier family 8 member B1
Sln	-	Sarcolipin

SNP	-	Single nucleotide polymorphism
Socs3	-	Suppressor of cytokine signaling 3
Sod1	-	Superoxide dismutase 1, soluble
Sod2	-	Superoxide dismutase 2, mitochondrial
Stat	-	Signal transducer and activator of transcription
sXbp1	-	Spliced X-box binding protein 1
T3	-	Triiodthyronin
TBS	-	Tris-buffered saline
Tcptp	-	T-cell protein tyrosine phosphatase
TG	-	Triacylglycerol
TH	-	Tyrosine hydroxylase
Tnf	-	Tumor necrosis factor
Trb3	-	Tribbles-related protein 3
Tris	-	Tris(hydroxymethyl)aminomethane
TX	-	Texas
Ucp1	-	Uncoupling protein 1
US	-	United States
USA	-	United States of America
VCO_2	-	Carbon dioxide production
VMH	-	Ventromedial (nucleus of the) hypothalamus
VO_2	-	Oxygen consumption
WAT	-	White adipose tissue
WI	-	Wisconsin
WT	-	Wildtype
Xbp1	-	X-Box binding protein 1
Xrn2	-	5’-3’ exoribonuclease 2
α-Msh	-	α-melanocyte-stimulating hormone
µ	-	Micro

Index of figures

Index of tables

List of publications

Pfuhlmann K., S. C. Schriever, P. Baumann, D. G. Kabra, L. Harrison, S. E. Mazibuko-Mbeje, R. E. Contreras, E. Kyriakou, S. E. Simonds, T. Tiganis, M. A. Cowley, S. C. Woods, M. Jastroch, C. Clemmensen, M. De Angelis, K. W. Schramm, M. Sattler, A. C. Messias, M. H. Tschöp and P. T. Pfluger (2018). ”Celastrol-Induced Weight Loss Is Driven by Hypophagia and Independent From UCP1.” Diabetes **67**(11): 2456-2465.

Pfuhlmann K., S. C. Schriever, B. Legutko, P. Baumann, L. Harrison, D. G. Kabra, E. V. Baumgart, M. H. Tschöp, C. Garcia-Caceres and P. T. Pfluger (2018). “Calcineurin A beta deficiency ameliorates HFD-induced hypothalamic astrocytosis in mice.“ Journal of Neuroinflammation **15**(1): 35.

Pfuhlmann K., P. T. Pfluger, S. C. Schriever, T. D. Müller, M. H. Tschöp and K. Stemmer (2017). "Dual specificity phosphatase 6 deficiency is associated with impaired systemic glucose tolerance and reversible weight retardation in mice." PLOS ONE **12**(9): e0183488.

Harrison L., S. C. Schriever, A. Feuchtinger, E. Kyriakou, P. Baumann, **K. Pfuhlmann**, A. C. Messias, A. Walch, M. H. Tschöp, P. T. Pfluger (2019). “Fluorescent blood-brain barrier tracing shows intact leptin transport in obese mice“. International Journal of Obesity **43**(6): 1305-1318.

Harrison L., **K. Pfuhlmann**, S. C. Schriever, P. T. Pfluger (2019). “Profound weight loss induces reactive astrogliosis in the arcuate nucleus of obese mice.“ Molecular Metabolism **24**: 149-155.

Kyriakou E., S. Schmidt, G. T. Dodd, **K. Pfuhlmann**, S. E. Simonds, D. Lenhart, A. Geerlof, S. C. Schriever, M. De Angelis, K. W. Schramm, O. Plettenburg, M. A. Cowley, T. Tiganis, M. H. Tschöp, P. T. Pfluger, M. Sattler, A. C. Messias (2018). “Celastrol Promotes Weight Loss in Diet-Induced Obesity by Inhibiting the Protein Tyrosine Phosphatases PTP1B and TCPTP in the Hypothalamus.” Journal of Medicinal Chemistry **61**(24): 11144-11157.

Schriever, S. C., A. Zimprich, **K. Pfuhlmann**, P. Baumann, F. Giesert, V. Klaus, D. G. Kabra, U. Hafen, A. Romanov, M. H. Tschöp, W. Wurst, M. Conrad, S. M. Hölter, D. Vogt Weisenhorn and P. T. Pfluger (2017). "Alterations in neuronal control of body weight and anxiety behavior by glutathione peroxidase 4 deficiency." Neuroscience **357**: 241-254.

Kabra, U. D., **K. Pfuhlmann**, A. Migliorini, S. Keipert, D. Lamp, O. Korsgren, M. Gegg, S. C. Woods, P. T. Pfluger, H. Lickert, C. Affourtit, M. H. Tschöp and M. Jastroch (2017). "Direct Substrate Delivery Into Mitochondrial Fission-Deficient Pancreatic Islets Rescues Insulin Secretion." Diabetes **66**(5): 1247-1257.

Kabra, D. G., **K. Pfuhlmann**, C. García-Cáceres, S. C. Schriever, V. Casquero García, A. F. Kebede, E. Fuente-Martin, C. Trivedi, K. Heppner, N. H. Uhlenhaut, B. Legutko, U. D. Kabra, Y. Gao, C. X. Yi, C. Quarta, C. Clemmensen, B. Finan, T. D. Müller, C. W. Meyer, M. Paez-Pereda, K. Stemmer, S. C. Woods, D. Perez-Tilve, R. Schneider, E. N. Olson, M. H. Tschöp and P. T. Pfluger (2016). "Hypothalamic leptin action is mediated by histone deacetylase 5." Nature Communications **7**: 10782.

Pfluger, P. T., D. G. Kabra, M. Aichler, S. C. Schriever, **K. Pfuhlmann**, V. C. García, M. Lehti, J. Weber, M. Kutschke, J. Rozman, J. W. Elrod, A. L. Hevener, A. Feuchtinger, M. Hrabe de Angelis, A. Walch, S. M. Rollmann, B. J. Aronow, T. D. Müller, D. Perez-Tilve, M. Jastroch, M. De Luca, J. D. Molkentin and M. H. Tschöp (2015). "Calcineurin Links Mitochondrial Elongation with Energy Metabolism." Cell Metabolism **22**(5): 838-850.

Literature

1. Schwartz MW, Gelling RW: **Rats lighten up with MCH antagonist**. *Nat Med* 2002, **8**(8):779-781.
2. Ng M, Fleming T, Robinson M, Thomson B, Graetz N, Margono C, Mullany EC, Biryukov S, Abbafati C, Abera SF *et al*: **Global, regional, and national prevalence of overweight and obesity in children and adults during 1980-2013: a systematic analysis for the Global Burden of Disease Study 2013**. *Lancet* 2014, **384**(9945):766-781.
3. World Health Organisation (WHO): **Obesity and Overweight.** 2017, http://www.who.int/mediacentre/factsheets/fs311/en/**.**
4. World Health Organisation (WHO): **Global Report on Diabetes***.* 2016, http://apps.who.int/iris/bitstream/10665/204871/1/9789241565257_eng.pdf.
5. Roh E, Song DK, Kim MS: **Emerging role of the brain in the homeostatic regulation of energy and glucose metabolism**. *Exp Mol Med* 2016, **48**:e216.
6. Tschop M, Smiley DL, Heiman ML: **Ghrelin induces adiposity in rodents**. *Nature* 2000, **407**(6806):908-913.
7. Timper K, Bruning JC: **Hypothalamic circuits regulating appetite and energy homeostasis: pathways to obesity**. *Dis Model Mech* 2017, **10**(6):679-689.
8. Rodgers RJ, Tschop MH, Wilding JP: **Anti-obesity drugs: past, present and future**. *Dis Model Mech* 2012, **5**(5):621-626.
9. Badman MK, Flier JS: **The gut and energy balance: visceral allies in the obesity wars**. *Science* 2005, **307**(5717):1909-1914.
10. Wynne K, Stanley S, McGowan B, Bloom S: **Appetite control**. *J Endocrinol* 2005, **184**(2):291-318.
11. Cypess AM, Kahn CR: **Brown fat as a therapy for obesity and diabetes**. *Curr Opin Endocrinol Diabetes Obes* 2010, **17**(2):143-149.
12. George M, Rajaram M, Shanmugam E: **New and emerging drug molecules against obesity**. *J Cardiovasc Pharmacol Ther* 2014, **19**(1):65-76.
13. Kim GW, Lin JE, Blomain ES, Waldman SA: **Antiobesity pharmacotherapy: new drugs and emerging targets**. *Clin Pharmacol Ther* 2014, **95**(1):53-66.
14. Marshall EM: **Valvular heart disease associated with fenfluramine-phentermine**. *N Engl J Med* 1997, **337**(24):1775; author reply 1775-1776.
15. Ost M, Keipert S, Klaus S: **Targeted mitochondrial uncoupling beyond UCP1 - The fine line between death and metabolic health**. *Biochimie* 2017, **134**:77-85.
16. Liu J, Lee J, Salazar Hernandez MA, Mazitschek R, Ozcan U: **Treatment of obesity with celastrol**. *Cell* 2015, **161**(5):999-1011.
17. Ma X, Xu L, Alberobello AT, Gavrilova O, Bagattin A, Skarulis M, Liu J, Finkel T, Mueller E: **Celastrol Protects against Obesity and Metabolic Dysfunction through Activation of a HSF1-PGC1alpha Transcriptional Axis**. *Cell metabolism* 2015, **22**(4):695-708.
18. Kim JE, Lee MH, Nam DH, Song HK, Kang YS, Lee JE, Kim HW, Cha JJ, Hyun YY, Han SY *et al*: **Celastrol, an NF-kappaB inhibitor, improves insulin resistance and attenuates renal injury in db/db mice**. *PLoS One* 2013, **8**(4):e62068.
19. Stroke NIoNDa: **Celastrol**. 2008, **1-11**.
20. Ni H, Zhao W, Kong X, Li H, Ouyang J: **NF-kappa B modulation is involved in celastrol induced human multiple myeloma cell apoptosis**. *PLoS One* 2014, **9**(4):e95846.
21. Ni H, Zhao W, Kong X, Li H, Ouyang J: **Celastrol inhibits lipopolysaccharide-induced angiogenesis by suppressing TLR4-triggered nuclear factor-kappa B activation**. *Acta haematologica* 2014, **131**(2):102-111.
22. Sethi G, Ahn KS, Pandey MK, Aggarwal BB: **Celastrol, a novel triterpene, potentiates TNF-induced apoptosis and suppresses invasion of tumor cells by inhibiting NF-kappaB-regulated gene products and TAK1-mediated NF-kappaB activation**. *Blood* 2007, **109**(7):2727-2735.

23. Shen YF, Zhang X, Wang Y, Cao FF, Uzan G, Peng B, Zhang DH: **Celastrol targets IRAKs to block Toll-like receptor 4-mediated nuclear factor-kappaB activation**. *J Integr Med* 2016, **14**(3):203-208.
24. Lee JH, Koo TH, Yoon H, Jung HS, Jin HZ, Lee K, Hong YS, Lee JJ: **Inhibition of NF-kappa B activation through targeting I kappa B kinase by celastrol, a quinone methide triterpenoid**. *Biochemical pharmacology* 2006, **72**(10):1311-1321.
25. Veerappan K, Natarajan S, Ethiraj P, Vetrivel U, Samuel S: **Inhibition of IKKbeta by celastrol and its analogues - an in silico and in vitro approach**. *Pharm Biol* 2017, **55**(1):368-373.
26. Pazhang Y, Jaliani HZ, Imani M, Dariushnejad H: **Synergism between NF-kappa B inhibitor, celastrol, and XIAP inhibitor, embelin, in an acute myeloid leukemia cell line, HL-60**. *Journal of cancer research and therapeutics* 2016, **12**(1):155-160.
27. Sha M, Ye J, Luan ZY, Guo T, Wang B, Huang JX: **Celastrol induces cell cycle arrest by MicroRNA-21-mTOR-mediated inhibition p27 protein degradation in gastric cancer**. *Cancer cell international* 2015, **15**:101.
28. Jiang QW, Cheng KJ, Mei XL, Qiu JG, Zhang WJ, Xue YQ, Qin WM, Yang Y, Zheng DW, Chen Y *et al*: **Synergistic anticancer effects of triptolide and celastrol, two main compounds from thunder god vine**. *Oncotarget* 2015, **6**(32):32790-32804.
29. Jiang F, Wang HJ, Bao QC, Wang L, Jin YH, Zhang Q, Jiang D, You QD, Xu XL: **Optimization and biological evaluation of celastrol derivatives as Hsp90-Cdc37 interaction disruptors with improved druglike properties**. *Bioorganic & medicinal chemistry* 2016, **24**(21):5431-5439.
30. Weisberg S, Leibel R, Tortoriello DV: **Proteasome inhibitors, including curcumin, improve pancreatic beta-cell function and insulin sensitivity in diabetic mice**. *Nutrition & diabetes* 2016, **6**:e205.
31. Choi SK, Park S, Jang S, Cho HH, Lee S, You S, Kim SH, Moon HS: **Cascade regulation of PPARgamma(2) and C/EBPalpha signaling pathways by celastrol impairs adipocyte differentiation and stimulates lipolysis in 3T3-L1 adipocytes**. *Metabolism: clinical and experimental* 2016, **65**(5):646-654.
32. Zhang Y, Geng C, Liu X, Li M, Gao M, Liu X, Fang F, Chang Y: **Celastrol ameliorates liver metabolic damage caused by a high-fat diet through Sirt1**. *Molecular metabolism* 2017, **6**(1):138-147.
33. Douglass JD, Dorfman MD, Thaler JP: **Glia: silent partners in energy homeostasis and obesity pathogenesis**. *Diabetologia* 2017, **60**(2):226-236.
34. Glickstein M: **Golgi and Cajal: The neuron doctrine and the 100th anniversary of the 1906 Nobel Prize**. *Curr Biol* 2006, **16**(5):R147-151.
35. Kabba JA, Xu Y, Christian H, Ruan W, Chenai K, Xiang Y, Zhang L, Saavedra JM, Pang T: **Microglia: Housekeeper of the Central Nervous System**. *Cellular and molecular neurobiology* 2017.
36. Wilhelm I, Nyul-Toth A, Suciu M, Hermenean A, Krizbai IA: **Heterogeneity of the blood-brain barrier**. *Tissue Barriers* 2016, **4**(1):e1143544.
37. Patching SG: **Glucose Transporters at the Blood-Brain Barrier: Function, Regulation and Gateways for Drug Delivery**. *Mol Neurobiol* 2017, **54**(2):1046-1077.
38. Chowen JA, Argente-Arizon P, Freire-Regatillo A, Frago LM, Horvath TL, Argente J: **The role of astrocytes in the hypothalamic response and adaptation to metabolic signals**. *Prog Neurobiol* 2016, **144**:68-87.
39. Brown AM, Ransom BR: **Astrocyte glycogen and brain energy metabolism**. *Glia* 2007, **55**(12):1263-1271.
40. Belanger M, Magistretti PJ: **The role of astroglia in neuroprotection**. *Dialogues Clin Neurosci* 2009, **11**(3):281-295.
41. Belanger M, Allaman I, Magistretti PJ: **Brain energy metabolism: focus on astrocyte-neuron metabolic cooperation**. *Cell metabolism* 2011, **14**(6):724-738.

42. Garcia-Caceres C, Quarta C, Varela L, Gao Y, Gruber T, Legutko B, Jastroch M, Johansson P, Ninkovic J, Yi CX *et al*: **Astrocytic Insulin Signaling Couples Brain Glucose Uptake with Nutrient Availability**. *Cell* 2016, **166**(4):867-880.
43. Halassa MM, Fellin T, Takano H, Dong JH, Haydon PG: **Synaptic islands defined by the territory of a single astrocyte**. *J Neurosci* 2007, **27**(24):6473-6477.
44. Giaume C, Koulakoff A, Roux L, Holcman D, Rouach N: **Astroglial networks: a step further in neuroglial and gliovascular interactions**. *Nat Rev Neurosci* 2010, **11**(2):87-99.
45. Bushong EA, Martone ME, Jones YZ, Ellisman MH: **Protoplasmic astrocytes in CA1 stratum radiatum occupy separate anatomical domains**. *J Neurosci* 2002, **22**(1):183-192.
46. Ogata K, Kosaka T: **Structural and quantitative analysis of astrocytes in the mouse hippocampus**. *Neuroscience* 2002, **113**(1):221-233.
47. Heller JP, Rusakov DA: **Morphological plasticity of astroglia: Understanding synaptic microenvironment**. *Glia* 2015, **63**(12):2133-2151.
48. Thaler JP, Yi CX, Schur EA, Guyenet SJ, Hwang BH, Dietrich MO, Zhao X, Sarruf DA, Izgur V, Maravilla KR *et al*: **Obesity is associated with hypothalamic injury in rodents and humans**. *The Journal of clinical investigation* 2012, **122**(1):153-162.
49. Sofroniew MV: **Molecular dissection of reactive astrogliosis and glial scar formation**. *Trends Neurosci* 2009, **32**(12):638-647.
50. Liddelow SA, Guttenplan KA, Clarke LE, Bennett FC, Bohlen CJ, Schirmer L, Bennett ML, Munch AE, Chung WS, Peterson TC *et al*: **Neurotoxic reactive astrocytes are induced by activated microglia**. *Nature* 2017, **541**(7638):481-487.
51. Gao Y, Ottaway N, Schriever SC, Legutko B, Garcia-Caceres C, de la Fuente E, Mergen C, Bour S, Thaler JP, Seeley RJ *et al*: **Hormones and diet, but not body weight, control hypothalamic microglial activity**. *Glia* 2014, **62**(1):17-25.
52. Canellada A, Ramirez BG, Minami T, Redondo JM, Cano E: **Calcium/calcineurin signaling in primary cortical astrocyte cultures: Rcan1-4 and cyclooxygenase-2 as NFAT target genes**. *Glia* 2008, **56**(7):709-722.
53. Klee CB, Crouch TH, Krinks MH: **Calcineurin: a calcium- and calmodulin-binding protein of the nervous system**. *Proc Natl Acad Sci U S A* 1979, **76**(12):6270-6273.
54. Norris CM, Kadish I, Blalock EM, Chen KC, Thibault V, Porter NM, Landfield PW, Kraner SD: **Calcineurin triggers reactive/inflammatory processes in astrocytes and is upregulated in aging and Alzheimer's models**. *J Neurosci* 2005, **25**(18):4649-4658.
55. Fernandez AM, Fernandez S, Carrero P, Garcia-Garcia M, Torres-Aleman I: **Calcineurin in reactive astrocytes plays a key role in the interplay between proinflammatory and anti-inflammatory signals**. *J Neurosci* 2007, **27**(33):8745-8756.
56. Pfluger PT, Kabra DG, Aichler M, Schriever SC, Pfuhlmann K, Garcia VC, Lehti M, Weber J, Kutschke M, Rozman J *et al*: **Calcineurin Links Mitochondrial Elongation with Energy Metabolism**. *Cell metabolism* 2015, **22**(5):838-850.
57. Brigelius-Flohe R, Maiorino M: **Glutathione peroxidases**. *Biochimica et biophysica acta* 2013, **1830**(5):3289-3303.
58. Flohe L, Toppo S, Cozza G, Ursini F: **A comparison of thiol peroxidase mechanisms**. *Antioxidants & redox signaling* 2011, **15**(3):763-780.
59. Ramming T, Appenzeller-Herzog C: **Destroy and exploit: catalyzed removal of hydroperoxides from the endoplasmic reticulum**. *Int J Cell Biol* 2013, **2013**:180906.
60. Ursini F, Maiorino M, Brigelius-Flohe R, Aumann KD, Roveri A, Schomburg D, Flohe L: **Diversity of glutathione peroxidases**. *Methods Enzymol* 1995, **252**:38-53.
61. Chen YI, Wei PC, Hsu JL, Su FY, Lee WH: **NPGPx (GPx7): a novel oxidative stress sensor/transmitter with multiple roles in redox homeostasis**. *American journal of translational research* 2016, **8**(4):1626-1640.

62. Wang L, Zhang L, Niu Y, Sitia R, Wang CC: **Glutathione peroxidase 7 utilizes hydrogen peroxide generated by Ero1alpha to promote oxidative protein folding**. *Antioxidants & redox signaling* 2014, **20**(4):545-556.
63. Lim JC, Choi HI, Park YS, Nam HW, Woo HA, Kwon KS, Kim YS, Rhee SG, Kim K, Chae HZ: **Irreversible oxidation of the active-site cysteine of peroxiredoxin to cysteine sulfonic acid for enhanced molecular chaperone activity**. *J Biol Chem* 2008, **283**(43):28873-28880.
64. Barford D: **The role of cysteine residues as redox-sensitive regulatory switches**. *Curr Opin Struct Biol* 2004, **14**(6):679-686.
65. Miki H, Funato Y: **Regulation of intracellular signalling through cysteine oxidation by reactive oxygen species**. *J Biochem* 2012, **151**(3):255-261.
66. Toppo S, Vanin S, Bosello V, Tosatto SC: **Evolutionary and structural insights into the multifaceted glutathione peroxidase (Gpx) superfamily**. *Antioxidants & redox signaling* 2008, **10**(9):1501-1514.
67. Tosatto SC, Bosello V, Fogolari F, Mauri P, Roveri A, Toppo S, Flohe L, Ursini F, Maiorino M: **The catalytic site of glutathione peroxidases**. *Antioxidants & redox signaling* 2008, **10**(9):1515-1526.
68. Maiorino M, Wissing JB, Brigelius-Flohe R, Calabrese F, Roveri A, Steinert P, Ursini F, Flohe L: **Testosterone mediates expression of the selenoprotein PHGPx by induction of spermatogenesis and not by direct transcriptional gene activation**. *FASEB J* 1998, **12**(13):1359-1370.
69. Rejraji H, Vernet P, Drevet JR: **GPX5 is present in the mouse caput and cauda epididymidis lumen at three different locations**. *Mol Reprod Dev* 2002, **63**(1):96-103.
70. Kryukov GV, Castellano S, Novoselov SV, Lobanov AV, Zehtab O, Guigo R, Gladyshev VN: **Characterization of mammalian selenoproteomes**. *Science* 2003, **300**(5624):1439-1443.
71. Nguyen VD, Saaranen MJ, Karala AR, Lappi AK, Wang L, Raykhel IB, Alanen HI, Salo KE, Wang CC, Ruddock LW: **Two endoplasmic reticulum PDI peroxidases increase the efficiency of the use of peroxide during disulfide bond formation**. *Journal of molecular biology* 2011, **406**(3):503-515.
72. Yan W, Chen X: **GPX2, a direct target of p63, inhibits oxidative stress-induced apoptosis in a p53-dependent manner**. *J Biol Chem* 2006, **281**(12):7856-7862.
73. Chu FF, Doroshow JH, Esworthy RS: **Expression, characterization, and tissue distribution of a new cellular selenium-dependent glutathione peroxidase, GSHPx-GI**. *J Biol Chem* 1993, **268**(4):2571-2576.
74. **GPX6 glutathione peroxidase 6 [Homo sapiens (human)]** [https://http://www.ncbi.nlm.nih.gov/gene/257202]
75. Utomo A, Jiang X, Furuta S, Yun J, Levin DS, Wang YC, Desai KV, Green JE, Chen PL, Lee WH: **Identification of a novel putative non-selenocysteine containing phospholipid hydroperoxide glutathione peroxidase (NPGPx) essential for alleviating oxidative stress generated from polyunsaturated fatty acids in breast cancer cells**. *J Biol Chem* 2004, **279**(42):43522-43529.
76. Raykhel I, Alanen H, Salo K, Jurvansuu J, Nguyen VD, Latva-Ranta M, Ruddock L: **A molecular specificity code for the three mammalian KDEL receptors**. *The Journal of cell biology* 2007, **179**(6):1193-1204.
77. Bosello-Travain V, Conrad M, Cozza G, Negro A, Quartesan S, Rossetto M, Roveri A, Toppo S, Ursini F, Zaccarin M *et al*: **Protein disulfide isomerase and glutathione are alternative substrates in the one Cys catalytic cycle of glutathione peroxidase 7**. *Biochimica et biophysica acta* 2013, **1830**(6):3846-3857.
78. Chang YC, Yu YH, Shew JY, Lee WJ, Hwang JJ, Chen YH, Chen YR, Wei PC, Chuang LM, Lee WH: **Deficiency of NPGPx, an oxidative stress sensor, leads to obesity in mice and human**. *EMBO Mol Med* 2013, **5**(8):1165-1179.

79. Maiorino M, Bosello-Travain V, Cozza G, Miotto G, Roveri A, Toppo S, Zaccarin M, Ursini F: **Understanding mammalian glutathione peroxidase 7 in the light of its homologs**. *Free radical biology & medicine* 2015, **83**:352-360.
80. Wei PC, Hsieh YH, Su MI, Jiang X, Hsu PH, Lo WT, Weng JY, Jeng YM, Wang JM, Chen PL *et al*: **Loss of the oxidative stress sensor NPGPx compromises GRP78 chaperone activity and induces systemic disease**. *Molecular cell* 2012, **48**(5):747-759.
81. Chen PJ, Weng JY, Hsu PH, Shew JY, Huang YS, Lee WH: **NPGPx modulates CPEB2-controlled HIF-1alpha RNA translation in response to oxidative stress**. *Nucleic Acids Res* 2015, **43**(19):9393-9404.
82. Wei PC, Lo WT, Su MI, Shew JY, Lee WH: **Non-targeting siRNA induces NPGPx expression to cooperate with exoribonuclease XRN2 for releasing the stress**. *Nucleic Acids Res* 2012, **40**(1):323-332.
83. Volkov P, Olsson AH, Gillberg L, Jorgensen SW, Brons C, Eriksson KF, Groop L, Jansson PA, Nilsson E, Ronn T *et al*: **A Genome-Wide mQTL Analysis in Human Adipose Tissue Identifies Genetic Variants Associated with DNA Methylation, Gene Expression and Metabolic Traits**. *PLoS One* 2016, **11**(6):e0157776.
84. Olsson AH, Volkov P, Bacos K, Dayeh T, Hall E, Nilsson EA, Ladenvall C, Ronn T, Ling C: **Genome-wide associations between genetic and epigenetic variation influence mRNA expression and insulin secretion in human pancreatic islets**. *PLoS Genet* 2014, **10**(11):e1004735.
85. Friedman LK, Mancuso J, Patel A, Kudur V, Leheste JR, Iacobas S, Botta J, Iacobas DA, Spray DC: **Transcriptome profiling of hippocampal CA1 after early-life seizure-induced preconditioning may elucidate new genetic therapies for epilepsy**. *Eur J Neurosci* 2013, **38**(1):2139-2152.
86. Song G, Nesil T, Cao J, Yang Z, Chang SL, Li MD: **Nicotine mediates expression of genes related to antioxidant capacity and oxidative stress response in HIV-1 transgenic rat brain**. *J Neurovirol* 2016, **22**(1):114-124.
87. Lacaille H, Duterte-Boucher D, Liot D, Vaudry H, Naassila M, Vaudry D: **Comparison of the deleterious effects of binge drinking-like alcohol exposure in adolescent and adult mice**. *J Neurochem* 2015, **132**(6):629-641.
88. Peng D, Hu T, Soutto M, Belkhiri A, Zaika A, El-Rifai W: **Glutathione peroxidase 7 has potential tumour suppressor functions that are silenced by location-specific methylation in oesophageal adenocarcinoma**. *Gut* 2014, **63**(4):540-551.
89. Peng DF, Razvi M, Chen H, Washington K, Roessner A, Schneider-Stock R, El-Rifai W: **DNA hypermethylation regulates the expression of members of the Mu-class glutathione S-transferases and glutathione peroxidases in Barrett's adenocarcinoma**. *Gut* 2009, **58**(1):5-15.
90. Guariniello S, Di Bernardo G, Colonna G, Cammarota M, Castello G, Costantini S: **Evaluation of the selenotranscriptome expression in two hepatocellular carcinoma cell lines**. *Anal Cell Pathol (Amst)* 2015, **2015**:419561.
91. Guerriero E, Capone F, Accardo M, Sorice A, Costantini M, Colonna G, Castello G, Costantini S: **GPX4 and GPX7 over-expression in human hepatocellular carcinoma tissues**. *Eur J Histochem* 2015, **59**(4):2540.
92. Li Y, Sun Z, Cunningham JM, Aubry MC, Wampfler JA, Croghan GA, Johnson C, Wu D, Aakre JA, Molina J *et al*: **Genetic variations in multiple drug action pathways and survival in advanced stage non-small cell lung cancer treated with chemotherapy**. *Clin Cancer Res* 2011, **17**(11):3830-3840.
93. Johnson C, Pankratz VS, Velazquez AI, Aakre JA, Loprinzi CL, Staff NP, Windebank AJ, Yang P: **Candidate pathway-based genetic association study of platinum and platinum-taxane related toxicity in a cohort of primary lung cancer patients**. *J Neurol Sci* 2015, **349**(1-2):124-128.
94. Gordeeva AE, Temnov AA, Charnagalov AA, Sharapov MG, Fesenko EE, Novoselov VI: **Protective Effect of Peroxiredoxin 6 in Ischemia/Reperfusion-Induced Damage of Small Intestine**. *Dig Dis Sci* 2015, **60**(12):3610-3619.

95. Teruya R, Ikejiri AT, Somaio Neto F, Chaves JC, Bertoletto PR, Taha MO, Fagundes DJ: **Expression of oxidative stress and antioxidant defense genes in the kidney of inbred mice after intestinal ischemia and reperfusion**. *Acta Cir Bras* 2013, **28**(12):848-855.
96. Bueno OF, Brandt EB, Rothenberg ME, Molkentin JD: **Defective T cell development and function in calcineurin A beta -deficient mice**. *Proc Natl Acad Sci U S A* 2002, **99**(14):9398-9403.
97. Bueno OF, Wilkins BJ, Tymitz KM, Glascock BJ, Kimball TF, Lorenz JN, Molkentin JD: **Impaired cardiac hypertrophic response in Calcineurin Abeta -deficient mice**. *Proc Natl Acad Sci U S A* 2002, **99**(7):4586-4591.
98. Divakaruni AS, Paradyse A, Ferrick DA, Murphy AN, Jastroch M: **Analysis and interpretation of microplate-based oxygen consumption and pH data**. *Methods Enzymol* 2014, **547**:309-354.
99. Zhang Y, Proenca R, Maffei M, Barone M, Leopold L, Friedman JM: **Positional cloning of the mouse obese gene and its human homologue**. *Nature* 1994, **372**(6505):425-432.
100. Cowley MA, Smart JL, Rubinstein M, Cerdan MG, Diano S, Horvath TL, Cone RD, Low MJ: **Leptin activates anorexigenic POMC neurons through a neural network in the arcuate nucleus**. *Nature* 2001, **411**(6836):480-484.
101. Bohmer FD, Friedrich K: **Protein tyrosine phosphatases as wardens of STAT signaling**. *JAKSTAT* 2014, **3**(1):e28087.
102. Sohn JW, Elmquist JK, Williams KW: **Neuronal circuits that regulate feeding behavior and metabolism**. *Trends Neurosci* 2013, **36**(9):504-512.
103. Newsholme P, Cruzat VF, Keane KN, Carlessi R, de Bittencourt PI, Jr.: **Molecular mechanisms of ROS production and oxidative stress in diabetes**. *Biochem J* 2016, **473**(24):4527-4550.
104. Matsuzawa-Nagata N, Takamura T, Ando H, Nakamura S, Kurita S, Misu H, Ota T, Yokoyama M, Honda M, Miyamoto K *et al*: **Increased oxidative stress precedes the onset of high-fat diet-induced insulin resistance and obesity**. *Metabolism: clinical and experimental* 2008, **57**(8):1071-1077.
105. Le Lay S, Simard G, Martinez MC, Andriantsitohaina R: **Oxidative stress and metabolic pathologies: from an adipocentric point of view**. *Oxid Med Cell Longev* 2014, **2014**:908539.
106. Even PC, Nadkarni NA: **Indirect calorimetry in laboratory mice and rats: principles, practical considerations, interpretation and perspectives**. *American journal of physiology Regulatory, integrative and comparative physiology* 2012, **303**(5):R459-476.
107. Zechner R, Kienesberger PC, Haemmerle G, Zimmermann R, Lass A: **Adipose triglyceride lipase and the lipolytic catabolism of cellular fat stores**. *J Lipid Res* 2009, **50**(1):3-21.
108. Lidell ME, Betz MJ, Enerback S: **Brown adipose tissue and its therapeutic potential**. *J Intern Med* 2014, **276**(4):364-377.
109. Cannon B, Nedergaard J: **Brown adipose tissue: function and physiological significance**. *Physiological reviews* 2004, **84**(1):277-359.
110. Fedorenko A, Lishko PV, Kirichok Y: **Mechanism of fatty-acid-dependent UCP1 uncoupling in brown fat mitochondria**. *Cell* 2012, **151**(2):400-413.
111. Xu Q, Tam M, Anderson SA: **Fate mapping Nkx2.1-lineage cells in the mouse telencephalon**. *J Comp Neurol* 2008, **506**(1):16-29.
112. Yee CL, Wang Y, Anderson S, Ekker M, Rubenstein JL: **Arcuate nucleus expression of NKX2.1 and DLX and lineages expressing these transcription factors in neuropeptide Y(+), proopiomelanocortin(+), and tyrosine hydroxylase(+) neurons in neonatal and adult mice**. *J Comp Neurol* 2009, **517**(1):37-50.

113. Poher AL, Altirriba J, Veyrat-Durebex C, Rohner-Jeanrenaud F: **Brown adipose tissue activity as a target for the treatment of obesity/insulin resistance**. *Frontiers in physiology* 2015, **6**:4.
114. Chouchani ET, Kazak L, Jedrychowski MP, Lu GZ, Erickson BK, Szpyt J, Pierce KA, Laznik-Bogoslavski D, Vetrivelan R, Clish CB *et al*: **Mitochondrial ROS regulate thermogenic energy expenditure and sulfenylation of UCP1**. *Nature* 2016, **532**(7597):112-116.
115. Li HY, Zhang J, Sun LL, Li BH, Gao HL, Xie T, Zhang N, Ye ZM: **Celastrol induces apoptosis and autophagy via the ROS/JNK signaling pathway in human osteosarcoma cells: an in vitro and in vivo study**. *Cell death & disease* 2015, **6**:e1604.
116. Chadalapaka G, Jutooru I, Safe S: **Celastrol decreases specificity proteins (Sp) and fibroblast growth factor receptor-3 (FGFR3) in bladder cancer cells**. *Carcinogenesis* 2012, **33**(4):886-894.
117. Kim JH, Lee JO, Lee SK, Kim N, You GY, Moon JW, Sha J, Kim SJ, Park SH, Kim HS: **Celastrol suppresses breast cancer MCF-7 cell viability via the AMP-activated protein kinase (AMPK)-induced p53-polo like kinase 2 (PLK-2) pathway**. *Cellular signalling* 2013, **25**(4):805-813.
118. Chen G, Zhang X, Zhao M, Wang Y, Cheng X, Wang D, Xu Y, Du Z, Yu X: **Celastrol targets mitochondrial respiratory chain complex I to induce reactive oxygen species-dependent cytotoxicity in tumor cells**. *BMC cancer* 2011, **11**:170.
119. Raja SM, Clubb RJ, Ortega-Cava C, Williams SH, Bailey TA, Duan L, Zhao X, Reddi AL, Nyong AM, Natarajan A *et al*: **Anticancer activity of Celastrol in combination with ErbB2-targeted therapeutics for treatment of ErbB2-overexpressing breast cancers**. *Cancer biology & therapy* 2011, **11**(2):263-276.
120. Rowland LA, Bal NC, Periasamy M: **The role of skeletal-muscle-based thermogenic mechanisms in vertebrate endothermy**. *Biol Rev Camb Philos Soc* 2015, **90**(4):1279-1297.
121. Wilson BD, Bagnol D, Kaelin CB, Ollmann MM, Gantz I, Watson SJ, Barsh GS: **Physiological and anatomical circuitry between Agouti-related protein and leptin signaling**. *Endocrinology* 1999, **140**(5):2387-2397.
122. Sutton GM, Begriche K, Kumar KG, Gimble JM, Perez-Tilve D, Nogueiras R, McMillan RP, Hulver MW, Tschop MH, Butler AA: **Central nervous system melanocortin-3 receptors are required for synchronizing metabolism during entrainment to restricted feeding during the light cycle**. *Faseb j* 2010, **24**(3):862-872.
123. Nogueiras R, Wiedmer P, Perez-Tilve D, Veyrat-Durebex C, Keogh JM, Sutton GM, Pfluger PT, Castaneda TR, Neschen S, Hofmann SM *et al*: **The central melanocortin system directly controls peripheral lipid metabolism**. *The Journal of clinical investigation* 2007, **117**(11):3475-3488.
124. Qian S, Chen H, Weingarth D, Trumbauer ME, Novi DE, Guan X, Yu H, Shen Z, Feng Y, Frazier E *et al*: **Neither agouti-related protein nor neuropeptide Y is critically required for the regulation of energy homeostasis in mice**. *Molecular and cellular biology* 2002, **22**(14):5027-5035.
125. Banks AS, Davis SM, Bates SH, Myers MG, Jr.: **Activation of downstream signals by the long form of the leptin receptor**. *J Biol Chem* 2000, **275**(19):14563-14572.
126. Bjorbaek C, Uotani S, da Silva B, Flier JS: **Divergent signaling capacities of the long and short isoforms of the leptin receptor**. *J Biol Chem* 1997, **272**(51):32686-32695.
127. Ukkola O, Santaniemi M: **Protein tyrosine phosphatase 1B: a new target for the treatment of obesity and associated co-morbidities**. *J Intern Med* 2002, **251**(6):467-475.
128. Tiganis T: **PTP1B and TCPTP--nonredundant phosphatases in insulin signaling and glucose homeostasis**. *FEBS J* 2013, **280**(2):445-458.

129. Loh K, Fukushima A, Zhang X, Galic S, Briggs D, Enriori PJ, Simonds S, Wiede F, Reichenbach A, Hauser C *et al*: **Elevated hypothalamic TCPTP in obesity contributes to cellular leptin resistance**. *Cell metabolism* 2011, **14**(5):684-699.
130. Dodd GT, Decherf S, Loh K, Simonds SE, Wiede F, Balland E, Merry TL, Munzberg H, Zhang ZY, Kahn BB *et al*: **Leptin and insulin act on POMC neurons to promote the browning of white fat**. *Cell* 2015, **160**(1-2):88-104.
131. Westerheide SD, Bosman JD, Mbadugha BN, Kawahara TL, Matsumoto G, Kim S, Gu W, Devlin JP, Silverman RB, Morimoto RI: **Celastrols as inducers of the heat shock response and cytoprotection**. *J Biol Chem* 2004, **279**(53):56053-56060.
132. Shrivastava S, Jeengar MK, Reddy VS, Reddy GB, Naidu VG: **Anticancer effect of celastrol on human triple negative breast cancer: possible involvement of oxidative stress, mitochondrial dysfunction, apoptosis and PI3K/Akt pathways**. *Experimental and molecular pathology* 2015, **98**(3):313-327.
133. Hu Y, Qi Y, Liu H, Fan G, Chai Y: **Effects of celastrol on human cervical cancer cells as revealed by ion-trap gas chromatography-mass spectrometry based metabolic profiling**. *Biochimica et biophysica acta* 2013, **1830**(3):2779-2789.
134. Guo J, Huang X, Wang H, Yang H: **Celastrol Induces Autophagy by Targeting AR/miR-101 in Prostate Cancer Cells**. *PLoS One* 2015, **10**(10):e0140745.
135. Furman JL, Sama DM, Gant JC, Beckett TL, Murphy MP, Bachstetter AD, Van Eldik LJ, Norris CM: **Targeting astrocytes ameliorates neurologic changes in a mouse model of Alzheimer's disease**. *J Neurosci* 2012, **32**(46):16129-16140.
136. Serrano-Perez MC, Martin ED, Vaquero CF, Azcoitia I, Calvo S, Cano E, Tranque P: **Response of transcription factor NFATc3 to excitotoxic and traumatic brain insults: identification of a subpopulation of reactive astrocytes**. *Glia* 2011, **59**(1):94-107.
137. Sama MA, Mathis DM, Furman JL, Abdul HM, Artiushin IA, Kraner SD, Norris CM: **Interleukin-1beta-dependent signaling between astrocytes and neurons depends critically on astrocytic calcineurin/NFAT activity**. *J Biol Chem* 2008, **283**(32):21953-21964.
138. Garcia-Caceres C, Fuente-Martin E, Burgos-Ramos E, Granado M, Frago LM, Barrios V, Horvath T, Argente J, Chowen JA: **Differential acute and chronic effects of leptin on hypothalamic astrocyte morphology and synaptic protein levels**. *Endocrinology* 2011, **152**(5):1809-1818.
139. Andrews ZB, Liu ZW, Walllingford N, Erion DM, Borok E, Friedman JM, Tschop MH, Shanabrough M, Cline G, Shulman GI *et al*: **UCP2 mediates ghrelin's action on NPY/AgRP neurons by lowering free radicals**. *Nature* 2008, **454**(7206):846-851.
140. Kim JG, Suyama S, Koch M, Jin S, Argente-Arizon P, Argente J, Liu ZW, Zimmer MR, Jeong JK, Szigeti-Buck K *et al*: **Leptin signaling in astrocytes regulates hypothalamic neuronal circuits and feeding**. *Nat Neurosci* 2014, **17**(7):908-910.
141. Herrmann JE, Imura T, Song B, Qi J, Ao Y, Nguyen TK, Korsak RA, Takeda K, Akira S, Sofroniew MV: **STAT3 is a critical regulator of astrogliosis and scar formation after spinal cord injury**. *J Neurosci* 2008, **28**(28):7231-7243.
142. Pleiss MM, Sompol P, Kraner SD, Abdul HM, Furman JL, Guttmann RP, Wilcock DM, Nelson PT, Norris CM: **Calcineurin proteolysis in astrocytes: Implications for impaired synaptic function**. *Biochimica et biophysica acta* 2016, **1862**(9):1521-1532.
143. Furman JL, Sompol P, Kraner SD, Pleiss MM, Putman EJ, Dunkerson J, Mohmmad Abdul H, Roberts KN, Scheff SW, Norris CM: **Blockade of Astrocytic Calcineurin/NFAT Signaling Helps to Normalize Hippocampal Synaptic Function and Plasticity in a Rat Model of Traumatic Brain Injury**. *J Neurosci* 2016, **36**(5):1502-1515.
144. Fernandez AM, Jimenez S, Mecha M, Davila D, Guaza C, Vitorica J, Torres-Aleman I: **Regulation of the phosphatase calcineurin by insulin-like growth factor I unveils a key role of astrocytes in Alzheimer's pathology**. *Mol Psychiatry* 2012, **17**(7):705-718.

145. Fernandez AM, Hervas R, Dominguez-Fraile M, Garrido VN, Gomez-Gutierrez P, Vega M, Vitorica J, Perez JJ, Torres Aleman I: **Blockade of the Interaction of Calcineurin with FOXO in Astrocytes Protects Against Amyloid-beta-Induced Neuronal Death**. *J Alzheimers Dis* 2016, **52**(4):1471-1478.
146. Chen Y, Holstein DM, Aime S, Bollo M, Lechleiter JD: **Calcineurin beta protects brain after injury by activating the unfolded protein response**. *Neurobiol Dis* 2016, **94**:139-156.
147. Matsuda T, Takuma K, Asano S, Kishida Y, Nakamura H, Mori K, Maeda S, Baba A: **Involvement of calcineurin in Ca2+ paradox-like injury of cultured rat astrocytes**. *J Neurochem* 1998, **70**(5):2004-2011.
148. Pyrzynska B, Lis A, Mosieniak G, Kaminska B: **Cyclosporin A-sensitive signaling pathway involving calcineurin regulates survival of reactive astrocytes**. *Neurochem Int* 2001, **38**(5):409-415.
149. Gabryel B, Chalimoniuk M, Stolecka A, Waniek K, Langfort J, Malecki A: **Inhibition of arachidonic acid release by cytosolic phospholipase A2 is involved in the antiapoptotic effect of FK506 and cyclosporin a on astrocytes exposed to simulated ischemia in vitro**. *J Pharmacol Sci* 2006, **102**(1):77-87.
150. Gabryel B, Pudelko A, Adamczyk J, Fischer I, Malecki A: **Calcineurin and Erk1/2-signaling pathways are involved in the antiapoptotic effect of cyclosporin A on astrocytes exposed to simulated ischemia in vitro**. *Naunyn Schmiedebergs Arch Pharmacol* 2006, **374**(2):127-139.
151. Szydlowska K, Zawadzka M, Kaminska B: **Neuroprotectant FK506 inhibits glutamate-induced apoptosis of astrocytes in vitro and in vivo**. *J Neurochem* 2006, **99**(3):965-975.
152. Furman JL, Artiushin IA, Norris CM: **Disparate effects of serum on basal and evoked NFAT activity in primary astrocyte cultures**. *Neurosci Lett* 2010, **469**(3):365-369.
153. Mordica WJ, Gallagher RJ, Kennedy JL, Chapes SK: **Male CD81 knockout genotype disrupts Mendelian distribution of offspring**. *Comp Med* 2010, **60**(3):196-199.
154. Schmidt CM, Hood WR: **Calcium availability influences litter size and sex ratio in white-footed mice (Peromyscus leucopus)**. *PLoS One* 2012, **7**(8):e41402.
155. Rosenfeld CS, Grimm KM, Livingston KA, Brokman AM, Lamberson WE, Roberts RM: **Striking variation in the sex ratio of pups born to mice according to whether maternal diet is high in fat or carbohydrate**. *Proc Natl Acad Sci U S A* 2003, **100**(8):4628-4632.
156. Trivers RL, Willard DE: **Natural selection of parental ability to vary the sex ratio of offspring**. *Science* 1973, **179**(4068):90-92.
157. Goundie TR, Vessey SH: **Survival and Dispersal of Young White-Footed Mice Born in Nest Boxes**. *Journal of Mammalogy* 1986, **67**(1):53-60.
158. Laukens D, Brinkman BM, Raes J, De Vos M, Vandenabeele P: **Heterogeneity of the gut microbiome in mice: guidelines for optimizing experimental design**. *FEMS microbiology reviews* 2016, **40**(1):117-132.
159. Ohoka N, Yoshii S, Hattori T, Onozaki K, Hayashi H: **TRB3, a novel ER stress-inducible gene, is induced via ATF4-CHOP pathway and is involved in cell death**. *EMBO J* 2005, **24**(6):1243-1255.
160. Du K, Herzig S, Kulkarni RN, Montminy M: **TRB3: a tribbles homolog that inhibits Akt/PKB activation by insulin in liver**. *Science* 2003, **300**(5625):1574-1577.
161. Schulz TJ, Tseng YH: **Systemic control of brown fat thermogenesis: integration of peripheral and central signals**. *Ann N Y Acad Sci* 2013, **1302**:35-41.
162. Harms M, Seale P: **Brown and beige fat: development, function and therapeutic potential**. *Nat Med* 2013, **19**(10):1252-1263.
163. Yamashita H, Sato Y, Mori N: **Difference in induction of uncoupling protein genes in adipose tissues between young and old rats during cold exposure**. *FEBS Lett* 1999, **458**(2):157-161.

Acknowledgements

I would like to express my gratitude to all the people who supported me during the many years of this PhD project and who made this work possible.

First of all I would like to thank

- Prof. Dr. Matthias Tschöp for giving me the opportunity to perform my PhD thesis at his renowned institute with its excellent research environment and great infrastructure.
- Dr. Paul Pfluger, who supervised my projects over all the years. Thank you for sharing your great insight in science, for giving me the opportunity to explore many different research fields and equipping me with a broad methodological spectrum. Thanks for being an excellent supervisor with a motivating and always positive and optimistic attitude.
- Prof. Dr. Martin Hrabě de Angelis for acting as the second supervisor of my thesis and for his interest in my research work.
- Dr. Sonja C. Schriever for her support throughout the years and her organizational talent.

Next, I would like to thank Dr. Dhiraj Kabra (“The master of western blot”), thanks for sharing your great biological knowledge and for your helpful advises.

Moreover, I would like to thank the whole former and current Neurobiology of Diabetes team. Thanks to Emily Baumgart, Peter Baumann, Luke Harrison, Verónica Casquero García, Raian Contreras and Sarah Jelenik. Thanks for the nice bench-environment, the team atmosphere and your support.

Thanks also to the master students and trainees in our group, Ksenija Martinovic, Louise Kaldjob, Celine Sundag and Carina Rupp, for their great work and the nice time together.

Next, I would like to thank Dr. Christoffer Clemmensen for sharing his pharmacological knowledge and for the fruitful discussions. Thanks also for providing the UCP1-KO mice for the celastrol project.

The astrocytes part of my thesis was one of my favorite projects. Thanks to Dr. Cristina García Cáceres for her support, advices and for making the method of primary astrocyte culture available for me.

I would also like to thank Dr. Beata Legutko for being an excellent teacher regarding the method of primary astrocyte culture. Thanks for your time, patients and your refreshing character.

Thanks to Dr. Martin Jastroch (MJ), Dr. Susanne Keipert and Daniel Lamp for sharing your seahorse expertise.

Thanks also to Marlene Kilian for all her work and support with the mice in A-stripe.

Further, I would like to thank Nirav Chhabra for teaching me the challenging method of islet isolation.

I would like to express my gratitude to my PhD colleagues from the S2 and S1 lab. Thanks for the joyful time together in and outside the lab. Thanks to Ines Pramme-Steinwachs, Lisa Suwandhi, Ingrid Fischer, Katrin Fischer, Ellen Walheim, Sigi Jall, Charlotte Hemmer, Michaela Bauer, Uma Kabra, Tim Gruber, Christian Gallus, Johannes Lichti, Matthias von Gamm, Annalisa Schraub and Sini Joseph.

Furthermore, I would like to thank all the group leaders, postdocs, and technicians at the IDO for the nice work environment and your helpfulness. In particular Christina Neff, Laura Sehrer, Luisa Müller, Daniela Heine, Heidi Hofmann, Clarita Layritz, Nicole Wiegert, Andreas Israel, Dr. Simone Hausmann, Ruth Karlina, Dr. Ming Gao, Dr. Theresa Schöttl, Dr. Kathrin Davari, Peggy Dörfelt, Dr. Alexandra Harger, Dr. Ken Dyar, Dr. Franziska Greulich, Dr. Sithandiwe Mazibuko-Mbeje, Dr. Kerstin Stemmer, Dr. Timo Müller, Dr. Brian Finan, Dr. Carmelo Quarta, Dr. Gustav Colldén, Dr. Robby Zachariah Tom, Dr. Fabi Zani and Dr. Petra Kotzbeck.

Thanks to the administrative staff: Ivonne Guderian, Armin Walter and Martina Antretter.

Ein großes Dankeschön geht auch an die Tierpflegerinnen Monika Klose, Michaela Wetzel und Petra Gabel.

Den größten Dank möchte ich Alex, meinen Eltern und meiner Schwester, sowie dem Rest meiner Familie schenken. Danke für eure unendliche Unterstützung.